Soil-Tool-Residue Interactions: Measurements and Modelling

by

Zhiwei Zeng

A Thesis submitted to the Faculty of Graduate Studies of

The University of Manitoba

in partial fulfillment of the requirements of the degree of

DOCTOR OF PHILOSOPHY

Department of Biosystems Engineering

University of Manitoba

Winnipeg

Abstract

Soil-tool-residue interactions are at the centre of many agricultural field operations. The study of soil-tool-residue interactions is one of the fundamental aspects of soil dynamics in agricultural engineering. The aim of this study was to investigate dynamic behaviours of soil-tool-residue interactions including soil cutting forces, soil displacement, soil loosening and furrow profile, straw displacement, residue cover and incorporation. Experimental studies of soil-tool-residue interactions were conducted for various soil-engaging tools (fluted coulter, rippled disc, and compact disc harrow) working on several field conditions (corn stubble, wheat stubble, and bare soil) at different operational parameters (working speed and depth). Numerical models of the soil-tool-residue interactions were developed for a micropenetrometer, a subsoiler, and a sweep using the discrete element method (DEM). The models were calibrated and validated by comparing simulation results with experimental data from soil bin and field tests. Field testing results of vertical tillage tools demonstrated that fluted coulters left less surface residue, incorporated more residue into the soil, created a wider furrow, and disturbed a larger area than rippled discs. The effect of working speed was more dominant than the coulter geometry on the tillage performance of the fluted coulters. Soil bin tests of a compact disc harrow indicated that disc spacing and offset had significant effects on soil disturbance characteristics, and the effects varied with the tillage depth. The DEM simulation results showed that the soil-micropenetrometer model produced comparable results to the laboratory measurements, in terms of the variation of cone index over penetration depth. The soil-subsoiler model was capable of predicting soil cutting resistance and soil disturbance characteristics with relative errors ranging from

i

2.63 to 10.2%. The straw-sweep-soil model was able to simulate dynamic attributes of bulk materials and individual particles, such as straw movement, moving trajectories and velocity contours. This study embraced a broad topic of soil-tool-residue interactions. The results have advanced the science of soil dynamics and contributed to the engineering knowledge required for the development of high-performance agricultural machinery that consumes minimal tractor power and creates optimal field conditions for crop growth.

Acknowledgements

I am profoundly grateful to my advisor, Dr. Ying Chen, for her excellent supervision, invaluable mentorship, and unwavering support throughout the duration of my doctoral studies. The energy and commitment she has for research and life is contagious and motivational, which has contributed enormously to my professional development and personal growth. She was, and continues to be, an inspiration. Words could never be enough to express my appreciation. My deepest thanks go to Drs. Chen and Sylvio Tessier who changed my life. I would also like to thank my thesis advisory committee members, Drs. Claude Laguë and Marolo Alfaro, for their constructive feedback and commitment over the years. The participation of Dr. John Fielke as the external examiner is highly appreciated.

Immense gratitude to the past and present members of the Soil Dynamics and Machinery Lab for their technical assistance and support. I would particularly like to thank Dr. Mohammad Sadek who helped me learn the discrete element modelling in the early days. My sincere thanks go to the teaching, administrative and technical staff of the Department of Biosystems Engineering, the University of Manitoba, especially Drs. Danny Mann and Jitendra Paliwal. A special thanks to Dr. Qiuyan Yuan for the friendship and moral support.

I acknowledge the financial support received from the following sources as research grants or scholarships during the course of my studies: Natural Sciences and Engineering Research Council of Canada, Government of Manitoba, Mitacs, Faculties of Graduate Studies, Engineering, and Agricultural and Food Sciences at the University of

谨以此书献给我亲爱的爸妈

This thesis is dedicated to my beloved parents

Table of Contents

viii

List of Tables

List of Figures

Chapter 1: General Introduction

1.1. Introduction

The soaring population of the world and limited land resources are requiring the agricultural industry to increase its productivity to provide a sufficient amount of food. Agricultural machinery is an extremely vital part of high-efficiency food production. There are many different types of agricultural machines, such as tillage and seeding implements. Soil-engaging tools are the main components of these implements, and thus their performance is critical for food production. Soil-engaging tools directly interact with the soil and crop residue in the field. The degree of interaction depends on the soil and residue conditions, tool types and their arrangement on the implement, as well as operational parameters (Unger and Cassel, 1991; Unger et al., 1997; McKyes and Maswaure, 1997). The performance of a soil-engaging tool is evaluated by the resultant soil dynamic attributes (such as soil displacement and cutting forces) and residue incorporation characteristics (such as residue cutting and sizing). A high-performance soil-engaging tool is one that creates the optimal soil and residue conditions for crop production while minimizing energy requirements.

One of the major concerns of conservation tillage is the presence of large quantities of residue (30% to 100% residue cover in percentage as shown in Fig. 1.1) that cause plugging of traditional tillage and seeding equipment, which can adversely affect crop emergence and yield. To tackle this problem, new tillage tools including vertical tillage (VT) and compact disc harrow (CDH) have been recently introduced to the market (Chen et al., 2016; Kanicki, 2014). A common feature of VT and CDH equipment (e.g., Fig. 1.2.) is the using of rotary soil-engaging tools, such as coulters, discs, rotary hoes,

knives, and rollers (Whitehair, 2014). Rotary tools cut crop residue into small segments while they work the soil, and small segments do not plug the equipment. Furthermore, rotary tools have lower draft force requirement and can travel faster as compared with traditional equipment (Chen et al., 2016). Therefore, VT and CDH can deal with heavy crop residue, while increasing field capacity and lowering energy consumption. Most importantly, VT and CDH maintain and anchor some residue on the soil surface for soil erosion protection, and therefore they are categorized as conservation tillage practices. The success of applying the concept of VT and CDH in the conservation tillage depends on the understanding of the interactions of new tillage tools with soil and residue.

Figure 1.1. Excessive residue cover in a corn field.

(a)

(b)

Figure 1.2. Examples of vertical tillage and compact disc harrow equipment: (a) Viking and (b) Fury of Buhler Industries Inc. (Source: https://www.versatile-ag.com)

Investigation on the soil-tool-residue interactions system has been carried out through two approaches: experimental and modelling studies. Experimental studies have generated data used to develop empirical models that related soil and tool variables (e.g.,

Liu et al., 2010). Modelling approaches could be categorized into either analytical modelling or numerical simulation. Analytical modelling predicts soil dynamic properties based on certain assumptions of soil failure pattern and simplifications of tool geometry (e.g., Liu et al., 2008). Numerical simulations can address complex soil deformation and tool geometry (e.g., Plouffe et al., 1999). One of the promising numerical simulation tools is the discrete element method (DEM), which can deal with the complex geometry of soil-engaging tools and non-homogeneous and non-linear behaviour of soil and residue (e.g., Sadek and Chen, 2015). Therefore, DEM simulations and experiments were carried out for the investigation of soil-tool-residue interactions in this study.

Research on soil-tool-residue interactions has progressed over the past decades, but challenges remain. The soil dynamic behaviours and residue incorporation characteristics of new tillage tools were not documented, notably the residue management associated with VT and the soil loosening associated with CDH. Most previous models were analytical or numerical models in which soil was treated as a continuous media, whereas soil is a discontinuous media in nature. The limited number of discrete element models developed in the literature had limitations on: a) the ability to represent the heterogeneity of agricultural soil and b) the capacity for integrating crop residue into soil-tool interaction models. This thesis was aimed to tackle these limitations of discrete element models and to advance the field of soil dynamics in the new era of conservation tillage.

1.2. Objectives

The overall goal of this study was to understand the soil-tool-residue interactions behaviours, which would lead to the development of new high-performance agricultural

machines, improvement of existing machines, and advancement of soil dynamics. A desired soil-engaging tool would consume minimal tractor power as assessed by soil cutting forces and create the optimal soil and residue conditions as evaluated by soil displacement, soil loosening and furrow profile, straw displacement, residue cover and incorporation. The specific objectives were to:

1. examine the soil and residue conditions as well as forces resultant from various VT tools working at different speeds (chapter 3 & 4),

2. investigate the soil furrow profiles and forces of a CDH as affected by tool arrangement (chapter 5),

3. calibrate and validate a DEM model of a micropenetrometer and its interaction with soil (chapter 6),

4. study the soil loosening characteristics of a deep tillage tool as effected by working depth using DEM modelling (chapter 7), and

5. investigate the straw movement behaviour of a sweep as affected by working speed using the DEM (chapter 8).

1.3. Thesis structure

This thesis has been structured in a paper format. General introduction and literature review are presented in chapters 1 and 2. Chapters 3 to 8 are major parts of the thesis written in the paper format and each chapter deals with specific objectives. Chapters 3, 4, and 5 report experimental studies of soil-tool-residue interactions, and chapters 6, 7 and 8 present modelling studies of the interactions. General conclusions are provided in chapter 9.

Chapters 3, 4, 5, 6, 7 and 8 have been published as Zeng and Chen (2018a), Zeng and Chen (2018b), Zeng et al. (2019), Zeng and Chen (2016), Zeng et al. (2017), and Zeng and Chen (2019) respectively. The published work has been formatted in this thesis for consistency. The candidate is the first author and Dr. Ying Chen, the candidate's advisor, is the corresponding author of all the manuscripts included in this thesis. Chapter 5 is co-authored by Dr. Long Qi, an adjunct professor in the Department of Biosystems Engineering at the University of Manitoba, who contributed to the testing protocol and discussion. Chapter 7 is co-authored by Dr. Xirui Zhang, a visiting scholar with the group in 2015-2016, who participated in the data collection and analysis for the soil bin experiment.

1.4. References

Chen, Y., Damphousse, S., Li, H., 2016. Vertical tillage and vertical seeding. Paper No. CSBE16-090. In: CSBE/SCGAB 2016 Annual Conference. Halifax, NS, Canada. July 3–6.

Kanicki, D., 2014. High Speed Compact Discs Are Not Vertical Tillage Tools? Special Report: Vertical Tillage. http://www.farm-equipment.com/articles. Accessed 11 September 2018.

Liu, J., Chen, Y., Kushwaha, R.L., 2010. Effect of tillage speed and straw length on soil and straw movement by a sweep. Soil & Tillage Research 109, 9–17.

Liu, J., Lobb, D.A., Chen, Y., Kushwaha, R.L., 2008. Steady-state models for the movement of soli and straw during tillage with a single sweep. Transactions of the ASABE 51(3), 781–789.

McKyes, E., Maswaure, J., 1997. Effect of design parameters of flat tillage tool on loosening of a clay soil. Soil & Tillage Research 43, 195–204.

Plouffe, C., Lague, C., Tessier, S., Richard, M.J., McLaughlin, N.B., 1999. Moldboard plow performance in a clay soil: simulation and experiment. Transactions of the ASAE 42(6), 1531–1540.

Sadek, M. A., Chen, Y., 2015. Feasibility of using PFC3D to simulate soil flow resulting from a simple soil engaging tool. Transactions of the ASABE 58(4), 987–996.

Unger, P.W., Cassel, D.K., 1991. Tillage implement disturbance effects on soil properties related to soil and water conservation: a literature review. Soil & Tillage Research 19(4), 363–382.

Unger, P.W., Schomberg, H.H., Dao, T.H., Jones, O.R., 1997. Tillage and crop residue management practices for sustainable dryland farming systems. Annals of Arid Zone 36(3), 209–232.

Whitehair, A., 2014. Vertical Tillage Effects on Yield, Disease and Pathogens, and Soil Properties. M.Sc. Thesis, Kansas State University, Manhattan, Kansas, USA.

Zeng, Z., Chen, Y., 2016. Simulation of soil-micropenetrometer interaction using the discrete element method (DEM). Transactions of the ASABE 59(5), 1157–1163.

Zeng, Z., Chen, Y., Zhang, X., 2017. Modelling the interaction of a deep tillage tool with heterogeneous soil. Computers and Electronics in Agriculture 143, 130–138.

Zeng, Z., Chen, Y., 2018a. Performance evaluation of fluted coulters and rippled discs for vertical tillage. Soil & Tillage Research 183, 93–99.

Zeng, Z., Chen, Y., 2018b. The performance of a fluted coulter for vertical tillage as affected by working speed. Soil & Tillage Research 175, 112–118.

Zeng, Z., Chen, Y., 2019. Simulation of straw movement by discrete element modeling of straw-sweep-soil interaction. Biosystems Engineering, in press.

Zeng, Z., Chen, Y., Qi, L., 2019. Soil cutting by a compact disc harrow having various disc arrangements. Transactions of the ASABE, in press.

Chapter 2: General Literature Review

2.1. Soil-engaging tools

Soil-engaging tools are tools for field operations, such as tillage, seeding, residue incorporation, and fertilizer applications (Srivastava et al., 2006). Soil-engaging tools are mechanical devices that are designed to manipulate soil by applying forces to the soil. The soil manipulation includes, but is not limited to, soil cutting, loosening, pulverization, inversion, and translocation (McKyes, 1985). In the context of conservation tillage system, residue management became the necessary part of a field operation (Lal, 1997). Soil-engaging tools are required to have functions of residue cutting and incorporation (Chen et al., 2004). Soil manipulation and residue management together constitute a field operation in conservation tillage system. Therefore, the performance of soil-engaging tools is evaluated by the soil and residue condition changes after tillage. Also, energy consumption used to cause the changes is critical as well (Tabatabaeefar et al., 2009).

2.2. Soil-tool-residue interactions

In the past decades, soil-tool interaction research has been the main focus of the area of soil dynamics and machinery (Ani et al., 2018). As conservation tillage, where 30 to 100% of crop residue is left in the fields, has gained popularity, crop residue has become a critical component of the soil dynamic system (Chen et al., 2016). A soil-engaging tool working in conservation tillage fields forms a system of soil-tool-residue interactions. Specific interactions in the soil-tool-residue system include interactions between soil particles, soil and tool, residue and tool, residue particles, as well as soil and residue. Dynamic characteristics of the interactions mainly include contact forces (e.g.,

tool draft, vertical, and lateral forces), displacement (e.g., soil movement and residue incorporation), and size reduction (e.g., soil pulverization and residue cutting) (McKyes, 1985). The importance of gaining a comprehensive understanding of soil dynamics involved in the soil-tool-residue interactions system is twofold: (1) It forms the foundation of the discipline of soil dynamics; (2) It is a prerequisite for designing high-performance soil-engaging tools to attain desired dynamic characteristics.

2.2.1. Soil-tool interaction

A soil-tool interaction can be depicted as a system with inputs and outputs, in other words, variables and measurements (Gill and Vanden Berg, 1967). The variables are mainly initial soil conditions, tool configurations, and operating conditions. The measurements are primarily final soil conditions and tool response. The tool response includes forces, energy requirement, and wear. Therefore, the investigation of soil-tool interaction in tillage can be generalized as the study of how these variables affect soil- and tool-related measurements. The dependence among the variables significantly increased the complexity of the investigation. The effect of tool working speed depending on soil conditions is a good example when studying the affecting variables of the draft force. The draft force is widely known to have a quadratic relationship with the tool working speed (ASABE Standard D497.7, 2015). However, the draft-speed relationship depends on the soil moisture content in which the polynomial curve transforms from a concave shape to a convex shape as the moisture content increases (Stafford, 1979a). Furthermore, the dependence on moisture content responds in an opposite direction in the context of clay soil (Wang and Gee-Clough, 1993). The relationship between draft force and speed has been also reported as linear, parabolic, and exponential functions under

different experimental conditions (Onwualu and Watts, 1998). To the best of the author's knowledge, there is no well-established theory or robust model that could explain all these interactions. Despite the tremendous efforts that have been made to understand soil-tool interaction in tillage, the statement of 'Tillage (research) is more an art than a science.' made decades ago by Gill and Vanden Berg (1967) is still arguably valid to some extent.

2.2.2. Role of residue

In conservation tillage systems, soil-tool interactions are centred on crop residues. Residue conditions resulting from tillage operations have been documented more and more frequently. Raper (2002) compared the effects of implement type, tillage depth, and tillage timing on residue cover and burial, and concluded that the tillage depth was a critical operational parameter affecting the residue burial. Six different tillage methods were compared in terms of residue incorporation in a heavy clay soil and found that the tandem disc incorporated the highest amount of residue (Chen et al., 2004). Empirical equations were derived to estimate the residue cover resulting from a tillage operation based on initial surface residue, tool dimensions, and tool operational parameters (Gregory et al., 1982; Koohestani and Gregory, 1985). However, only a few studies focused on the dynamic motion of individual residue, which was attributed to its interaction with soil and tool. Also, in turn, how residue affected soil dynamics and tool performance are not fully understood at present. Flat residue and standing stubble of oat had different impacts on soil moisture content and the performance of seeding operation (Doan et al., 2005a, b). Tracers of soil and straw were used to characterize the soil and residue movement in three dimensions (Eltom et al., 2015a; Liu et al., 2010). For

example, straw movements of a straw-soil-rotary blade interaction were measured using straw tracers and showed that straw burial was correlated with straw vertical movement (Fang et al., 2016).

The role that residue plays in the soil-tool-residue interactions process is complex due to the heterogeneous nature of residue, non-uniform distribution in field, and non-linear behaviours. The significance of understanding the role of residue is to better predict dynamic attributes of soil behaviour and tool performance in field operations involving residues. The importance of the work is sufficient to warrant further investigation.

2.3. New tillage tools

New tillage tools including vertical tillage (VT) and compact disc harrow (CDH) have been proposed to create field condition that facilitates soil conservation against erosion, residue decomposition, and field operations in a cost-effective manner. The definitions of VT and CDH equipment have not been standardized and confusion exists regarding their marketing names (Kanichi, 2014), although various sources attempted to provide generic definitions (Chen et al., 2016). Some of the common characteristics of VT and CDH equipment include rotary soil-engaging tools (e.g., coulters, discs, rotary hoes, knives, and rollers) and higher working speeds (e.g., 12 to 20 km h^{-1}). The working speed of traditional tillage equipment, such as mouldboard plow and sweep cultivator, typically ranges between 5 and 11 km h^{-1} (ASABE Standard D497.7, 2015). However, a working speed of 20 km h^{-1} is common in today's tillage practice. As farm scales are becoming bigger, producers are consistently looking for tillage implement that can be operated at high speeds in order to increase field efficiency (the number of acres that can

12

be tilled per hour) without compromising tillage performance. The working speed is one of the most dominant variables that affect the dynamics attributes of tillage operation (Stafford, 1979a; Wheeler and Godwin, 1996). Soil-tool-residue interactions behaviours in the modern high-speed tillage differ significantly from that in the traditional tillage. Higher speeds typically increase the draft forces (forces required to pull the tools by tractor) and cause high soil movement (the translocation of soil in forward, lateral, and vertical directions), which is typically not desired in conservation tillage systems. This poses two questions to agricultural engineers: a) how to lower the draft forces of soil engaging tools to reduce the tractor power requirement; b) how to minimize the undesired soil movements in tillage operations. The key to answering the two questions is to understand the soil dynamics involved in the soil-tool-residue interactions system.

2.3.1. Vertical tillage

A VT tool is a soil-engaging tool that interacts with soil in a vertical plane perpendicular to the soil surface and along the travel direction. For example, a plain coulter as commonly seen in front of a subsoiler (Zhang et al., 2007) or planter (Fallahi and Raoufat, 2008) is a typical VT tool. The concept of VT was initially proposed in the 1990's by no-till farmers in the Midwest of USA in dealing with excessive corn residue, where the heavy residue layer resisted decomposition and adversely affected seeding operations, crop emergence, and yield. Although the concept has been there for about two decades, the adoption of VT worldwide only happened in recent years as witnessed by VT implement released from agricultural manufacturers all over the world (Kanichi, 2014). Very recently, the history, definitions, functions, current field evaluation, and measurement methods of VT were reviewed by Chen et al. (2016). The VT was designed

13

for residue management in two ways: a) cutting and sizing crop residues so that they do not plug the equipment in tillage and seeding operation; b) disturbing soil and mixing it with residue for faster decomposition. The performance of residue management can be evaluated by measuring the size of residue, residue cover, and residue incorporation using rulers, the rope method, and the soil core sampling method respectively. Effects of VT practice on agronomic and environmental aspects have been studied. Those studies focused on soil temperature and moisture content, crop emergence, plant stand, grain yield (Walther, 2017), crop disease and pathogens (Whitehair, 2014), and water quality in runoffs (Smith and Warnemuende-Pappas, 2015). The knowledge of soil-tool-residue interactions in VT is lacking and a solid understanding of the dynamic characteristics and affecting factors of VT is urgently needed to develop new VT machines and improve existing VT machines.

2.3.2. Compact disc harrow

The CDH is a European version of new tillage tool to deal with heavy residue in conservation tillage systems. CDH was originally from Western Europe in the 1990's and was recently introduced to North America. The main differences between CDH and conventional disc harrows are the machine configuration and tool geometry. A CDH typically consists of two parallel beams where the discs are individually mounted at a certain angle. The discs have a shallow concavity. These differences enabled CDH travelling at a higher speed (12 to 20 km h^{-1}) and reduced the tractor power requirement. For example, a commercial CDH required a 16% lower draft force and resulted in a smoother soil surface as compared with a conventional cultivator (Knechtges et al., 2010). The CDH usually has greater disc angles than VT, which means a greater level of

soil disturbance is expected for CDH. The draft and vertical forces of CDH were modelled as a function of disc angles and working depth by introducing pressure area of the disc (Kogut et al., 2016). Information on soil and residue behaviours of CDH is lacking in the literature.

2.4. Experimental studies

Experimental investigation of soil-tool-residue interactions came naturally to researchers as the first attempt to understand the soil dynamics. Experimental studies can be classified as laboratory and field studies. There are several advantages of laboratory soil bin experiments, including independence of weather (Barnes et al., 1960), precise setting of operation variables (Wegscheid and Myers, 1967), and better control of soil conditions (Stafford, 1979b). However, indoor soil bin conditions are not always the same as field conditions, in terms of crop residue and roots conditions. In addition, the soil in the soil bin that undergoes frequent tillage and compaction cycle may show different behaviours as compared with undisturbed soil in the field (Dexter and Bird, 2001). A sweep test was conducted in field and soil bin with similar residue condition and showed that the soil displacement in the field doubled that in the soil bin (Liu et al., 2007). Therefore, field tests are necessary for soil-engaging tools, which deal with crop residues, such as VT and CDH. Recently, a tillage tool testing platform was proposed by adapting a tool carrier and drive system of the indoor soil bin to field testing (Yang et al., 2016). The field testing platform combined some of the advantages of soil bin and tractor-based field tests and was reviewed in the section of field testing.

2.4.1. Soil bin testing

The attempt of using soil bin to study soil dynamics can be traced back to a century ago (Ademosun, 2014). The idea was to have a facility where one can test soil-engaging tools in a controlled environment on a year-round basis. Most often, soil bin tests were geared toward fundamental studies of soil dynamics. The historical background, concepts, past and present studies and future research direction of soil-machine interaction studies in soil bins were reviewed by Ani et al. (2018). A typical soil bin facility consists of several components, such as soil container, tool carriage, drive system, soil preparation equipment, and measuring instrumentation. Design of soil bins differs from one facility to another depending on design specifications, such as available space, operational parameter range, and tool performance of interest. Among the existing soil bins, most of them can travel at different speeds with a value up to 10 m s^{-1} (Rosa and Wulfsohn, 2008). Various types of soil container have been used, for example, adjustable width and length (Godwin et al., 1980), a circular soil container (Bobobee and Kumi, 2013), and multiple soil containers in parallel with different soil types (Gill, 1990). The system for driving the carriage could be a hydraulic power and an electric motor system (Onwualu and Watts, 1989) or a tractor in an outdoor soil bin (Manuwa et al., 2011). Most soil bins were equipped with a dynamometer to measure soil cutting forces (Mahadi et al., 2017); Each soil bin facility has unique features and has contributed to the understanding of soil dynamics in different aspects.

2.4.2. Field testing

Field tests have higher confidence in representing farming operations and true soil and residue conditions than soil bin tests. There are two different types of field testing:

full-scale machine-based tests and tool-based tests. Field tests of full-scale machines are usually conducted for prototyping purpose or field evaluation of existing machines. There have been numerous field tests of full-scale machines. For example, Chen et al. (2004) tested six full-scale tillage machines in a field to evaluate their performance, in terms of soil loosening and residue incorporation. Tool-based tests are conducted using smaller scale machines, for example, a field testing frame that pulled by a tractor or a field testing platform that moved along stationary rails. An instrumented field testing frame was designed to test various VT soil-engaging tools at high speeds up to 35 km h^{-1} (Sumanth et al., 2018). In the study of soil-machine interaction of traction, Upadhyaya et al. (1986) designed a mobile wheel traction testing device to conduct controlled field experiments of tires in situ. Similarly, a mobile tillage tool testing platform was developed to improve the controlling and repeatability of tillage tool field tests (Yang et al., 2016). The testing platform has been utilized to investigate the effect of trash board attachment on moldboard plough performance under different field straw conditions (Eltom et al., 2015a, b), as well as the effect of working depth and speed on double-disc furrow opener's soil cutting forces and straw cutting efficiency (Fiaz et al., 2015).

2.5. Modelling studies

Measurements of soil dynamic behaviours in the soil-tool-residue system are time consuming. Some of them, for example, soil particle movement, are difficult, if not impossible. Therefore, modelling approaches have been used to simulate soil dynamic behaviours. Generally speaking, the modelling methods can be grouped into analytical simulation and numerical simulation, where the latter group includes finite element

method (FEM), computational fluid dynamics (CFD), and discrete element method (DEM).

2.5.1. Analytical modelling

Analytical modelling describes the soil-tool-residue interactions system using a set of mathematical analytic functions, which are based on elastoplasticity or critical state soil mechanics, including proper constitutive relationships, yield criteria, and associated flow rules of plasticity. The Universal Earthmoving Equation, which was derived from the theory of passive earth pressure, is one example of analytical modelling methods, which has been used by many researchers (Hettiaratchi and Reece, 1967; McKyes and Ali, 1977; Godwin and Spoor, 1977). Results of analytical models explained some of the results of experimental studies. A good example is calculating the draft force of a simple blade either in two-dimension or three-dimension (Shen and Kushwaha, 1998). For a wide blade, a two-dimensional equation for calculating the soil resistance was developed based on the logarithmic spiral method of Terzaghi (1959) and has been widely used. In the case of a narrow blade where the edge effect of soil movement outside of the width of blade is significant, several three-dimensional soil cutting models were proposed to calculate the soil cutting forces based on different soil failure assumptions (e.g., Hettiaratchi and Reece, 1967; Godwin and Spoor, 1977; McKyes and Ali, 1977). However, researchers later found that the analytical method is challenged in incorporating some variables involved in the tillage operations, such as complex tool geometry and working speed, and also difficult to provide information on soil deformations and displacements, due to the simplified sol failure pattern.

18

2.5.2. Numerical modelling

Several numerical methods, including FEM, CFD, and DEM, have been used for modelling soil dynamic behaviours in agriculture. FEM can be used to investigate the failure zone, field of stress, soil deformation, and acting forces of soil-engaging tools in various soil conditions. The accuracy of FEM results highly depends on the constitutive law used for soil. Two constitutive models have been most popular for agricultural soil: a nonlinear elastic model (Chi and Kushwaha, 1989) and an elastic-plastic model (Drucker and Prager, 1952). FEM has been widely used to simulate soil-tool interaction. The late studies included predicting soil resistance on the tillage tools (e.g., Fielke, 1999; Gebregziabher et al., 2007; Topakci et al., 2010), soil failure patterns (Tagar et al., 2015), and interaction of tool with residue stubble (Li et al., 2017).

Karmakar and Kushwaha (2006) reviewed the available numerical simulation methods for tillage tool modelling and concluded that CFD was feasible to predict soil failure pattern and soil disturbance area. The pressure distribution on the plow surface was simulated using CFD to evaluate the relative wear of the tool at different working speeds and depths (Zhu et al., 2017). Although the success of FEM and CFD has been seen in some aspects of soil-machine interaction research, the two continuum numerical simulation methods failed to deal with soil and residue disturbances around a soil-engaging tool, which are discontinuous in nature.

The discrete element method (DEM) is an explicit numerical method of modelling dynamic behaviours of distinct particles moving independently. The domain of interest in a physical system is modelled as an assemblage of particles that interact at contacts. Certain contact laws govern the particle displacements and contact forces. Different

19

contact laws can be chosen to reflect the dynamic behaviour of the material to be

modelled. Using the DEM, dynamic behaviours of a system can be monitored at micro

levels of the individual particles and at macro levels of the bulk material. The DEM has

emerged from the infant stage to a rapidly developing stage and has the potential to

become a robust simulation tool in the field of soil dynamics. Therefore, the DEM is

chosen to simulate the soil-tool-residue interactions in this study. The DEM has been

successfully applied to soil-tool interactions in agriculture (e.g., van der Linde, 2007;

Mak et al., 2012; Chen et al., 2013). The major challenges of using DEM are to

determine the appropriate contact model and associated parameters for agricultural soils

so that the model reflects the behaviours of the soils. There were a few studies focused on

selecting appropriate contact models for agricultural soils (e.g., Momozu et al., 2002;

Ucgul et al., 2014a, b; Ucgul et al., 2015). There were many studies conducted to

calibrate model parameters. The sensitivity of model parameters on model behaviours has

been studied (Sadek and Chen, 2015; Keppler et al., 2016), providing information for

determining which model parameters should be calibrated. Numerous methods were used

for calibrations, e.g., analytical assumptions (Liao et al., 1997), trial-and-error method

(Tanaka et al., 2000), inverse solution technique (Franco et al., 2005), in-situ tests, and

optimization method (Asaf et al., 2007). Most existing models employed the contact

models implemented in DEM software. These contact models may not be the best for

modelling agricultural soils. For example, Sadek and Chen (2015) pointed out that their

discrete element model under predicted soil movement resulting from a blade, possibly

attributable to the contact model used. Inappropriate contact models could be one of the

reasons for discrepancies between simulations and measurements reported by many other

researchers. In summary, appropriate contact models and robust calibration methods need

to be developed. Also, many past DEM studies only investigated one parameter such as

draft and could not be calibrated for accurate draft, vertical and soil translocation all at

once. Furthermore, there is a lack of modelling soil-tool-residue interactions using the

DEM in the literature.

2.6. References

Ademosun, O.C., 2014. Soil tillage dynamics in Nigeria: potentials, prospects and challenges. In: Proceedings of the International Soil Tillage Research Organization (ISTRO) Nigeria Symposium. Akure, Nigeria. November 3–6.

Ani, O.A., Uzoejinwa, B.B., Ezeama, A.O., Onwualu, A.P., Ugwu, S.N., 2018. Overview of soil-machine interaction studies in soil bins. Soil & Tillage Research 175, 13–27.

ASABE Standards. 2015. D497.7 Agricultural Machinery Management Data. St. Joseph, Mich.: ASABE.

Asaf, Z., Rubinstein, D., Shmulevich, I., 2007. Determination of discrete element model parameters required for soil tillage. Soil & Tillage Research 92, 227–242.

Barnes, K.K., Bockhop, C.W., McLeod, H.E., 1960. Similitude studies of tillage implement forces. Agricultural Engineering 41(1), 32–37.

Bobobee, E.Y.H., Kumi, F., 2013. Development and performance evaluation of an abrasive wear testing equipment for tillage tools. Journal of Science and Technology 33(1), 55–67.

Chen, Y., Damphousse, S., Li, H., 2016. Vertical tillage and vertical seeding. Paper No. CSBE16-090. In: CSBE/SCGAB 2016 Annual Conference. Halifax, NS, Canada. July 3–6.

Chen, Y., Monero, F.V., Lobb, D., Tessier, S., Cavers, C., 2004. Effects of six tillage methods on residue incorporation and crop performance in a heavy clay soil. Transactions of the ASAE 47(4), 1003–1010.

Chen, Y., Munkholm, L.J., Nyord, T., 2013. A discrete element model for soil-sweep interaction in three different soils. Soil & Tillage Research 126, 34–41.

Chi, L., Kushwaha, R.L., 1989. Finite element analysis of forces on a plane soil blade. Canadian Agricultural engineering 31, 135–140.

Dexter, A., Bird, N.R.A., 2001. Methods for predicting the optimum and range of soil water contents for tillage based on the water retention curve. Soil & Tillage Research 57(4), 203–212.

Doan, V., Chen, Y., Irvine, B., 2005a. Effect of residue type on the performance on no-till drill openers. Canadian Biosystems Engineering 47(2), 29–35.

Doan, V., Chen, Y., Irvine, B., 2005b. Effect of oat stubble height on the performance of no-till drill openers. Canadian Biosystems Engineering 47(2), 37–44.

Drucker, D.C., Prager, W., 1952. Soil mechanics and plastic analysis or limit design. Quarterly of Applied Mathematics 10(2), 157–165.

Eltom, A.E.F., Ding, W., Ding, Q., Tagar, A.A., Talha, Z., Gamareldawla., 2015a. Field investigation of a trash-board, tillage depth and low speed effect on the displacement and burial of straw. Catena 133, 385–393.

Eltom, A.E.F., Ding, W., Ding, Q., Ali, A.B., Adam, A.E., 2015b. Effect of trash board on moldboard plough performance at low speed and under two straw conditions. Journal of Terramechanics 59, 27–34.

Fallahi, S., Raoufat, M.H., 2008. Row-crop planter attachments in a conservation tillage system: a comparative study. Soil & Tillage Research 98, 27–34.

Fang, H., Zhang, Q., Chandio, F.A., Guo, J., Sattar, A., Arslan, C., Ji, C., 2016. Effect of straw length and rotavator kinematic parameter on soil and straw movement by a rotary blade. Engineering in Agriculture, Environment and Food 9, 235–241.

Fiaz, A., Ding, W., Ding, Q., Mubshar, H., Khawar, J., 2015. Forces and straw cutting performance of double disc furrow opener in no-till paddy soil. PLOS ONE 10(3), e0119648.

Fielke, J.M., 1999. Finite element modelling of the interaction of the cutting edge of tillage implements with soil. Journal of Agricultural Engineering Research 74(1), 91–101.

Franco, Y., Rubinstein, D., Shmulevich, I., 2005. Determination of discrete element model parameters for soil-bulldozer blade interaction. In: Proceedings of the 15th international conference of the ISTVS, Hayama, Japan. September 25–29.

Gebregziabher, S., Mouazen, A.M., Brussel, H.V., Ramon, H., Meresa, F., Verplancke, H., Nyssenf, J., Behailuf, M., Deckersg, J., Baerdemaeker, J.D., 2007. Design of the Ethiopian ard plough using structural analysis validated with finite element analysis. Biosystems Engineering 97(1), 27–39.

Gill, W.R, Vanden Berg, G.E., 1967. Soil Dynamics in Tillage and Traction. Agriculture Handbook No. 316. United States Department of Agriculture.

Gill, W.R., 1990. A History of the USDA National Tillage Machinery Laboratory. Agricultural Research Service. United States Department of Agriculture.

Godwin, R.J., Spoor, G., 1977. Soil failure with narrow tines. Journal of Agricultural Engineering Research 22(4), 213–228.

Godwin, R. J., Spoor, G., Kilgour, J., 1980. The design and operation of a simple low-cost soil bin. Journal of Agricultural Engineering Research 25(1), 99–104.

Gregory, J.M., McCarty, T.M., Ghidey, F., Pfost, D.L., 1982. Tillage equation for residue management. Paper No. 82-1513. In: ASAE 1982 Annual Conference. Chicago, Illinois, USA. December 14–17.

Hettiaratchi, D.R.P., Reece, A.R., 1967. Symmetrical three-dimensional soil failure. Journal of Terramechanics 4(3), 45–67.

Kanicki, D., 2014. What is Vertical Tillage Anyway? Special Report: Vertical Tillage. http://www.farm-equipment.com/articles. Accessed 11 September 2018.

Karmakar, S., Kushwaha, R.L., 2006. Dynamic modelling of soil-tool interaction: an overview from a fluid flow perspective. Journal of Terramechanics 43, 411–425.

Keppler, I., Safranyik, F., Oldal, I., 2016. Shear test as calibration experiment for DEM simulation: a sensitivity study. Engineering Computations 33(3), 742–758.

Knechtges, H.J., Koch, F., Meyer, T., Scheit, S., 2010. Comparison of stubble working with cultivator or compact disc harrow. Landtechnik 65, 51–53.

Kogut, Z., Sergiel, L., Zurek, G., 2016. The effect of the disc setup angles and working depth on disc harrow working resistance. Biosystems Engineering 151, 328–337.

Koohestani, M., Gregory, J.M., 1985. Measurement of tillage parameters that affect residue cover. Paper No. 85-2045. In: ASAE 1985 Annual Conference.

Lal, R., 1997. Residue management, conservation tillage and soil restoration for mitigating greenhouse effect by CO2-enrichment. Soil & Tillage Research 43, 81–107.

Li, M., Xu, S., Yang, Y., Guo, L., Tong, J., 2017. A 3D simulation model of corn stubble cutting using finite element method. Soil & Tillage Research 166, 43–51.

Liao, C.L., Chang, T.P., Young, D.H., 1997. Stress strain relationship for granular materials based on the hypothesis of best fit. International Journal of Solids and Structures 34(31–32), 4087–4100.

Liu, J., Chen, Y., Lobb, D.A., Kushwaha, R.L., 2007. Soil-straw-tillage tool interaction: field and soil bin study. Canadian Biosystems Engineering 49, 2.1–2.6.

Liu, J., Chen, Y., Kushwaha, R.L., 2010. Effect of tillage speed and straw length on soil and straw movement by a sweep. Soil & Tillage Research 109, 9–17.

Mahadi, M.R., Chen, Y., Botha, P., 2017. Instrumented soil bin for testing soil-engaging tools. Applied Engineering in Agriculture 33(3), 357–366.

Mak, J., Chen, Y., Sadek, M.A., 2012. Determining parameters of a discrete element model for soil-tool interaction. Soil & Tillage Research 118, 117–122.

Manuwa, S.I., Ademosun, O.C., Agbetoye, L.A.S., Adesina, A., 2011. Development of outdoor soil bin facility for soil tillage dynamics research. Journal of Agricultural Engineering and Technology 19, 1–8.

McKyes, E., 1985. Soil Cutting and Tillage. New York, NY. Elsevier.

McKyes, E., Ali, O.S., 1977. The cutting of soil by narrow blades. Journal of Terramechanics 14(2), 43–58.

Momozu, M., Oida, A., Yamazaki, M., Koolen, A.J., 2002. Simulation of soil loosening process by means of the modified distinct element method. Journal of Terramechanics 39(4), 207–220.

Onwualu, A.P., Watts, K.C., 1989. Development of soil bin test facility. Paper No. 89-1106. In: ASAE 1989 Annual Conference. New Orleans, Louisiana, USA.

Onwualu, A., Watts, K., 1998. Draft force and vertical forces obtained from dynamic soil cutting by plane tillage tools. Soil & Tillage Research 48, 239–253.

Raper, R., 2002. The influence of implement type, tillage depth, and tillage timing on residue burial. Transactions of the ASAE 45, 1281–1286.

Rosa, U.A., Wulfsohn, D., 2008. Soil bin monorail for high speed testing of narrow tillage tools. Biosystems Engineering 99(3), 444–454.

Sadek, M.A., Chen, Y., 2015. Feasibility of using PFC3D to simulate soil flow resulting from a simple soil-engaging tool. Transactions of the ASABE 58(4), 987–996.

Shen, J., Kushwaha, R.L., 1998. Soil-Machine Interactions. Marcel Dekker Inc., New York.

Smith, D.R., Warnemuende-Pappas, E.A., 2015. Vertical tillage impacts on water quality derived from rainfall simulations. Soil & Tillage Research 153, 155–160.

Stafford, J.V., 1979a. The performance of rigid tine in relation to soil properties and speed. Journal of Agricultural Engineering Research 24(1), 41–56.

Stafford, J.V. 1979b. A versatile high-speed soil tank for studying soil and implement interaction. Journal of Agricultural Engineering Research 24(1), 57–66.

Srivastava, S. K., Goering, C. E., Rohrbach, R. P., Buckmaster, D. R., 2006. Engineering Principles of Agricultural Machines, 2nd Edition. St. Joseph, MI: ASABE.

Sumanth, K., Chen, Y., Peng, Q., 2018. Development of a field testing unit for vertical
    tillage and seeding. Paper No. 1801237. In: ASABE 2018 Annual Conference.
    Detroit, Michigan, USA. July 29–August 1.

Tabatabaeefar, A., Emamzadeh, H., Ghasemi Varnamkhasti, M., Rahimizadeh, R.,
    Karimi, M., 2009. Comparison of energy of tillage systems in wheat production.
    Energy 34, 41–45.

Tagar, A.A., Ji, C., Adamowski, J., Malard, J., Chen, S., Ding, Q., Abbasi, N.A., 2015.
    Finite element simulation of soil failure patterns under soil bin and field testing
    conditions. Soil & Tillage Research 145, 157–170.

Tanaka, H., Momozo, M., Oida, A., Yamazaki, M., 2000. Simulation of soil deformation
    and resistance at bar penetration by distinct element method. Journal of
    Terramechanics 37, 41–56.

Topakci, M., Celik, H.K., Canakci, M., Rennie, A.E.W., Akinci, I., Karayel, D., 2010.
    Deep tillage tool optimization by means of finite element method: case study for a
    subsoiler tine. Journal of Food Agriculture and Environment 8(2), 531–536.

Terzaghi, K., 1959. Theoretical Soil Mechanics. Wiley & Sons Inc., New York.

Ucgul, M., Fielke, J.M., Saunders, C., 2014a. 3D DEM tillage simulation: validation of a
    hysteretic spring (plastic) contact model for a sweep tool operating in a
    cohesionless soil. Soil & Tillage Research 144, 220–227.

Ucgul, M., Fielke, J.M., Saunders, C., 2014b. Three-dimensional dicrete element
    modelling of tillage: determination of a suitable contact model and parameters for
    a cohesionless soil. Biosystems Engineering 121, 105–117.

Ucgul, M., Fielke, J.M., Saunders, C., 2015. Three-dimensional discrete element modelling (DEM) of tillage: accounting for soil cohesion and adhesion. Biosystems Engineering 129, 298–306.

Upadhyaya, S.K., Mehlschau, J., Wulfsohn, D., Glancey, J.L., 1986. Development of a unique, mobile, single wheel traction testing machine. Transactions of the ASAE 29(5), 1243–1246.

van der Linde, J., 2007. Discrete Element Modelling of a Vibratory Subsoiler. M.Sc. Thesis, University of Stellenbosch, Matieland, South Africa.

Walther, P.A., 2017. Corn Residue Management for Soybean Production: On-Farm Experiment. M.Sc. Thesis, University of Manitoba, Winnipeg, Manitoba, Canada.

Wang, J., Gee-Clough, D., 1993. Deformation and failure in wet clay soil, Part 2: Soil bin experiments. Journal of Agricultural Engineering Research 54(1), 57–66.

Wegscheid, E.L., Myers, H.A., 1967. Soil bin instrumentation. Agricultural Engineering 48(8), 442–445.

Wheeler, P.N., Godwin, R.J., 1996. Soil dynamics of single and multiple tines at speeds up to 20 km/h. Journal of Agricultural Engineering Research 63, 243–250.

Whitehair, A., 2014. Vertical Tillage Effects on Yield, Disease and Pathogens, and Soil Properties. M.Sc. Thesis, Kansas State University, Manhattan, Kansas, USA.

Yang, Y., Ding, Q., Ding, W., Xue, J., Qiu, W., He, R., 2016. Design and application of multipurpose in-situ tillage tool testing platform. Transactions of the Chinese Society for Agricultural Machinery 47(1), 68–74.

Zhang, J.G., Raper, R.L., Balkcom, K.S., Arriaga, F.J., Kornecki, T.S., Schwab, E.B., 2007. Drawbar power requirements and soil disruption of in-row subsoiler points for conservation tillage. In: Proceeding of the 2007 Southern Conservation Agricultural System Conference 214–222.

Zhu, L., Ge, J., Cheng, X., Peng, S., Qi, Y., Zhang, S., Zhu, D., 2017. Modelling of share/soil interaction of a horizontally reversible plow using computational fluid dynamics. Journal of Terramechanics 72, 1–8.

Chapter 3: Performance Evaluation of Fluted Coulters and Rippled Discs for Vertical Tillage *

3.1. Abstract

Vertical tillage (VT) is the latest form of conservation tillage dealing with excessive residue. Information on the performance of VT equipment is lacking in the literature. In this study, five VT tools were tested in a corn stubble field to compare their performance. They were two coulters with 8 flutes (C8) and 13 flutes (C13), and three rippled discs with different diameters: 457 mm (D457), 508 mm (D508), and 559 mm (D559). All the five tools were tested at a working speed of 16 km h^{-1} and tillage depth of 100 mm. The results showed that increasing disc diameter from 457 to 559 mm resulted in significantly increased residue incorporation (44%), soil opening width (30%), soil disturbance area (127%), and lateral cutting force (79%), as well as decreased residue cover (5%). Increasing the number of flutes from 8 to 13 resulted in significantly lower soil sticking (39%) and soil opening width (29%), but a significantly higher residue cover (7%). Overall, the fluted coulters performed more aggressively than the rippled discs in disturbing soil and incorporating residue, and had a higher draft force and a higher soil sticking. Among all the tools, the D457 conserved the most amount of residue on the soil surface and disturbed the least amount of soil, whereas the C8 was the most intensive VT tool in these regards. The D559 had the highest soil loosening efficiency, defined as the soil loosening area divided by the draft force.

3.2. Introduction

Conservation tillage has received tremendous attention in most of the agricultural systems as it improves soil quality (Madejon et al., 2009; He et al., 2011), increases crop yields (de Vita et al., 2007; Naudin et al., 2010), controls soil erosion (Prasuhn, 2012), and reduces production cost (Tullberg et al., 2007). However, excessive residue in the conservation tillage systems is detrimental to seeding operation, seed germination, and early plant growth. Other than equipping planters with various coulters as leading tools to cut residues (Erbach, 1981; Raoufat and Mahmoodieh, 2005), agricultural producers have been seeking alternative conservation tillage systems to alleviate the problems of excessive residue. Vertical tillage (VT) was proposed as an alternative conservation tillage that cuts residue aggressively to improve seeding conditions while protecting soil and the environment. Although many agricultural machinery manufacturers, e.g., John Deere (Moline, Illinois, USA) and Great Plains (Salina, Kansas, USA), have released their VT machines, performance of those machines has not been well documented. Some studies on VT have been recently reported in the literature, and most of them concerned about the effects of VT equipment on agronomic and environmental aspects such as soil temperature and moisture content (Langseth and Daigh, 2016), crop emergence, plant stand, grain yield (Walther, 2017), and water quality in runoffs (Smith and Warnemuende-Pappas, 2015). In a recent study, the resultant soil and residue conditions of fluted coulters for VT were examined (Zeng and Chen, 2018). No other literature has been found on evaluations of VT tools in terms of engineering aspects, such as soil cutting forces and soil disturbance.

The common soil-engaging tools of VT equipment are various rotary tools, such as coulters and concave discs (Chen et al., 2016). Each rotary tool can be characterized by its diameter and edge shapes such as plain, notched, bubble, and rippled (ASABE Standard S477.1, 2013). The concave discs with different concavities and edge shapes are the major soil-engaging tools of disc tillage implements, such as disk harrow and disk plow (ASABE standard S414.2, 2009). The coulters with different edge shapes, such as bubble and fluted coulters, are typically found in seeding machines of conservation tillage systems as soil and residue cutting components (ASABE standard S477.1, 2013). The concave discs for tillage purposes are usually operated at a gang angle, while the coulters are set at a zero gang angle. Those rotary tools were widely adopted in VT equipment to size crop residue and shatter soil in the top layer. The intention is to create a field condition that facilitates seeding operation, residue decomposition, soil conservation, crop growth, and other field operations in a cost-effective manner.

With the focus of dealing with excessive residue, several indicators including residue cover, incorporated residue, and size of residue have been suggested to assess the performance of VT soil-engaging tools (Chen et al., 2016). The residue cutting capacity of various rotary blades has been extensively studied. In general, the use of rotary blades significantly decreased the residue cover (Raoufat and Mahmoodieh, 2005). Resultant residue conditions depend on the type and shape of the tool as well as the field conditions. The amount of residue cut by plain coulters was inversely proportional to residue density and proportional to working depth (Kushwaha et al., 1986). The coulter sharpness was an important parameter affecting cornstalk residue shearing, where the amount of sheared residue increased with the increases in coulter sharpness (Choi and

33

Erbach., 1986). The smooth and rippled coulters worked superiorly to notched coulters in terms of cutting residue (Karll et al., 1978). Meanwhile, a comparative soil bin test between a toothed, notched, and smooth coulter on sugar cane residue found that the toothed coulter cut the most amount of residue with lowest energy requirements (Bianchini and Magalhaes, 2008). These existing studies were for traditional tillage and seeding, not for VT involving high-speed operations.

The performance of rotary tools is affected by several geometrical and operational parameters of the tools, as well as soil and residue conditions. A comprehensive investigation on the performance of different coulters in a residue-free field indicated that coulter shape and style had no significant effect on draft and vertical forces, but influenced furrow formation and the level of soil disturbance (Schaaf et al., 1980). Soil dynamics of a single rotary blade is sensitive to blade diameter (Kushwaha et al., 1986), wedge tip curvature (Choi and Erbach, 1986), blade thickness (Tice and Hendrick, 1992), disc angle and rotational speed (Salokhe and Quang, 1995). Although an empirical power model explained the variation of coulter forces with the cutting depth (Tice and Hendrick, 1991), none of these soil and coulter geometrical parameters were considered in the model. An investigation of the interaction among discs in a gang found that the interaction had a stronger effect on the draft force than the vertical force (Chapman et al., 1988). Most of the existing studies focused on plain rotary blades working at low speeds in conventional tillage systems. However, the tillage performance of a fluted coulter was significantly affected by high working speeds ranging from 12 to 20 km h^{-1} (Zeng and Chen, 2018).

In summary, the information on tillage performance and its affecting factors of VT soil-engaging tools are lacking in assessing this new conservation tillage practice. The objective was to evaluate the performance of five typical VT soil-engaging tools in terms of soil cutting forces, as well as soil and residue conditions.

3.3. Material and methods

3.3.1. Site description

A field experiment of fall tillage was conducted in the fall of 2016 at a research farm in Portage la Prairie, Manitoba, Canada. A corn stubble field with corn stover being chopped and evenly spread over was used for the experiment. The field had a silty clay soil (43% clay, 48% silt, and 9% sand) within normal tillage depth. Soil moisture content and bulk density were measured using the core sampling method. Soil shear strength and penetration resistance were measured using a Vane Shear Meter (Geovane, New Zealand) and a Pocket Penetrometer (Geotester, Italy), respectively. Residue cover and density were measured using the image thresholding method and the quadrat sampling method, respectively. Details regarding those measurements can be found in Zeng and Chen (2018). Initial soil and residue conditions are summarized in Table 3.1.

Table 3.1. Initial soil and residue conditions

Measurement		Unit	Value
Soil	Moisture content	%	35.7 ± 2.4
	Dry bulk density	kg m^{-3}	1325.2 ± 62.8
	Penetration resistance	kPa	367.8 ± 114.6
	Shear strength	kPa	72.0 ± 23.1
Residue	Cover percentage	%	98.1 ± 0.8
	Standing density	kg ha^{-1}	1853.8 ± 462.1
	Flat density	kg ha^{-1}	7375.6 ± 3326.1

3.3.2. Description of the VT tools

The VT soil-engaging tools tested were two fluted coulters and three rippled discs (Fig. 3.1a). The two fluted coulters had the same diameter (559 mm), but one had 8 flutes and the other had 13 flutes. The flutes of the coulters formed a wavy circumference that was designed to enhance lateral soil shattering. The rippled discs had different diameters, i.e., 559 mm (22 in), 508 mm (20 in), 457 mm (18 in), but they all had 25 ripples and 25 "saw teeth". The saw tooth edge was designed to aggressively cut crop residue and self-sharpening. For the purpose of data interpretation, some common geometrical parameters were defined for the coulters and discs (Fig. 3.1b). The terms, flute and ripple were interchanged with wave. The working width of the coulters was the overall width of the waves along the circumference. The working width of the discs was the concavity. The wave radial length was the length of the wave along the tool radius. These geometrical parameters are independent of working conditions. The following parameters depend on the working depth. The cutting angle was the angle between the circular cutting edge of

36

the tool and the soil surface. The number of engaging waves was the equivalent number of waves working in the soil at any moment. The pressure area was the surface area of the tool below the soil surface projected onto a vertical plane perpendicular to the travel direction. The soil trapping volume was the volume confined by the soil surface, tool surface and an imaginary vertical plane parallel to the travel direction. Given a specific working depth of 100 mm, the values of these parameters were calculated and listed in Table 3.2.

In field tests, a single tool was mounted on a toolbar through a coiled shank (Fig. 3.1c). The shank was attached to a testing frame through a dynamometer. Two gauge wheels of the frame controlled the tillage depth. The frame was pulled by a tractor through a three-point hitch.

(a)

(b)

(c)
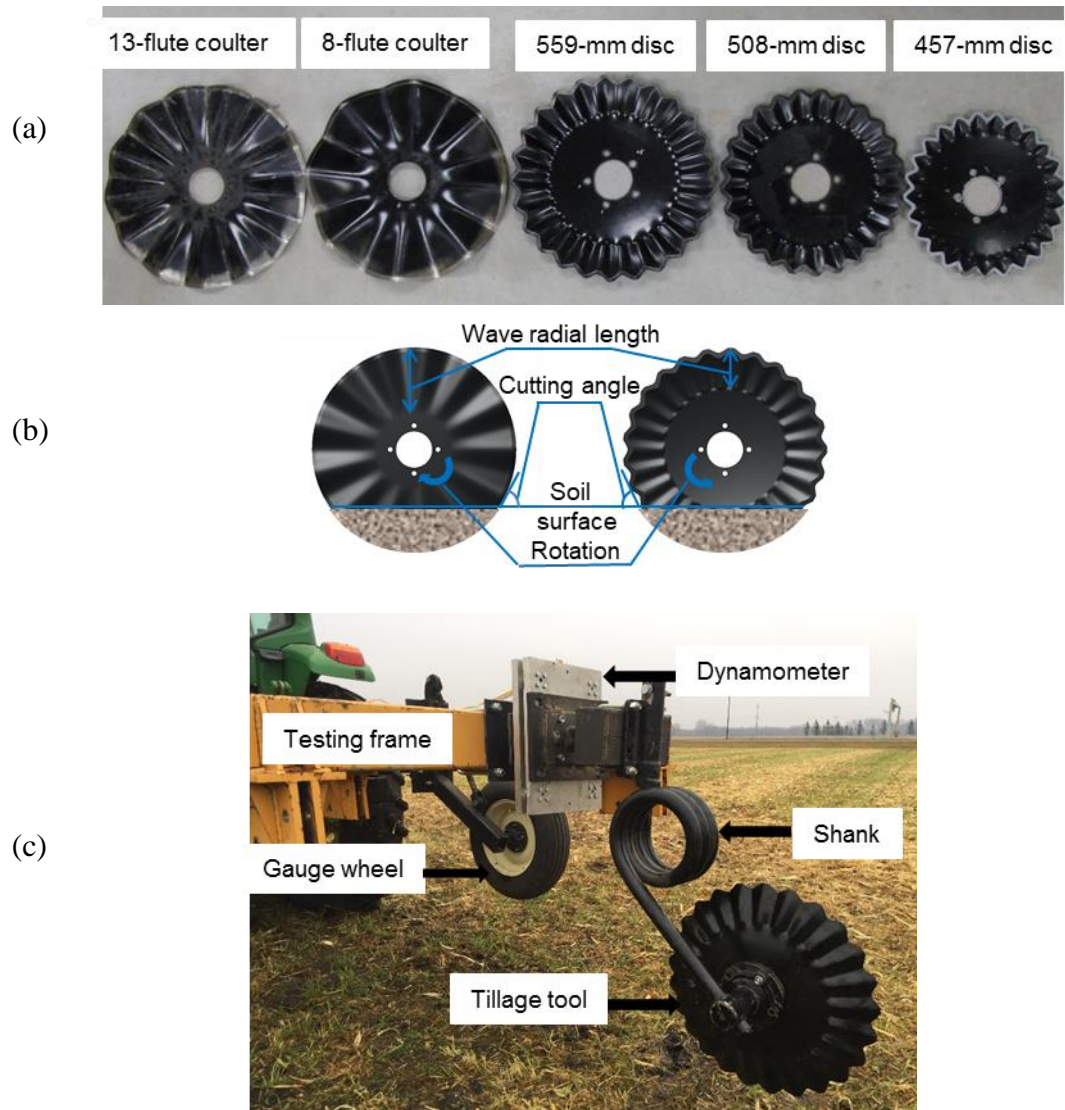
Figure 3.1. Five tillage tools tested (a) and some common tool geometrical parameters (b); a field testing unit (c).

Table 3.2. Summary of principal geometrical parameters of the tools

Term	13-flute coulter	8-flute coulter	559-mm disc	508-mm disc	457-mm disc
Working width, mm	44.5	63.5	55.0	45.0	35.0
Wave radial length, mm	180	180	100	75	50
Cutting angle[*], °	50.1	50.1	50.1	52.7	55.8
Engaging waves[*]	3.61	2.22	6.95	7.32	7.75
Pressure area[*], mm^2	3660	5220	984	885	765
Trapping volume[*], mm^3	1480000	2140000	141000	119000	96400

[*] Values were calculated at a working depth of 100 mm.

3.3.3. Experimental design

A completely randomized design was used for the experiment. Treatments were five different tools: the 8-flute coulter (C8), 13-flute coulter (C13), and 559 mm (D559), 508 mm (D508), 457 mm (D457) rippled discs. Each treatment was replicated five times. Thus, a total of 25 field plots were used in the experiment. The plots were 3 m wide to accommodate one pass of the tractor. The plots were 30 m long and laid out perpendicular to the previous crop rows. The working speed and the cutting depth of the tools were set at 16 km h^{-1} and 100 mm respectively for all the treatments. There were buffer areas at two ends of the field for tractor acceleration and deceleration to ensure a constant working condition within the 30 m plots.

3.3.4. Measurements

All the measurements were conducted at three random locations in each plot, unless specified otherwise.

3.3.4.1. Soil cutting forces

The force data was measured by the dynamometer as shown in Fig. 3.1c. As the tillage tool travelled in the soil, force signals were recorded by a data acquisition system at 65 Hz. The data were then retrieved to calculate the soil cutting forces including draft (F_D), lateral (F_L), and vertical (F_V) forces. Each force reported was the average value of data curves recorded for the 30-m long plots.

3.3.4.2. Residue cover and incorporation

Following the tillage, a 1x1 m quadrat was placed on the ground and centred with the path of the tillage tool to confine the area for residue cover (R_C) measurement. A camera was mounted on a tripod facing toward the quadrat and took the image of soil surface including the quadrat (Fig. 3.2a). Images (Fig. 3.2b) were analyzed in MATLAB using the image thresholding method to determine the percentage of the corn residue on the soil surface (Chen et al., 2004).

The surface residue was manually removed after residue cover measurement. A large core sampler with an inner diameter of 140 mm was pushed into the furrow to a depth of 100 mm (Fig. 3.2c). The core sampler was then carefully dug out. Fresh residue in the sample was manually extracted. Extracted residues were oven-dried at 55°C for 72 hours (ASABE Standard S358.3, 2012) and weighed to determine the dry mass of the residue incorporated (R_I).

(a)	(b)
	(c)
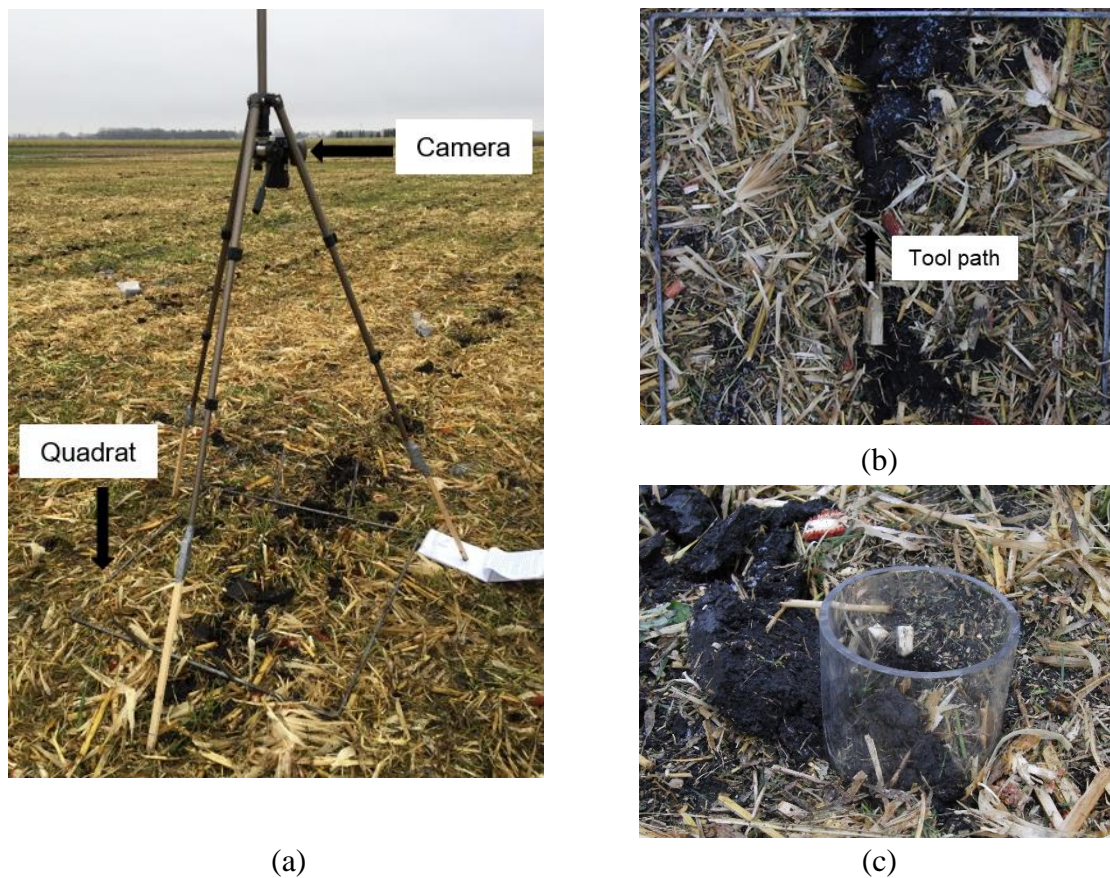
Figure 3.2. Residue-related measurements: camera setup (a); a soil surface image confined by a 1 x 1 m quadrat after tillage (b); and soil core sampling for residue incorporation measurement (c).

3.3.4.3. Furrow profile

Loosened soil was removed from the tool path to expose the tillage furrow. A soil profiler was made by confining skewers between two transparent plastic plates using two clamps (Fig. 3.3a). The skewers were marked at the same height. Then, the soil profiler was placed across the furrow and the skewers slid down until their bottom tips being in contact with the furrow surface. The soil furrow profile reflected by the height of the skewers was digitalized in a camera. The furrow profile was then characterized by soil opening width (S_W), soil cutting depth (S_D), and soil disturbance area (S_A) (Fig. 3.3b).

(a)   (b)
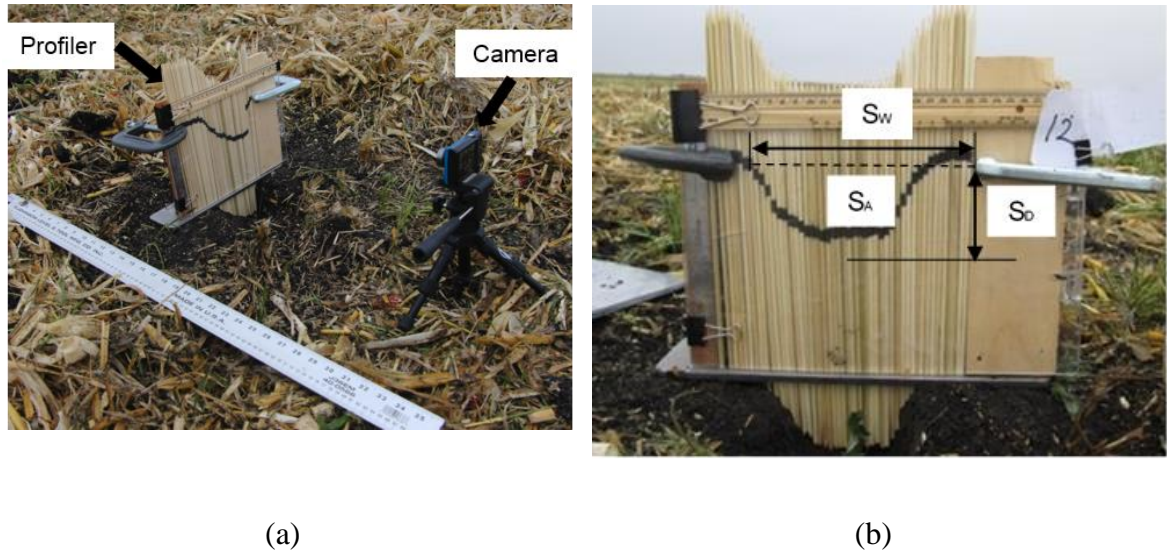
Figure 3.3. A soil furrow profiler (a) for measuring furrow characteristics including soil opening width (S_W), soil cutting depth (S_D), and soil disturbance area (S_A) (b).

3.3.4.4. Soil sticking

At the completion of the test run of a plot, the tillage tool was gently lifted above the ground. The soil (contained some residue) stuck on the tool were scraped, collected, oven-dried at 55°C for 72 hours, and weighed. The dry mass of the soil was named as soil sticking (S_S). There was only one measurement of S_S in each plot.

3.3.5. Data analysis

Analysis of variance (ANOVA) was performed using statistical software (SAS for Windows v 9.4). The means between five treatments were compared with Duncan's multiple range tests at the significance level of 0.05. The averages of the two different groups of tools, i.e., the disc and coulter, were also compared with T-test at the significance level of 0.05. The effects of treatments were examined.

42

3.4. Results

While the tillage performance indicators were compared between the five different tools, the results were also compared between the type of two coulters and the type of three discs as well as within a type. Thus, the outcomes would be useful not only to determine which of the five tools, as general VT tools, was ideal for a certain function, but also to determine which type of tools was advantageous or disadvantageous over the other group for certain tasks, and which tool within a type overperformed or underperformed the other tools. Therefore, in the following sections, data interpretations were made among all the five tools and between the two types, as well as among each type.

3.4.1. Soil cutting forces

The draft force (F_D) required by a single tillage tool ranged from 345 to 809 N. The D457 had the minimum draft force and C8 had the maximum draft force, which was significantly different. The F_D did not differ statistically among the same type of tools, but differed between two tool types. In general, the coulters required a 73% higher F_D than the discs on average. The F_D of C8 was 30.4% higher than that of C13. The D457 experienced a 26% lower F_D than D559. The difference in vertical force (F_V) was significant only between C13 and D559. The other three tillage tools had similar F_V. Further statistical tests revealed that the average F_V of the coulter did not significantly differ from that of the disc. The lateral force (F_L) were significantly different among the tools, especially between two tool types. The discs had an average F_L of 356.7 N, which was 6.9 times larger than the coulters. Also, the F_L of the discs was of the same order of magnitude than the corresponding F_D mainly due to their concavities. The two coulters

43

had almost identical F_V (4.5% in difference). D457 had the smallest F_V among the discs, which was 31.2% and 44.2% less than D508 and D559 respectively.

Table 3.3. Soil cutting forces (in N) of different tillage tools

Forces / *Tools	Draft (F_D)	Vertical (F_V)	Lateral (F_L)
C13	620.2 ± 134.9^{ab}	176.0 ± 50.2^{b}	53.2 ± 32.9^{c}
C8	809.0 ± 232.9^{a}	218.6 ± 42.9^{ab}	50.8 ± 34.8^{c}
D559	464.0 ± 157.4^{bc}	297.2 ± 116.5^{a}	451.8 ± 108.1^{a}
D508	430.0 ± 95.7^{bc}	259.2 ± 63.5^{ab}	366.2 ± 93.2^{a}
D457	345.0 ± 82.4^{c}	232.4 ± 96.6^{ab}	252.0 ± 104.9^{b}

Means within a column followed by the same letters are not significantly different according to Duncan's multiple range test at the significance level of 0.05.

* C13: 13-flute coulter; C8: 8-flute coulter; D559: 559 mm disc; D508: 508 mm disc, D457: 457 mm disc.

3.4.2. Residue cover and incorporation

The measured residue cover (R_C) differed significantly among the tools (Fig. 3.4a). The C8 had the lowest R_C (74.9%) among all tools. The discs had an average residue remained of 84.9%, which was significantly higher than an average R_C of 77.6% for the coulters. Between the two coulters, C13 left more residue of 5.3% on the ground than C8. For the discs, two smaller discs had more residue left than D559. Those differences were found to be significant, whereas the difference in R_C between D508 and D457 was not significant.

The residue incorporated into the soil (R_I) was significantly affected by tool type (Fig. 3.4b). The coulters mixed 10.4 g of residue on average, which was significantly higher than an average R_I of 7.8 g for the discs based on the T-test result (not shown in Fig. 3.4b). The C8 had the maximum R_I of 10.6 g and was statistically equal to that of

C13. The D559 had an R_I of 9.2 g, which was 19.5% and 43.8% significantly higher than D508 and D457 respectively.

<center>(a)</center>
<center>(b)</center>
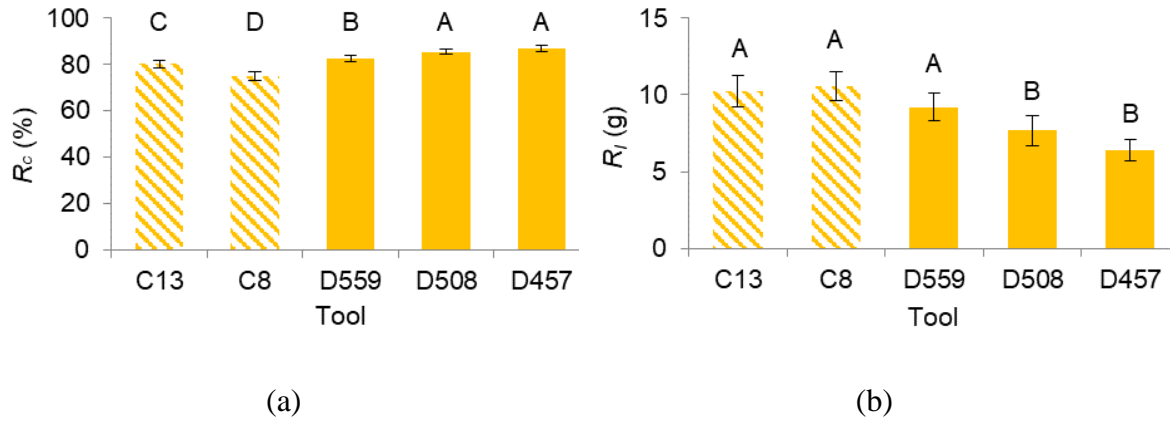
Figure 3.4. Residue measurements of different tillage tools (C13: 13-flute coulter; C8: 8-flute coulter; D559: 559 mm disc; D508: 508 mm disc, D457: 457 mm disc): (a) residue cover (R_C) and (b) residue incorporated (R_I). Means followed by different letters are significantly different according to Duncan's multiple range test at the significance level of 0.05; error bars are standard deviations.

3.4.3. Soil sticking

The soil stuck (S_S) on the coulters was primarily soil clods with some small pieces of the corn stalk. No big chunks of soil sticking were observed on the discs in the experiment. The C8 had the most S_S of 163 g, which was 64.6% higher than that of C13 and more than six times higher than any of the discs. The coulters showed a significantly higher capacity to hold soil with an average S_S of 131 g, as compared with 15.8 g average S_S of the discs.
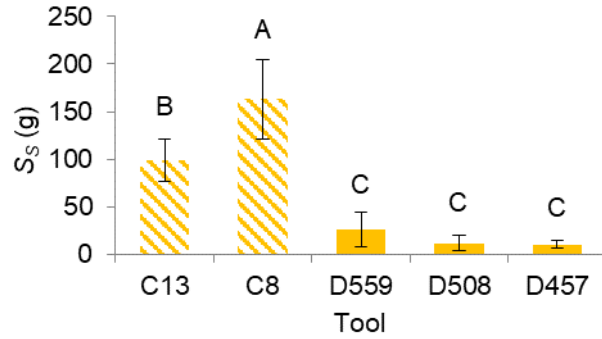
Figure 3.5. Soil sticking (S_S) on different tillage tools (C13: 13-flute coulter; C8: 8-flute coulter; D559: 559 mm disc; D508: 508 mm disc, D457: 457 disc); means followed by different letters are significantly different according to Duncan's multiple range test at the significance level of 0.05; error bars are standard deviations.

3.4.4. Furrow profile

No significant differences were found between the soil cutting depth (S_D) of different tillage tools (Fig. 3.6a). The average S_D of all tillage tools was 98 mm, which was close to the target depth (100 mm). The average S_D of the coulters (96.7 mm) was slightly smaller than that of the discs (98.9 mm). The C8 had the widest soil opening (S_W) (179.8 mm), which was significantly higher than that of C13 (127.3 mm) (Fig. 3.6b). The D559 had a similar S_W to C13 and that was significantly higher than both D508 and D457. For the soil disturbance area (S_A), C8 had an 11.1% higher value than C13, which was not significant. The D559 disturbed a 49.7% and 61.7% significantly larger area than D508 and D457 respectively. Comparing the average S_A, the coulters had a 55.6% greater value than the discs.
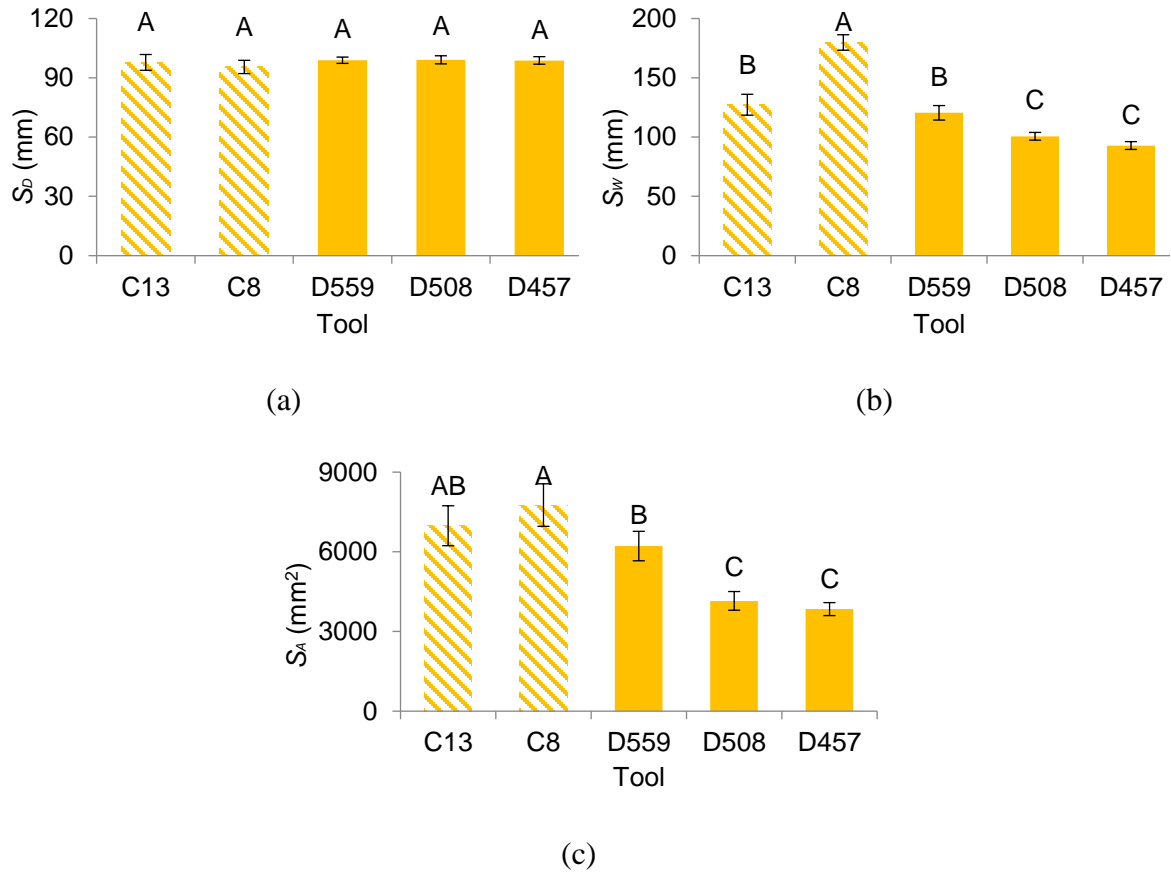
Figure 3.6. Furrow profile characteristics of different tillage tools (C13: 13-flute coulter; C8: 8-flute coulter; D559: 559 mm disc; D508: 508 mm disc, D457: 457 mm disc): (a) soil cutting depth (S_D); (b) soil opening width (S_W); and (c) soil disturbance area (S_A). Means followed by different letters are significantly different according to Duncan's multiple range test at the significance level of 0.05; error bars are standard deviations.

3.5. Discussions

While not all of the tillage performance indicators were significantly different among the five tools, the overall direction of the results showed that it is feasible to achieve desired tillage performance by selecting different tillage tools for VT. The variations on the performance indicators between the two different tool types were larger than that within each type. The fluted coulters performed more aggressively than the

rippled discs in disturbing soil and residue with a tendency to allow soil build-up on the tool surface. The differences within the coulters and discs can be attributed to the different number of wave and disc diameter respectively, which are related to the geometrical parameters of the tools listed in Table 3.2.

The direct proportional relationships between the disc diameter and soil cutting forces agreed with previous studies (Magalhaes et al., 2007; Choi and Erback, 1986; Kushwaha et al., 1986). The coulters were expected to have a zero lateral force due to their symmetric geometry. However, they experienced none zero lateral forces, which might be resulted from the offset position of the coil shank. The lateral force of the discs had three sources including (a) soil lateral throwing from the concave side, (b) soil cutting resistance acting on the forward convex face, and (c) scrubbing action between furrow wall and the backward convex face (Chapman et al., 1988). The first source pointed from the concave side to the convex side, while the latter two were in an opposite direction. Measured lateral forces of the discs were all in the latter direction, which was expected as the discs were operated at a zero gang angle and thus had large convex surface areas.

It was interesting to note that on average the coulter had a 25% lower vertical force and a 73% higher draft force than the disc with similar working width and depth. The vertical force indicated the machine weight that was required to maintain a specified cutting depth. Tools which have higher draft forces also have higher vertical forces as shown in previous studies (e.g., Murray, 2016). However, this was not the case in this study due possibly to the geometrical differences between the coulters and discs. The concavity of the discs contributed greatly to the vertical force while the wider waves of

48

the coulters resulted in larger draft forces. The draft force was associated with the pressure area. Generally speaking, the larger the area is, the bigger the resistance. This explained the higher draft forces of the discs as compared with the coulters.

Given the sampling area, the average amount of 10.4 g residue incorporated by the coulters was equivalent to an amount of 6759.4 kg ha^{-1} residue, which accounted for more than 70% of the residue mass on the soil surface, 9229.4 kg ha^{-1}, prior to the tillage. This implied that the coulters were effective in mixing the surface residue. The average residue incorporated by the discs was 5069.5 kg ha^{-1}, which was significantly lower than that of a tandem disc working at a 16-degree gang angle (Chen et al., 2004). The soil inversion action of conventional disc plowing with large disc concavities and gang angle facilitates residue incorporation (Hanna et al., 1995). On the contrary, the residue incorporation of VT tools was achieved mainly by pushing residues and mixing soil through their elaborately designed geometry, i.e., flutes of the coulters and the concavity of the discs.

The field prior to the tillage had a residue cover of 98.1% and a total above-ground residue density of 9229.4 kg ha^{-1}, which almost doubled a density of 5433.5 kg ha^{-1} that found in a conservation corn field in southern Ontario, Canada (Beyaert and Voroney, 2011). Given the heavy residue condition, the tools were considered effective in disturbing residue indicated by the after-tillage residue cover ranging from 74.9 to 86.8% with an average of 82%. Similar residue cover results have been reported for VT equipment on corn fields. Klingberg and Weisenbeck (2010) measured the residue cover varying from 69 to 94% and Walther (2017) found an average residue cover of 64.6%. These results supported VT being a conservation tillage practice. The difference in R_C

between the two coulters showed a similar trend with that in Zeng and Chen (2018), where C8 left less residue on the soil surface than C13. However, the difference was significant in the corn field, as opposed to the marginal value in a wheat stubble field (Zeng and Chen, 2018).

The most striking observation from the data comparison between two types of tools was the difference in S_S. The coulters had a strong possibility of catching soil as compared with the discs. The tool geometrical parameters including trapping volume and pressure area were possibly responsible for the soil being stuck. Soil was confined in a trapping volume, which prevented trapped soil from sliding off. Thus, more soil was stuck on the coulters than the discs due to the larger trapping volumes of the former tools. Due to the same reason, C8 had a significantly higher S_S than that of C13. The amount of soil stuck on the tool surface also depends on other factors, e.g., soil moisture content and tool surface properties which affect the adhesion between soil and tool. The data thus need to be interpreted with caution. Further research would be needed to determine how tool geometry and operational parameters would affect soil sticking phenomenon.

Soil cutting depth of a tillage tool affects the resultant cutting forces and soil disturbance based on the soil dynamic theory (McKyes, 1985). Therefore, it is important to compare tillage tools under the same cutting depth. The soil cutting depth results from this study showed that the actual depths of the five tools were all close to the target cutting depth (100 mm), and they were all at the same statistical level. The low standard deviations of cutting depth demonstrated that the ground-driven tools were able to maintain a high uniformity in the heavy residue field. Rotary tools tend to float up out of the ground, especially when travelling at high speed. To maintain the tools at the desired

depth, researchers (e.g. Smith and Benock, 1977) have proposed several solutions, such as powered discs and ballasting toolbars. However, this was not a concern in this study. The ability of the rotary tools to maintain uniform working depth at the speed of 16 km h^{-1} showed that they were suitable for high-speed operations, such as VT. It was mainly attributed to the toothed edge of the discs and the fluted design of the coulters as well as their large cutting angle, which together facilitated tool penetration and depth maintenance. A uniform cutting depth would result in a uniformly loosened seedbed, which was desired for seeding and plant growth.

The C8 had a significant higher S_W as compared with C13, which agreed with the finding reported by Zeng and Chen (2018). Both coulters were considered as wide coulters based on ASABE standard S477.1 (2013), which explained their wider furrow opening than those from the discs. Both the S_W and S_A shared a similar trend: increasing with the working width of the tools. Two smaller discs had significant narrower S_W and smaller S_A than the others, which was also attributed to their shorter wave radial length. Given the working depth of 100 mm, two smaller discs had wave radial lengths that less than the working depth and thus less aggressive in disturbing soil as compared with these had full wavy section being in contact with soil.

Among the soil cutting forces, F_D is the most critical one, as it determines the tractor power required. A lower F_D is always desired to reduce the energy input for field operations. Among the soil disturbance variables, S_A represents the extent of soil loosening. A greater S_A is often desired in a tillage operation. When examining the results of S_A and F_D, one found that a tillage tool disturbed more soil had a higher draft force requirement. The soil loosening efficiency, defined as soil disturbance area divided by the

51

draft force (S_A/F_D) in McKyes (1985), was calculated for all tools. D559 had the maximum soil loosening efficiency and followed by D457 and C8 being the least. Thus, the disc with 559 mm diameter performed the best in terms of the soil loosening efficiency.

3.6. Conclusions

In this study, five vertical tillage (VT) tools: 8-flute and 13-flute coulters, as well as 457, 508, and 559 mm rippled discs, were tested in a corn stubble field to evaluate their tillage performance. Soil and residue disturbance, soil sticking on the tools, and soil cutting forces were measured as performance indicators. The tillage performance of the VT tools was greatly affected by the tool type. On average, the fluted coulters left less residue, incorporated more residue into the soil, created a wider furrow, and disturbed a larger area, as compared with the rippled discs. The coulters had a 73% higher draft force demand and a 729% higher possibility of soil sticking than the discs. Among the five tools, the 8-flute coulter was the most aggressive tool in disturbing residue and soil, and in this regard, it would be beneficial for solving the problem of excessive residue in fields. On the contrary, the 457 mm disc would be preferred to minimize the impact of tillage on soil and residue conditions as it resulted in the least soil and residue disturbance. From the perspective of soil loosening efficiency, the 559 mm disc was the most desirable tool as it disturbed the most amount of soil per unit draft force consumed. The limitation of this study was using a single tool in the field tests, which did not allow to evaluate the effectiveness of residue cutting, an important performance indicator for VT. Field evaluations of the VT tools using farm scale equipment will be carried out in future studies.

3.7. Acknowledgement

3.8. References

ASABE Standards. 2009. S414.2 Terminology and Definitions for Agricultural Tillage Implements. St. Joseph, Mich.: ASABE.

ASABE Standards. 2012. S358.3 Moisture Measurement - Forages. St. Joseph, Mich.: ASABE.

ASABE Standards. 2013. S477.1 Terminology for Soil-Engaging Components for Conservation-Tillage Planters, Drills, and Seeders. St. Joseph, Mich.: ASABE.

Beyaert, R., Voroney, R.P., 2011. Estimation of decay constants for crop residues measured over 15 years in conventional and reduced tillage systems in a coarse-textured soil in southern Ontario. Canadian Journal of Soil Science 91, 985–995.

Bianchini, A., Magalhaes, P.S.G., 2008. Evaluation of coulters for cutting sugar cane residue in a soil bin. Biosystems Engineering 100, 370–375.

Chapman, M.L., Johnson, C.E., Schafer, R.L., Gill, W.R., 1988. Some performance characteristics of disc gangs. Journal of Agricultural Engineering Research 39, 1–7.

Chen, Y., Damphousse, S., Li, H., 2016. Vertical tillage and vertical seeding. Paper No. CSBE16-090. In: CSBE/SCGAB 2016 Annual Conference. Halifax, NS, Canada. July 3–6.

Chen, Y., Monero, F., Lobb, D., Tessier, S., Cavers, C., 2004. Effects of six tillage methods on residue incorporation and crop performance under a heavy clay soil. Transactions of the ASABE 47(4), 1003–1010.

Choi, C.H., Erbach, D.C., 1986. Cornstalk residue shearing by rolling coulter. Transactions of the ASAE 29(6), 1530–1535.

De Vita, P., Di Paolo, E., Fecondo, G., Di Fonzo, N., Pisante, M., 2007. No-tillage and conventional tillage effects on durum wheat yield, grain quality and soil moisture content in southern Italy. Soil & Tillage Research 92, 69–78.

Erbach, D.C., 1981. Planting for crop production with conservation. In: Crop Production with Conservation in the 1980s. ASAE Publication, St. Joseph, MI.

Hanna, H.M., Melvin, S.W., Pope, R.O., 1995. Tillage implement operational effects on residue cover. Applied Engineering in Agriculture 11(2), 205–210.

He, J., Li, H., Rabi, G.R., Wang, Q., Cai, G., Su, Y., Qiao, X., Liu, L., 2011. Soil properties and crop yields after 11 years of no tillage farming in wheat-maize cropping system in North China Plain. Soil & Tillage Research 113, 48–54.

Karll, J.L., Larsen, W.E., Dubbs, A.L., 1978. No-till drill studies for seeding small grain. Paper No. 78-1514. In: ASAE 1978 Annual Conference.

Klingberg, K., Weisenbeck, C., 2011. Shallow vertical tillage: impact on soil disturbance and crop residue. In: Proceeding of the 2011 Wisconsin Crop Management Conference 50, 46–49.

Kushwaha, R.L., Vaishnav, A.S., Zoerb G.C., 1986. Soil bin evaluation of disc coulters under no-till crop residue conditions. Transactions of the ASAE 29(1), 40–44.

Madejon, E., Murillo, J.M., Moreno, F., Lopez, M.V., Arrue, J.L., Alvaro-Fuentes, J., Cantero, C., 2009. Effect of long-term conservation tillage on soil biochemical properties in Mediterranean Spanish areas. Soil & Tillage Research 105, 55–62.

Magalhaes, P.S.G., Bianchini, A., Braunbeck, O.A., 2007. Simulated and experimental
analyzes of a toothed rolling coulter for cutting crop residues. Biosystems
Engineering 96(2), 193–200.

McKyes, E., 1985. Soil Cutting and Tillage. Elsevier, New York.

Murray, S., 2016. Modelling of Soil-Tool Interactions Using the Discrete Element
Method (DEM). M.Sc. Thesis, University of Manitoba, Winnipeg, Manitoba,
Canada.

Naudin, K., Goze, E., Balarabe, O., Giller, K.E., Scopel, E., 2010. Impact of no tillage
and mulching practices on cotton production in North Cameroon: a multi-
locational on-farm assessment. Soil & Tillage Research 108, 68–76.

Prasuhn, V., 2012. On-farm effects of tillage and crops on soil erosion measured over 10
years in Switzerland. Soil & Tillage Research 120, 137–146.

Raoufat, M.H., Mahmoodieh, R.A., 2005. Stand establishment responses of maize to
seedbed residue, seed drill coulters and primary tillage systems. Biosystems
Engineering 90(3), 261–269.

Salokhe, V.M., Quang, N.B., 1995. Dynamics of a powered disk in clay soil. Journal of
Terramechanics 32(5), 231–244.

Schaaf, D.E., Hann, S., Lindwall. C.W., 1980. Development of performance data on seed
drill coulters. Paper No. 80-303. In: Proceedings of 1980 CSAE Annual Meeting.
Edmonton, Alberta, Canada.

Smith, E.M., Benock, G., 1977. Power tillage compared with conventional tools for
grassland renovation. Paper No. 77-1003, In: ASAE 1977 Annual Conference.

56

Smith, D.R., Warnemuende-Pappas, E.A., 2015. Vertical tillage impacts on water quality derived from rainfall simulations. Soil & Tillage Research 153, 155–160.

Tice, E.M., Hendrick, J.G., 1991. Disc coulter forces: evaluation of mathematical models. Transactions of the ASAE 34(6), 2291–2298.

Tice, E.M., Hendrick, J.G., 1992. Disc coulter operating characteristics. Transactions of the ASAE 35(1), 3–10.

Tullberg, J.N., Yule, D.F., McGarry, D., 2007. Controlled traffic farming: from research to adoption in Australia. Soil & Tillage Research 97, 272–281.

Walther, P.A., 2017. Corn Residue Management for Soybean Production: On-farm Experiment. M.Sc. Thesis, University of Manitoba, Winnipeg, Manitoba, Canada.

Zeng, Z., Chen, Y., 2018. The performance of a fluted coulter for vertical tillage as affected by working speed. Soil & Tillage Research 175, 112–118.

Chapter 4: The Performance of a Fluted Coulter for Vertical Tillage as Affected by Working Speed *

4.1. Abstract

Vertical tillage is an efficient and effective tillage practice for conservation agriculture. However, the performance of vertical tillage tools has not been well documented. In this study, two vertical tillage tools: 8-wave and 13-wave coulters, were tested in a wheat stubble field at three different working speeds: 12, 16, and 20 km h^{-1}, to examine the effects of tool geometry and working speed on the tillage performance of the fluted coulters. Soil disturbance width, soil throw width, and soil sticking on the coulter as well as residue cover were measured. The results showed that the soil disturbance width was significantly different among the working speeds and between two coulters while the other measured variables were only affected by the working speed. The 13-wave coulter had a 17% lower soil disturbance width as compared with the 8-wave coulter. Increasing the working speed (from 12 to 16 km h^{-1} and from 12 to 20 km h^{-1}) increased the soil disturbance width by 7.0 and 13.1% and the soil throw width by 14.3 and 45.1% respectively, but decreased the soil sticking by 1.4 and 76.6% and the residue cover by 5.1 and 11.0% respectively. Generally speaking, the effect of working speed was more dominant than the coulter geometry on the tillage performance of the fluted coulters. For long-term no-tillage farmers with excessive residue concerns, the 8-wave coulter working at 20 km h^{-1} would be beneficial for sustainable farming practice.

4.2. Introduction

Conservation tillage, including no-tillage, aims to increase the profitability and sustainability of crop production, and its main advantage over traditional tillage is leaving at least 30% residue cover in the field to protect the soil and environment. In no-tillage systems, crop residue cover is often as high as 100%. A dilemma in conservation tillage systems is that the crop residue causes plugging of tillage and seeding equipment. Vertical tillage (VT) has been recently proposed to tackle the dilemma. In VT, crop residue is cut into small pieces, which avoids plugging seeding equipment in the subsequent seeding operation. The residue is partially mixed with soil for fast decomposition, while an essential amount of residue is maintained on the soil surface for soil protection. Thus, VT is a conservation tillage practice. In addition, VT has several other advantages over conventional tillage. An on-farm study of several commercially available VT machines showed that VT is more desirable in terms of soil and water conservation as compared with traditional tillage equipment on a site-specific basis (Klingberg and Weisenbeck, 2011). As for crop yields, the literature reported mixed results. A comparative study between VT and no-till found that VT significantly increased the plant population and yield with a marginally higher lodging resistance regardless of seeding rates (Watters and Douridas, 2013). Whitehair (2014) reported that VT did not yield more grain at any of nine site locations over a two-year period as compared with conventional, no-till, and reduced tillage systems. Vertical tillage successfully delayed runoff initiation in rainfall simulations; however, the steady-state rate and total amount of runoff were significantly higher in VT as compared with no-tillage (Smith and Warnemuende-Pappas, 2015). Vertical tillage is a recent concept, and little research has been done in this area.

In VT, soil-engaging tools interact with soil in a vertical plane perpendicular to the soil surface and along the travel direction (Chen et al., 2016). To date, vertical tillage equipment has been developed by many agricultural manufacturers, such as Great Plains (Salina, Kansas, USA), Salford Group (Salford, ON, Canada), and Kongskilde Industries (Soroe, Denmark) (Kanicki, 2014). The VT machines varied significantly in configuration, size, and functionality. For example, two different arrangement of VT implements were demonstrated in Chen et al. (2016) as disc-roller arrangement and disc-tine-roller arrangement. The leading and major working components of VT equipment are mostly coulters, but concave discs with small gang angles have also been used. Coulters are the least intrusive yet effective vertical tools that slice soil, cut residue, partially incorporate residue, and loosen soil. Coulters can be either configured on gangs or individually mounted using shanks. As compared with the gang configuration, the individual shank systems have several advantages: no interaction between coulters, more uniform tillage depth in an uneven condition, rock protection, less residue collection, and more accessible for maintenance. However, the individual shank configuration is usually more expensive to manufacture than the gang configuration. Traditionally, coulters were used on planters as seed openers and fertilizer banding openers (Fallahi and Raoufat, 2008). Coulters were also used on some conventional tillage equipment as auxiliary tools, for example, in the front of subsoiling tools (Zhang et al., 2007). Those coulters were typically straight coulters for the purpose of cutting residue and opening slots in the soil. The working speed of seeding and traditional tillage equipment typically ranges between 5.5 and 11 km h^{-1} (ASABE Standard D497.7, 2015). Coulters for VT are larger in diameters, and have more complex geometries as well as more aggressive residue cutting

60

abilities. They are varied significantly in shape, dimension, and operating angles. These coulters are designed to travel at much higher speeds: 12 to 20 km h^{-1} (Chen et al., 2016).

The working speed is one of the most dominant operator-controlled variables that affect the performance of the soil-engaging tool (Stafford, 1979; Wheeler and Godwin, 1996). Tice and Hendrick (1992) inferred that a high speed may contribute to effective residue cutting by observing the kinematic behaviour of straight coulters in soil bin tests. Sarauskis et al. (2013) and Fiaz et al. (2015) experimentally confirmed that the coulter at increased speeds had an increasing residue cutting efficiency in wheat and rice fields respectively. However, coulters for VT that work at high speeds have not been well documented.

Soil and residue conditions resulting from a tillage operation is also affected by the geometry of the tillage tools. Experimental studies on the performance of different coulters in the residue-free condition indicated that furrow characteristics and soil disturbance varied with coulter geometry (Schaaf et al., 1980; Godbole, 1997). After a comprehensive study of four coulters with different shapes, Godbole (1997) concluded that the lateral soil displacement depended on the specific coulter surface area that contacted with soil, rather than the general geometrical characteristics of the coulters. Sarauskis et al. (2013) compared four different notched coulters on their residue cutting ability in a winter wheat field and found the one with the most notches and the deepest notches performed the best. Although Choi and Erbach (1986) reported that the coulter shape had no significant effect on cornstalk residue shearing, the coulter sharpness was the most important coulter geometrical characteristics influencing residue shearing. Similarly, a coulter with toothed geometry significantly improved the residue cutting

efficiency (Magalhaes et al., 2007). As for the residue cover, several models and databases have been proposed by Stott et al. (1988) and Soil Conservation Service and the Equipment Manufacturers Institute (1992) regarding the effect of tillage tool geometry on the residue cover after field operations. There is a lack of information on the resultant soil and residue conditions from VT coulters. This information is crucial to guide the design of high-performance VT equipment.

In summary, previous coulter-related studies were carried out for small, straight coulters at low working speeds in traditional tillage. Little research has been done on large coulters at high working speeds in VT. This study focused on a specific type of VT tool, fluted coulters, rather than performing a comprehensive investigation of all VT tools. The objective of this study was to evaluate the tillage performance of two fluted coulters working at different speeds, in terms of soil disturbance and residue cover.

4.3. Material and methods

4.3.1. Site description

A field experiment was conducted in the fall of 2016 at a research farm in Portage la Prairie, Manitoba, Canada. The soil type was silty clay with 46% clay, 49% silt, and 5% sand content. The field had winter wheat stubble with a row spacing of 0.25 m and a stubble height of approximately 0.15 m, and wheat straw was chopped by the combine straw chopper and evenly spread over the field in July 2016.

4.3.2. Equipment description

The VT tools tested were two fluted coulters with 8 and 13 waves, named as 8-wave and 13-wave coulters respectively (Fig. 4.1a). They were identical to 8-flute and

13-flute coulters used in Chapter 3. For each test, a single coulter was mounted to a toolbar through a coil shank (Fig. 4.1b). The toolbar had a three-point hitch and two gauge wheels for controlling the tillage depth. The original mounting of the shank allowed the coulter floating with a range of gang angle of 0-20 degrees. In the tests, the gang angle of the coulters was fixed at zero degrees to avoid effects of the gang angle variation. The tilt angle of the coulter was also set as zero for the tests.

| (a) | (b) |
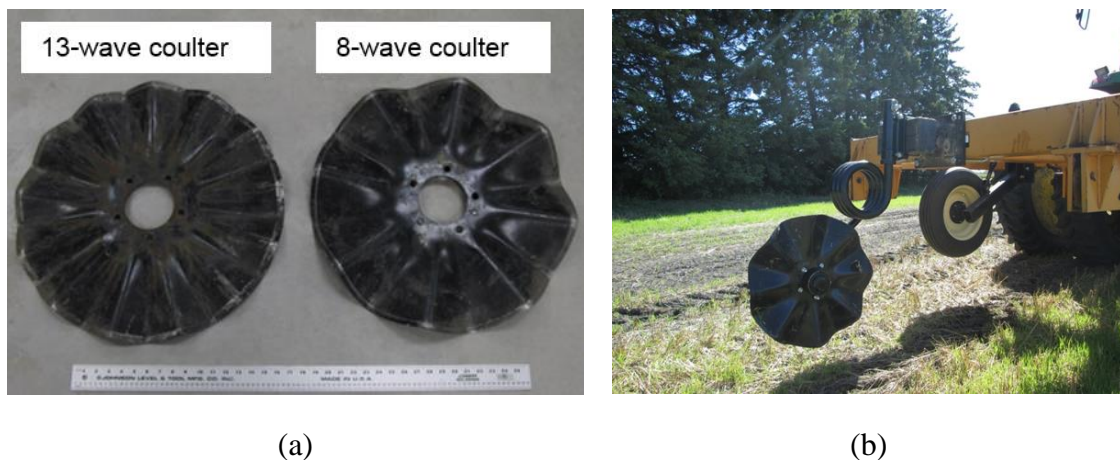
Figure 4.1. Coulters tested: (a) two different fluted coulters; (b) coulter and shank mounted on the toolbar.

Both the fluted coulters had a diameter of 559 mm with formed flutes radiating from the outer periphery toward the centre. The fluted coulters consisted of equal-spaced waves along the thrust direction. Geometrical parameters of the coulters are listed in Table 4.1. These parameters are of importance in relation to the resultant soil and residue conditions. The working width is the maximum width measured at the periphery of the coulter. The coulter flutes can be characterized with wave gang angle and wave tilt angle. The wave gang angle was defined as the angle between the wave plane and the travel direction on the horizontal plane that was parallel to the soil surface. The wave tilt angle

is defined as the angle that the wave plane makes with the vertical axis on the vertical plane that was perpendicular to the travel direction. The engaging waves referred to the number of waves that come into contact with soil at any given time for a specific working depth, 76 mm in this study. The contacting area was the coulter surface area of the engaging waves in contact with the soil at any moment. Assuming that each wave was forming a closed space by adding a plane that was parallel to the coulter plane, the space could be partially filled with soil during the operation. Thus, the total volume of the soil-filled spaces of the engaging waves was defined as soil trapping volume. The relative differences in these parameters between two coulters are provided in Table 4.1.

Table 4.1. The comparison of principal geometrical parameters between the two coulters

Term	8-wave coulter	13-wave coulter	Relative difference (%)[+]
Working width, mm	63.5	44.5	-29.9
Wave gang angle, °	30.1	33.4	11.0
Wave tilt angle, °	6.5	4.6	-29.2
Engaging waves	1.93	3.13	62.2
Contacting area, m^2	0.0322	0.0334	3.7
Trapping volume, m^3	0.00154	0.00108	-30.0

[+]The relative difference was calculated using the measurement of the 8-wave coulter as the reference value; positive value means the measurement of 13-wave is greater than that of 8-wave, and vice versa for the negative value.

4.3.3. Experimental design

A completely randomized factorial design was used for the experiment. Treatments were the six combinations of the two coulters (8-and 13-wave coulters) and three working speeds (12, 16, and 20 km h^{-1}). Each treatment was replicated five times.

Therefore, a total of 30 plots were used in the field experiment. The plots were 3 m wide to accommodate one pass of the tractor. The plots were 30 m long, and laid out perpendicular to the previous crop rows. Each plot had buffer areas at two ends for tractor acceleration and deceleration to ensure the tractor travelled at a specified constant speed within the plot. The working depth of the coulters was set constant at 76 mm for all the treatments.

4.3.4. Measurements

Measurements of soil and residue characteristics were conducted before and after the tillage operation. All the initial soil and residue samplings were taken at five random locations over the entire field. All the post-tillage measurements were conducted at three random locations in each plot, unless specified otherwise.

4.3.4.1. Initial soil conditions

Before the tillage operation, soil shear strength was measured using a Vane Shear Meter (Geovane, New Zealand). The blades were pushed in the soil till the top edge was in level with the soil surface. The meter was then rotated at the speed of approximately 1 rpm till the soil failed. The reading on the meter dial was recorded as the soil shear strength (kPa). Soil penetration resistance at the surface was measured using a Pocket Penetrometer (Geotester, Italy). The penetrometer foot was pushed into the soil until the top of the foot was leveled with the soil surface. The reading was recorded and the meter was reset for the next test. Soil samples were also taken using a core sampler that was 50 mm in diameter and 76 mm in height. The sampling depth was the same as the target tillage working depth (76 mm). Soil cores were weighed, oven-dried for 24 hours at

105°C, and weighed again to determine the gravimetric soil moisture content and dry bulk density.

4.3.4.2. Initial dry mass of surface residue

The amount of residue on the surface was measured prior to the tests. A 1-m by 1-m quadrat was placed on the soil surface. Loose residue within the quadrat was collected first; then standing stubble in the quadrat was cut and collected separately. The collected residue samples were oven-dried at 55°C for 72 hours (ASABE Standard S358.3, 2012) and weighed to determine the dry mass of standing stubble and flat residue per hectare.

4.3.4.3. Residue cover

Residue cover measurements were done both before and after tillage using digital images taken above the 1x1 m quadrat. For the undisturbed soil surface, the quadrat was placed in random locations of the field (Fig. 4.2a). For the disturbed surface, the quadrat was centred with the path of the coulter (Fig. 4.2b). Images were analyzed in Matlab using the image thresholding method to determine the percentage of the residue on the soil surface (Chen et al., 2004).
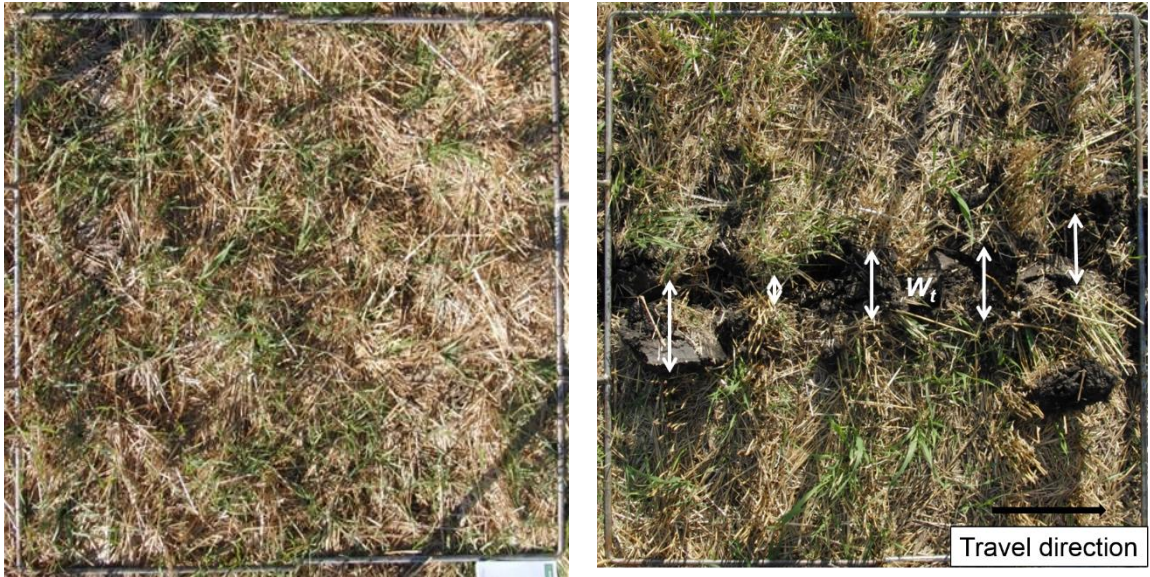
Figure 4.2. Soil surface images confined by a 1 x 1 m quadrat: (a) residue cover before tillage; (b) residue cover after tillage and soil throw width (W_t) resulting from the tillage.

4.3.4.4. Soil throw and disturbance width

The soil throw width (W_t) was manually measured as the lateral width of the disturbed soil on the surface. Measurements were taken at five locations along the coulter path equally spaced within each quadrat, as demonstrated in Fig. 4.2b. Some scattered soil aggregates that were thrown away from the coulter path were not included in measuring the W_t. To measure soil furrow opening width (W_d), the furrow was exposed by carefully removing top loose soil and residue. A transparent film (216 mm by 279 mm) was placed over the furrow, and the furrow surface shape was traced on the film (Fig. 4.3). The soil disturbance width was measured as the average of five furrow widths equally distributed along the film.
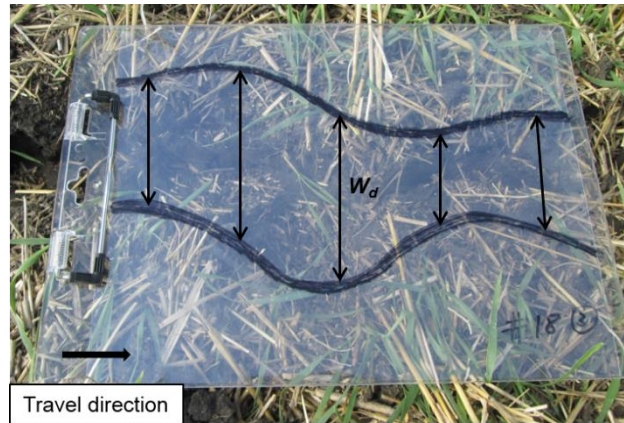
Figure 4.3. Furrow surface shape on a transparent film for measuring soil disturbance width (W_d).

4.3.4.5. Soil sticking

At the completion of the test run of a plot, the coulter was gently lifted above the ground. The soil and residue stuck on the coulter (Fig. 4.4) were scraped and collected in a zipper bag. The collected material was later oven-dried at 55°C for 72 hours. The dry mass was reported as soil sticking (*SS*). There was only one measurement of *SS* from one coulter in each plot.

Figure 4.4. Soil and residue stuck on the coulter.

4.3.5. Data analysis

Analysis of variance (ANOVA) was performed using statistical software (SAS for Windows v 9.4). The means between treatments were compared with Duncan's multiple range tests at the significance level of 0.05. The main effects of coulter geometry and working speed were presented when the interaction effects were not significant; otherwise, the simple effects of working speed for both coulters were examined and presented.

4.4. Results and discussions

4.4.1. Initial soil and residue conditions

Measurements of field initial conditions are listed in Table 4.2. The field had a higher amount of flat residue than the standing residue. The total amount of residue (standing plus flat residue) was 5377 ± 1250 kg ha^{-1}, which was similar to that of a long-term no-till wheat field reported by Bahrani et al. (2007) and slightly higher than the typical wheat straw biomass in no-till fields ranging from 1 to 5 t ha^{-1} reported by Kushwaha et al. (1986). This much residue covered 97.5% of the field surface. The moisture content (dry basis) of the tillage layer was 31.1% that was suitable for field operations on a silty clay soil. The values of soil dry bulk density, soil resistance, and shear strength were typical for this type of soil.

Table 4.2. Initial soil and residue conditions

Measurements	Moisture content	Dry bulk density	Soil resistance	Shear strength	Residue cover	Standing residue	Flat residue
Unit	%	kg m^{-3}	kPa	kPa	%	kg ha^{-1}	kg ha^{-1}
Means	31.1	1234.2	439.7	77.8	97.5	1039.6	4337.4
SD^{+}	3.3	100.8	50.6	12.5	1.5	133.5	1242.1

[+]SD stands for the standard deviation resulting from 5 replications of each measurement.

4.4.2. Soil sticking

The working speed had a pronounced effect on the amount of soil stuck on the coulters regardless of the coulter geometry (P<0.0001). The *SS* decreased with the increase in working speed (Fig. 4.5). The coulters operating at 20 km h^{-1} had the least *SS* (47.7 g), which was 66% and 77% lesser than that of 16 and 12 km h^{-1}, respectively. As shown in Fig. 4.4, most of the stuck soil and residue was located within the fluted regions of the coulter, indicating that the flutes tended to trap soil, as the coulter rotated. The soil stuck on the coulter would affect the gravity, adhesion, and rotational momentum. The adhesion between the stuck soil and the coulter provides resistance against the peeling-off force that is the resultant force of the gravity and rotational momentum. The smaller *SS* at a higher speed implied that the rotational momentum could be dominant over the gravity in the peeling-off force, since the momentum is proportional to the rotational speed of the coulter which is determined by the coulter working speed.
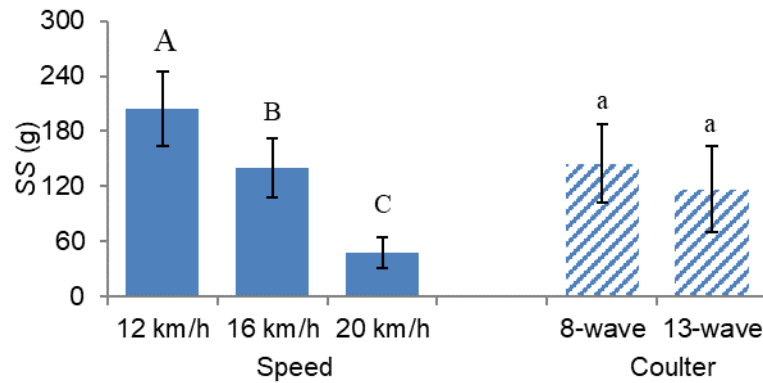
Figure 4.5. Soil sticking (*SS*) dry weight of different coulter geometries at different working speeds; means followed by different lower case letters or upper case letters are significantly different according to Duncan's multiple range test at the significance level of 0.05; error bars are standard deviations.

The 13-wave coulter had a 9% lesser *SS* than the 8-wave coulter, which was expected as the 13-wave had a 30% smaller trapping volume. However, the statistical difference in *SS* between the two coulters was not detected due to the variation of the field data, as shown by the high standard deviations. The effect of coulter trapping volume might have been "diluted" by the effect of rotational momentum. The 8-wave coulter with more trapped soil would have higher rotational momentum, causing the stuck soil to be more easily spanned out the coulter. The coulter contacting area would also affect the *SS* by changing the magnitude of the adhesion. However, this effect was considered to be minor, due to the small difference in the contacting surface (3%) between the two coulters. The study conducted by Godbole (1997) showed the opposite effect in relation to the number of waves, where a 25-wave coulter had a significantly higher *SS* than an 8-wave coulter. The detailed description of the coulter geometry was not found in that study, and the working speed, 8 km h^{-1}, was much lower than the speeds

71

used in this study. Besides, the field in this study was covered by 97.5% residue, whereas the previous study was conducted in a residue-free soil condition. All these explained the different results from these two studies. Further research is required to better understand the soil sticking phenomenon of fluted coulters.

4.4.3. Soil disturbance width

A higher tillage speed resulted in a wider soil surface disturbance (Fig. 4.6). The significant difference in W_d was only observed between the lowest and highest speeds. The W_d increased by 7% and 5.7% when the working speed increased from 12 to 16 km h^{-1} and from 16 to 20 km h^{-1}, respectively, although these increases were not statistically significant. That W_d increased with the increasing speed was expected since the zone of influence expanded when the working speed increased. However, the change in the W_d was not of a large magnitude. For example, a 66.7% increase in the speed from 12 to 20 km h^{-1} resulted in only 13.1% increase in W_d. Therefore, altering working speed would be not very effective for changing the soil disturbance width.
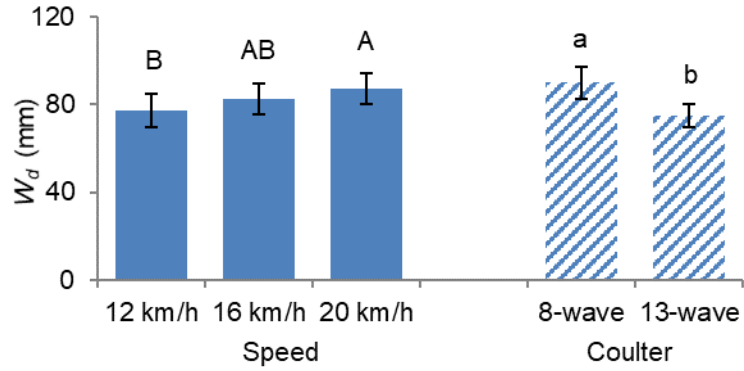
Figure 4.6. Soil disturbance width (W_d) of different coulter geometries at different working speeds; means followed by different lower case letters or upper case letters are significantly different according to Duncan's multiple range test at the significance level of 0.05; error bars are standard deviations.

The fluted coulters disturbed the soil in a wavy pattern as shown in Fig. 4.3, which was consistent with the findings in Godbole (1997) due to the wavy shape of the coulters. The 13-wave coulter disturbed a 17% narrower furrow opening than the 8-wave coulter, which was statistically significant. The working width of the 13-wave coulter was smaller than that of the 8-wave coulter. Typically, a narrower tool creates a smaller furrow (McKyes, 1985). A smaller gang angle and tilt angle would cause lower soil disturbance (O'Dogherty et al., 1996). The 13-wave coulter had a smaller wave tilt angle but a greater wave gang angle as compared with the 8-wave coulter. The lower value of W_d of the 13-wave coulter implied that the effect of the wave gang angle might have been suppressed by the effects of the working width and the wave tilt angle.

4.4.4. Soil throw width

Since both the interaction effect and the working speed effect were statistically significant, the working speed effect was examined within each coulter (Fig. 4.7). For the

8-wave coulter, the speed of 20 km h^{-1} produced a significantly higher W_t than the two lower speeds that resulted in W_t of the same statistical level. In the case of the 13-wave coulter, the values of W_t at the speeds of 20 and 16 km h^{-1} were at the same statistical level, which were significantly greater than that at the 12 km h^{-1}. These were the reasons why slightly significant interactions (P=0.04) between the coulter geometry and working speed were detected. Generally speaking, a higher speed resulted in a greater W_t regardless of the coulter geometry, which demonstrated the significant main effects of the working speed.
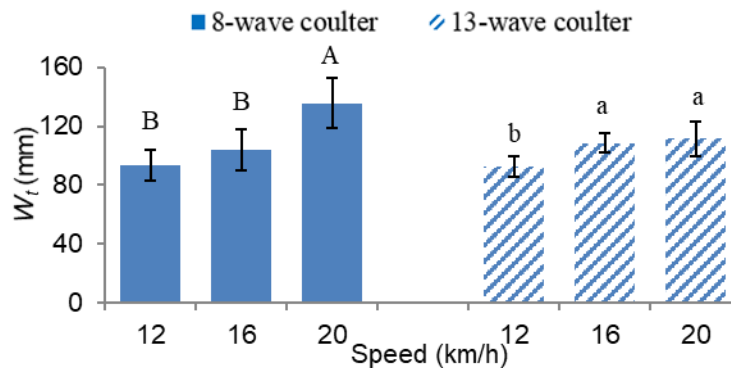
Figure 4.7. Soil throw width (W_t) at different working speeds of two coulter geometries (8- and 13-wave); means followed by different lower case letters or upper case letters are significantly different according to Duncan's multiple range test at the significance level of 0.05; error bars are standard deviations.

Two coulters did not result in significant differences in W_t (P=0.17). As indicated in Godbole (1997), the contacting area had a stronger effect on soil lateral displacement than other coulter geometries, such as the coulter width and the number of waves. The similar contacting areas of two studied coulters were responsible for their similar values of W_t. The 13-wave coulter had approximately one more wave working in the soil at any

given time as compared with the 8-wave coulter, which produced finer and thus more homogeneous soil aggregates in the tillage zone. The smaller standard deviation in the W_t of the 13-wave coulter as compared with the 8-wave coulter at any speed indirectly reflected the difference in the size of soil aggregates as the 13-wave produced a more uniform soil throw distribution along the coulter path due to the finer size of the soil aggregates. Similarly, the soil surface roughness results in Godbole (1997) showed that the variation of surface roughness resulting from the 25-wave coulter was lesser than that from the 8-wave coulter.

4.4.5. Residue cover

The working speed significantly affected the residue cover (RC) (P<0.0001), while the coulter geometry did not result in different RC (P=0.51). The RC at 20 km h^{-1} significantly differed from that at 16 km h^{-1} by a relative reduction of 6.2%. Similarly, the speed of 16 km h^{-1} significantly decreased the RC by a relative difference of 5.1% as compared with that at 12 km h^{-1}. The 13-wave coulter created an almost identical RC to the 8-wave coulter. Since the W_t represents the degree of lateral soil movement, it would associate with the residue burying and mixing, which in turn associated with the results of RC. The insignificant effect of coulter geometry on the RC was in agreement with the insignificant effect on the W_t.
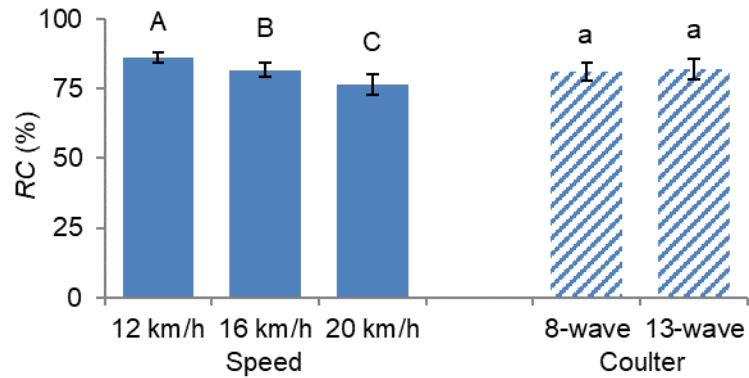
Figure 4.8. Residue cover (*RC*) of different coulter geometries and at different working speeds; means followed by different lower case letters or upper case letters are significantly different according to Duncan's multiple range test at the significance level of 0.05; error bars are standard deviations.

The amount of residue incorporation or burial could be implied by the surface residue remaining after tillage. Therefore, a lower *RC* of the tillage at 20 km h^{-1} reflected more residue incorporation, which might improve soil fertility with appropriate nitrogen application. In the fall, it is critical for the soil fertility maintenance in the area suffering from a cold and long winter fallow, e.g., the Canadian Prairies. The decreased levels of surface crop residue from the operation at 12 to 20 km h^{-1} would also result in warmer and drier soils in the spring, which might advance seeding and extend the growing season. This is desirable in a short-season region, e.g., the Canadian Prairies, where the soil temperature and moisture content in the spring are the concerns. The increasing trend of residue incorporation or anchoring from 12 to 20 km h^{-1} would also alleviate residue blowing and drifting in windy conditions on the Prairies.

4.4.6. Discussions

In this study, it was observed that the working speed and coulter geometry affected soil disturbance and residue cover. The effect of working speed was more dominant than that of coulter geometry. Increasing working speed resulted in a reduction in the *SS* and *RC*, and an increase in the W_d and W_t. Smaller *SS* is always preferred in any tillage operations, and in this regard, fluted coulters will perform better when operated at a higher speed. Smaller W_t is typically desired, as a higher amount of soil throw reflects indirectly higher energy requirement. However, it is difficult to determine whether a smaller or larger value of W_d or *RC* has better tillage performance. The advantages and disadvantages of higher or lower W_d and *RC* depend on the specific application, e.g., tillage purpose, soil and environment conditions, and subsequent seeding practices.

Fluted coulters have a more complex geometry than flat coulters, and as the result, the soil dynamics resulting from the coulters was complex. The waved coulter surface of the fluted coulters provided a discontinuous disking function for soil pulverizing and residue cutting. Small or zero disk angles and symmetric structure of the coulters allowed the tillage operation to be performed at a very high speed. This will lead to greater efficiency, in terms of tillage work performed within a unit time. For traditional disk plows, the gang angle affects the amount of soil being pushed forward and sideways, and the tilt angle is designed for lifting the soil along the disk's forward face. For the fluted coulters, the wave gang angles (30.1° and 33.4°) and wave tilt angles (6.5° and 4.6°) are smaller than the typical gang and tilt angles of disk plows ranging from 35° to 55° and 15° to 25° respectively (Kepner et al., 1978). Therefore, the pushing and lifting actions of the fluted coulters were not as aggressive. This would prevent excessive soil

77

being disturbed, which is desired in conservation tillage. The main action of the fluted

coulters was to cut soil downward, that facilitated residue cutting, which is the primary

purpose of the VT. In addition, the waves of the coulter potentially twist soil from side to

side when they travel in the soil. This twisting action favours fracturing the soil and

mixing residue with the soil, resulting in uniform soil bulk density and rapid residue

decomposition.

4.5. Conclusions

Tests of a vertical tillage tool using two different fluted coulters (8-wave and 13-

wave) were performed at three different working speeds in a field with wheat stubble.

The working speed and coulter geometry significantly affected the tillage performance of

the fluted coulters. The 13-wave coulter created a 13% lower soil disturbance width as

compared with the 8-wave coulter. Increasing the working speed from 12 to 20 km h^{-1}

significantly increased the soil disturbance width and soil throw width by 13.2% and

32.9%, respectively, while significantly decreasing the soil sticking and residue cover by

77% and 12.4%, respectively. The results facilitated the understanding of the soil-coulter

interaction and could serve as references when selecting tillage and residue management

practices, as well as studying soil erosion. Except for the soil throw width, the working

speed and coulter geometry could be employed as independent variables in altering

tillage-resulted soil and residue conditions. The working speed had more significant

effects on both soil disturbance and residue management than the coulter geometry.

Therefore, the working speed is the primary strategy, with the coulter geometry as a

secondary strategy, to improve the tillage performance. However, the field tests were

conducted only in the given field conditions for one of many VT tools. Therefore,

cautions should be taken when applying the results to other field conditions and when using other VT tools. For long-term no-tillage farmers with excessive residue concerns, the 8-wave coulter working at 20 km h^{-1} would be a better choice.

4.6. Acknowledgement

4.7. References

ASABE Standards. 2012. S358.3 Moisture Measurement - Forages. St. Joseph, Mich.: ASAE.

ASABE Standards. 2015. D497.7 Agricultural Machinery Management Data. St. Joseph, Mich.: ASAE.

Bahrani, M.J., Raoufat, M.H., Ghadiri, H., 2007. Influence of wheat residue management on irrigated corn grain production in a reduced tillage system. Soil & Tillage Research 94, 305–309.

Chen, Y., Damphousse, S., Li, H., 2016. Vertical tillage and vertical seeding. Paper No. CSBE16-090. In: CSBE/SCGAB 2016 Annual Conference, Halifax, NS, Canada. July 3–6.

Chen, Y., Monero, F., Lobb, D., Tessier, S., Cavers, C., 2004. Effects of six tillage methods on residue incorporation and crop performance under a heavy clay soil. Transactions of the ASABE. 47(4), 1003–1010.

Choi, C., Erbach, D., 1986. Cornstalk residue shearing by rolling coulters. Transactions of the ASAE 29(6),1530–1535.

Fallahi, S., Raoufat, M.H., 2008. Row-crop planter attachments in a conservation tillage system: a comparative study. Soil & Tillage Research 98, 27–34.

Fiaz, A., Ding, W., Ding, Q., Mubshar, H., Khawar, J., 2015. Forces and straw cutting performance of double disc furrow opener in no-till paddy soil. PLOS ONE 10(3), e0119648.

Godbole, R.D., 1997. Comparing Rolling Coulters Based on Soil Disturbance. Ph.D.
Thesis, Iowa State University, Ames, Iowa, USA.

Kanicki, D., 2014. What is vertical tillage anyway? https://www.farm-
equipment.com/articles/10122. Accessed 11 September 2018.

Kepner, R.A., Barger, R., Bainer, E.L., 1978. Principles of Farm Machinery. AVI
Publishing Company.

Klingberg, K., Weisenbeck, C., 2011. Shallow vertical tillage: impact on soil disturbance
and crop residue. In: Proceeding of the 2011 Wisconsin Crop Management
Conference 50, 46–49.

Kushwaha, R.I., Vaishnav, A.S., Zoerb, C.C., 1986. Soil bin evaluation of disc coulter
under no till crop residue conditions. Transactions of the ASAE 29, 40–44.

Magalhaes, P.S.G., Bianchini, A., Braunbeck, O.A., 2007. Simulated and experimental
analyzes of a toothed rolling coulter for cutting crop residues. Biosystems
Engineering 96(2), 193–200.

McKyes, E., 1985. Soil Cutting and Tillage. Elsevier, New York.

O'Dogherty, M.J., Godwin, R.J., Hann, M.J., Al-Ghazal, A.A., 1996. A geometrical
analysis of inclined and tilted spherical plough discs. Journal of Agricultural
Engineering Research 63, 205–218.

Sarauskis, E., Masilionyte, L., Romanechas, K., Krianuciuniene, Z., Jasinskas, A., 2013.
The effect of the disc coulters forms and speed ratios on cutting of crop residue in
no-tillage system. Bulgarian Journal of Agricultural Science 19(3), 620–624.

Schaaf, D.E., Hanna, S., Lindwall, C.W., 1980. Development of performance data on seed drill coulters. Paper No. CSAE80-303. In: CSAE 1980 Annual Conference. Edmonton, Alberta, Canada.

Smith, D.R., Warnemuende-Pappas, E.A., 2015. Vertical tillage impacts on water quality derived from rainfall simulations. Soil & Tillage Research 153, 155–160.

Soil Conservation Service and the Equipment Manufacturers Institute, 1992. Estimates of residue cover remaining after single operation of selected tillage machines. Washington, D.C.: USDA Soil Conservation Service.

Stafford, J., 1979. The performance of a rigid tine in relation to soil properties and speed. Journal of Agricultural Engineering Research 24(1), 41–56.

Stott, D.E., Stuart, B.L., Barrett, J.R., 1988. Residue management decision support system. Paper No. 88-7541. In: ASAE 1998 Annual Conference.

Tice, E., Hendrick, J., 1992. Disc coulter operating characteristics. Transactions of the ASAE 35(1), 3–10.

Watters, H.D., Douridas, N.N., 2013. Soybean seeding rates by tillage – no-till vs vertical till. http://agcrops.osu.edu/sites/agcrops/files/ofr_reports/Soybean-Seeding-Rate-and-Tillage.pdf. Accessed 11 September 2018.

Wheeler, P.N., Godwin, R.J., 1996. Soil dynamics of single and multiple tines at speeds up to 20 km/h. Journal of Agricultural Engineering Research 63, 243–250.

Whitehair, A., 2014. Vertical Tillage Effects on Yield, Disease and Pathogens, and Soil Properties. M.Sc. Thesis, Kansas State University, Manhattan, Kansas, USA.

Zhang, J. G., Raper, R.L., Balkcom, K.S., Arriaga, F.J., Kornecki, T.S., Schwab, E.B., 2007. Drawbar power requirements and soil disruption of in-row subsoiler points for conservation tillage. In: Proceeding of the 2007 Southern Conservation Agricultural System Conference 214–222.

Chapter 5: Soil Loosening of a Compact Disc Harrow as Affected by Disc Spacing and Offset *

*Published in Transactions of the ASABE (in press).

5.1. Abstract

The Compact disc harrow (CDH) is a relatively new type of conservation tillage implement. Its disc arrangement on the implement is critical to the tillage performance. The objective of this study was to investigate the effects of disc spacing and offset on the tillage performance of a CDH. Tests were conducted in an indoor soil bin using a three-disc unit. The spacing of the two rear discs was set at 203, 254, or 305 mm, and the front disc was set at one of three offset positions: left, centre, or right, relative to the rear two discs. The discs were operated at two different tillage depths: shallow (63.5 mm) and deep (127 mm). The results showed that the soil cutting area ratio (the ratio of disturbed area to the total area of the furrow) decreased as the spacing increased from 203 to 305 mm; in contrast, the soil loosening efficiency (the ratio of soil disturbance area to draft force) remained constant in the shallow tillage depth, and increased in the deep tillage depth. As for the effect of offset, the centre position resulted in a soil cutting area ratio of more than 80%, which was superior to the other offset positions. However, the left offset had the highest efficiency of 15.3 and 22 $mm^2 N^{-1}$ in shallow and deep harrowing, respectively. The common standard disc spacing of 254 mm with the centre offset was not necessarily the optimal setting, depending on working depth and tillage performance indicators of interest.

5.2. Introduction

Sustainable farming has progressed from a conventional system of deep tillage to a conservation system of shallow tillage or no-tillage (Khosravani et al., 2004; Lal et al., 2007). Shallow tillage aims to leave some crop residue on the soil surface for soil protection and to prepare seedbeds at minimal cost. Compact disc harrow (CDH) is one of the latest forms of shallow tillage equipment. CDH was originated in Western Europe during 1990's and was introduced recently to North America (Kanicki, 2014). Several agricultural machinery manufacturers have released their CDH machines, e.g., Speedtiller of K-Line Ag (Cavalier, North Dakota, USA), Rubin of Lemken (Alpen, North Rhine-Westphalia, Germany), and Fury of Versatile (Winnipeg, Manitoba, Canada). A CDH typically consists of two rows of discs followed by finishing tools, such as finger tines or roller baskets. Unlike the gang angle arrangement of conventional discs, the individually-mounted discs of a CDH can have a gang angle, while keeping the front row parallel to the rear row, which is compact, versatile, and capable of travelling at high speeds. According to Knechtges et al., 2010, a commercial CDH requires about 16% lesser draught force and leaves a smoother soil surface as compared to a conventional cultivator.

However, the large disc spacing of CDH may negatively affect the uniformity of the tillage layer that is crucial for plant growth and yield (Hakansson et al., 2002; Atkinson et al., 2009; Celik et al., 2013). The tillage layer produced by disc harrows has untilled ridges at the bottom of the tilled layer (Gill and Hendrick, 1976; Celik et al., 2008). Therefore, soil furrow bottom profile should be carefully examined prior to the use of CDH to assess the uniformity of tillage layer. Among the parameters affecting soil

uniformity, disc spacing and offset of front row relative to the rear row are of great importance (Willatt and Willis, 1965; Spoor and Godwin, 1978; Godwin et al., 1984). Increasing disc spacing resulted in increased height of the unloosened soil ridge in the furrow profiles (Hang et al., 2018). Typical CDHs on the market have discs spaced at 254 mm (10 in) apart in each of the two rows and discs on the front row passed the centreline of the rear discs. It was worth investigating whether such an arrangement would result in the optimal uniformity of tillage layer. A higher degree of soil disturbance uniformity may correspond to a larger draft force and thus a higher power requirement. Therefore, draft force is also an important performance indicator of a tillage equipment. An index, soil loosening efficiency, considering both soil disturbance and draft force, was recommended to assess the overall performance of a tillage implement (McKyes, 1985).

For disc implements, most existing studies focused on soil cutting forces as affected by design parameters (such as disc diameter and concavity) and operational parameters (such as gang and tilt angles, and tillage depth). A mathematical model for predicting soil reaction forces on discs with gang and tilt angles was proposed and experimentally verified to account for disc geometries, soil properties, and tillage depth (Alam, 1989). An analytical examination of the effects of disc geometrical and operational parameters on its areas of contact with soil showed that the gang angle and tillage depth had more effects on soil disturbance area than the tilt angle and disc concavity (O'Dogherty et al., 1996). Few studies have been conducted on field-scale disc implements and the interactions of soil disturbance between discs. A field study on a disc harrow demonstrated that decreasing the gang angle would enable an operation at higher speeds, which would increase the work rate and decrease the fuel consumption with a

86

similar soil disturbance level (Serrano et al., 2003). Soil cutting forces of a disc gang were linearly correlated with the interaction between discs occurred in terms of the draft force (Chapman et al., 1988). The previous studies were mainly limited to conventional discs such as tandem discs, offset discs, and disc plows, which are different from a CDH in the range and scale of design parameters. The only study on CDH found was on the draft force as affected by gang angle and tilt angle (Kogut et al., 2016). The objectives of this study were to investigate the soil loosening characteristics of a CDH as affected by (1) disc spacing and (2) offset of the front disc relative to the rear discs.

5.3. Material and methods

5.3.1. Testing facility and discs

An indoor soil bin test of CDH was conducted in the Soil Dynamics and Machinery Lab, University of Manitoba, Canada. The soil in the bin was a sandy loam with 70% sand, 16% silt, and 14% clay. The soil had an average moisture content of 21.2 $\pm$ 0.8% (dry basis) and an average bulk density of 1.73 $\pm$ 0.14 Mg m^{-3}, measured using the soil core (50 mm in diameter and 150 mm in depth) and oven-drying method. The soil was prepared to a similar soil condition before each test by following the cultivating-leveling-compacting soil preparation procedure described in Hasimu and Chen (2014).

The CDH studied had individually mounted discs which were 508 mm (20 in) shallow-concavity discs. The shanks were mounted on the toolbar through rubber-cushion brackets. Discs were arranged in two rows and the gang angles of the front and rear rows were in the opposite direction (Fig. 5.1a). For soil bin tests, a small unit of three discs (labeled with highlighted stars) was used with two discs in the rear and one in the front. Figure 5.1b shows that such a three-disc unit would create a soil furrow with two

untilled soil ridges. Arraying these two ridges in an end-to-end fashion would form the

entire soil furrow bottom of a whole CDH implement. This demonstrated that the three-

disc unit would represent a CDH implement in terms of soil loosening pattern. The three-

disc unit was fabricated, and it was connected to the hitch of the soil bin carriage (Fig.

5.2). The disc position could be adjusted sideways along the toolbar to achieve the

desired disc spacing and offset distance for the tests. The distance between the front and

rear rows was 800 mm. The front disc and rear discs had a gang angle of 17° and 15°,

respectively. All discs were tilted at an angle of 20°. These parameters were selected

based on the disc configurations in the CDH implement.

(a)

Travel direction

Gang angle

(b)

Tilt angle

Offset

Spacing

A unit
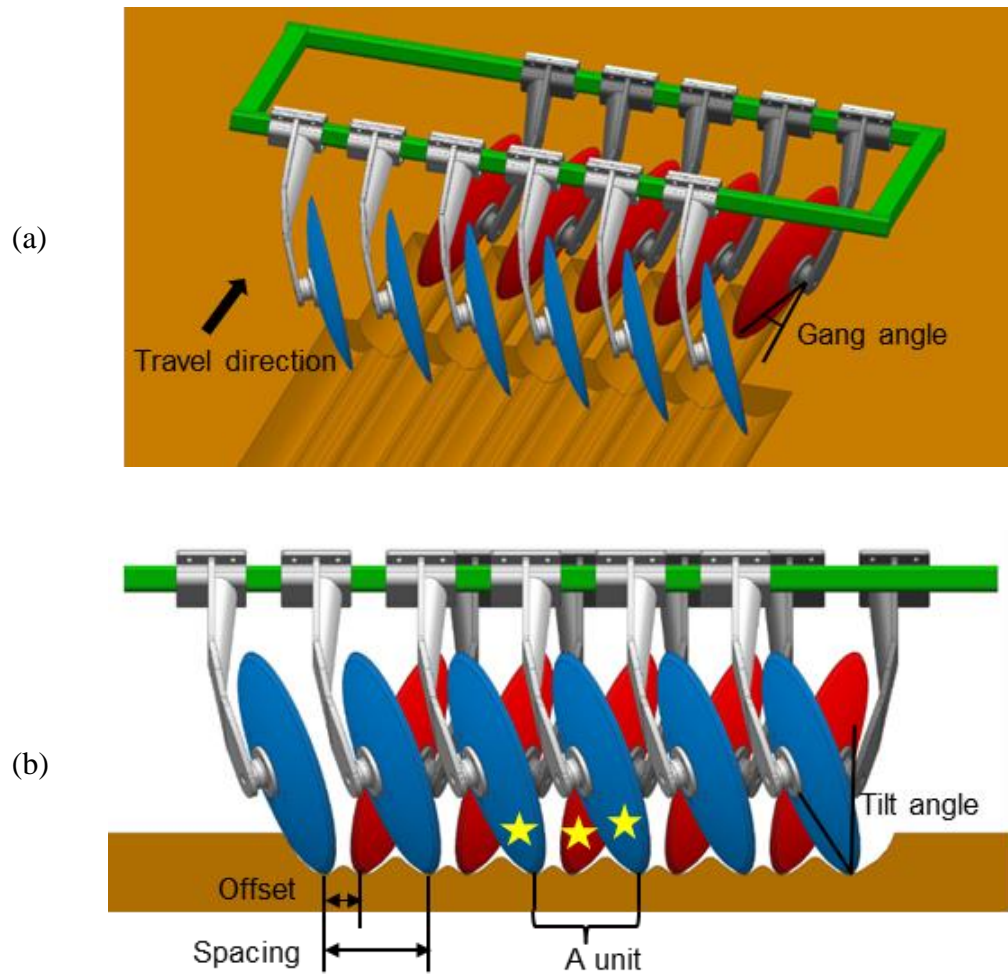
Figure 5.1. An illustrative sketch of a compact disc harrow: (a) the front and rear discs are staggered to each other along the travel direction; (b) the rear view demonstrates the definitions of disc spacing and offset. The furrow bottom profile features untilled ridges across the tillage layer. Note: loosened soil in the furrow is not shown here.
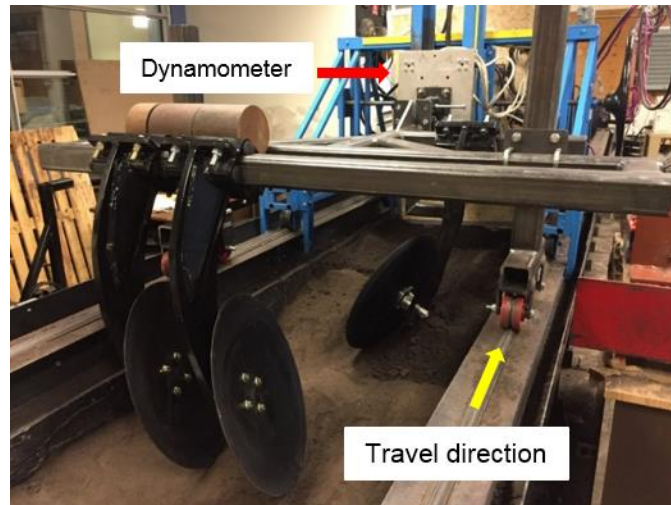
Figure 5.2. The three-disc testing unit connected with the soil bin carriage through a dynamometer.

5.3.2. Experimental design

A completely randomized experimental design was followed. The experimental factors were spacing of rear discs and offset position of the front disc relative to the rear discs, as defined in Fig. 5.1b. Nine treatments combined of three disc spacings and three offset positions were tested in a random order with four replications. The three spacings of narrow (S_N), standard (S_S), and wide (S_W) were at values of 203 mm, 254 mm, and 305 mm, respectively. The three offset positions were at ¼, ½, and ¾ of each spacing value, namely the positions: the left (O_L), the centre (O_C), and the right (O_R). Experiments were conducted at two different tillage depths of 63.5 and 127 mm representing shallow and deep harrowing, respectively. A constant working speed of 2.78 m s^{-1} (10 km h^{-1}) was used for all tests, which was the highest speed could achieve using the testing facility.

5.3.3. Measurements

5.3.3.1. Furrow profile

Soil furrow profile, measured on transects perpendicular to the tractor travel direction, has been proved to be a reliable characteristic to evaluate soil disturbance (Tessier, 1988). In this study, a soil profile meter consisting of a row of 3 mm square steel pins (Tessier et al., 1989) was used to measure the furrow bottom profile (Fig. 5.3a). There was no space between adjacent pins and 200 pins provided a measuring width of 600 mm. After each run, the loosened soil was carefully removed away from the furrow to expose the undisturbed furrow bottom. The soil profile meter was placed across the furrow. The handles of the profile meter were then triggered, and the pins fell to follow the furrow profile. The furrow profile, as depicted by the relative position of the pins to the original soil surface, was traced on a drafting paper. The recorded furrow profile was scanned (Fig. 5.3b). The section of interest was the segment between the bottom points of the two rear discs, which also included the soil disturbance of the front disc. A rectangle with a width of the disc spacing and a height of the tillage depth was placed as the top edge aligned with the soil surface to confine the section of interest (Fig. 5.3c). The rectangular section was then extracted and the undisturbed soil ridges were painted in dark colour (Fig. 5.3d). This measurement was performed at three random locations along the tool path for each run. Readers should note that the measured furrow profile is the bottom profile after removing loosened soil, which is related to soil compactness and preparedness for seeding and plant growth, whereas the furrow profile without removing loosened soil as is usually seen in the literature (e.g., Zobeck and Onstad, 1987) is associated with soil erosion.
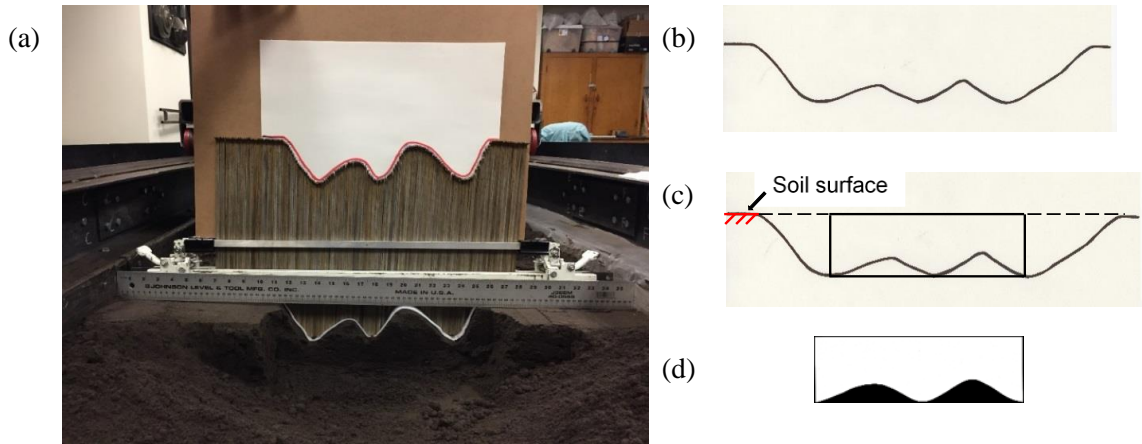
Figure 5.3. Furrow profile measurement using a soil profile meter (a); traced furrow profile (b); the section of interest confined by a rectangle with a width of the disc spacing and a height of the tillage depth (c); extracted rectangular section showing soil furrow bottom with ridges in dark colour (d).

5.3.3.2. Furrow characteristics

A typical furrow bottom included two unequal ridges (Fig. 5.4), which reflected two features. One was that not all area in the tillage layer was disturbed, and the other was that the furrow bottom was not even, but ridged. If the actual tillage depth was D and the height of the large ridge was H, the soil layer completely disturbed by the discs was the layer above the large ridge, and the loosened layer had a thickness of (D-H). The ΔH was the difference between the heights of the two ridges, which reflected the variation of the ridge height. Large values of H and ΔH were considered to be unfavourable for soil uniformity within the tilled cross-section area. The soil furrow profiles were then imported to MATLAB to obtain the total area of two ridges (A_{ridge}) by counting the dark-coloured pixels. Another important performance indicator was the ratio of disturbed area to the total area of the section of interest, which represented the fraction of the area

disturbed by the discs, relative to the cross-sectional area of the total area targeted for loosening. The area ratio was calculated by the equation (1):

$$A_\Phi = \frac{S \times D - A_{ridge}}{S \times D} \times 100\% \qquad (5.1)$$

where

A_Φ = the area ratio (dimensionless),

A_{ridge} = the total area of ridges (mm^2),

S = the disc spacing (mm),

D = the tillage depth (mm).

A larger cutting area ratio indicates better uniformity of soil disturbance.
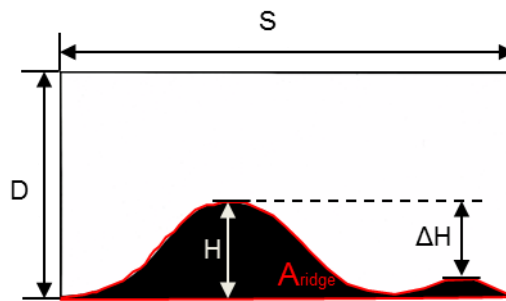
Figure 5.4. Diagram showing furrow profile characteristics: disc spacing (*S*), actual tillage depth (*D*), ridge height (*H*), ridge height variation (Δ*H*), and the total area of ridges (*A$_{ridge}$*).

5.3.3.3. Soil loosening efficiency

The draft force (*F*) of the testing unit was measured using a compact dynamometer as shown in Fig. 5.2a. The dynamometer was specifically designed for the

soil bin by placing four 3D load cells (Michigan Scientific, Model TR3D-A-5K, Michigan Scientific Corporation, Charlevoix, Mich., USA) in between two rectangular aluminum plates with one sensor in each corner (Mahadi et al., 2017). The dynamometer had a negligible cross sensitivity between three directions (longitudinal, lateral, and vertical), i.e., the measured draft force was statistically independent of the lateral and vertical forces. The soil loosening efficiency (η) (McKyes, 1985) was defined as follows:

$$\eta = \frac{A}{F} \qquad\qquad (5.2)$$

where

η = the soil loosening efficiency ($mm^2\ N^{-1}$),

A = the soil disturbance area of the three-disc unit and equals to $(S \times D - A_{ridge})$ (mm^2),

F = the draft force of the three discs (N).

5.3.4. Data analysis

Analysis of variance (ANOVA) was performed using statistical software (SAS for Windows v 9.4) to examine the main effects of the experimental factors (disc spacing and offset) as well as their interactions on the A_Φ and η at each tillage depth. The means between treatments were compared with Duncan's multiple range tests at the significance level of 0.05.

5.4. Results and discussions

5.4.1. Furrow profile

A representative furrow profile was randomly selected from each treatment to qualitatively assess the soil uniformity (Fig. 5.5). All furrow profiles comprised untilled

ridges and the two ridges had different sizes. The left ridge lay between the front disc and the rear disc on the left. The right ridge lay between the front disc and the rear disc on the right. Having small ridges with uniform height gives for better performance of tillage, allowing to achieve uniform bulk density all over the furrow for even plant growth.

In the shallow harrowing (Fig. 5.5a), a ridge was as high as the original soil surface at three disc arrangements of S_S-O_L, S_W-O_L, and S_W-O_R, which were not desirable, and two were observed for the case of O_L. This was not seen for the O_C with any disc spacing. These results indicated that the left offset position was more vulnerable to undesired furrow profile than the centre position. Also, more uniform ridge heights were observed for the O_C, as compared with the O_R. By shifting the front disc from the centre position either to the left or to the right, it caused larger ridges and more uneven ridge height, as expected.

In the deep harrowing, untilled ridge with a height of tillage depth was not observed in any of the treatments (Fig. 5.5b). The ridge on the left tended to be convex and that on the right tended to be concave. This might be due to the orientation of the discs where one ridge was formed between two concave surfaces of the discs and the other was between two convex surfaces. The O_C had the most symmetric furrow profiles. Unlike the shallow harrowing, the differences in the furrow profile between the O_L and O_R were marginal in the deep harrowing. The furrow profile of the O_L basically mirrored that of the O_R at the same spacing. The differences in the furrow profile were more remarkable as the spacing increased from S_S to S_W, as compared to that resulting from an increase of spacing from S_N to S_S.

The disc geometry is also projected along with the soil furrow profile (Fig. 5.5). The concave ridge had a close match with the projected disc geometry; while the convex ridge differed significantly from the geometry. The soil pulverization action between the two concave surfaces of the discs contributed to the large difference in the convex ridge, which made it is impossible to predict the theoretical height of the ridge based on the projected disc geometry. Overlaying the soil furrow profiles of shallow and deep harrowing found that the overall trend was similar at the same tool arrangement (results not shown). The variation of soil furrow profiles among replications was smaller at the deep harrowing than that of the shallow harrowing, which indicated different soil fracture modes at different working depths.
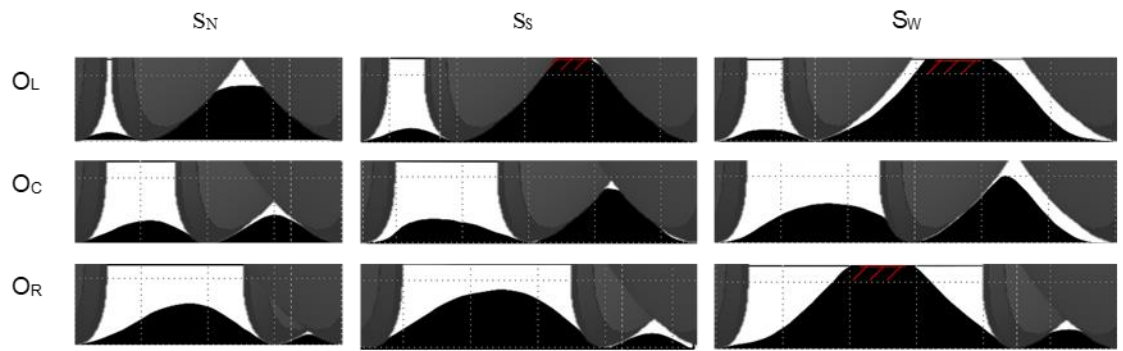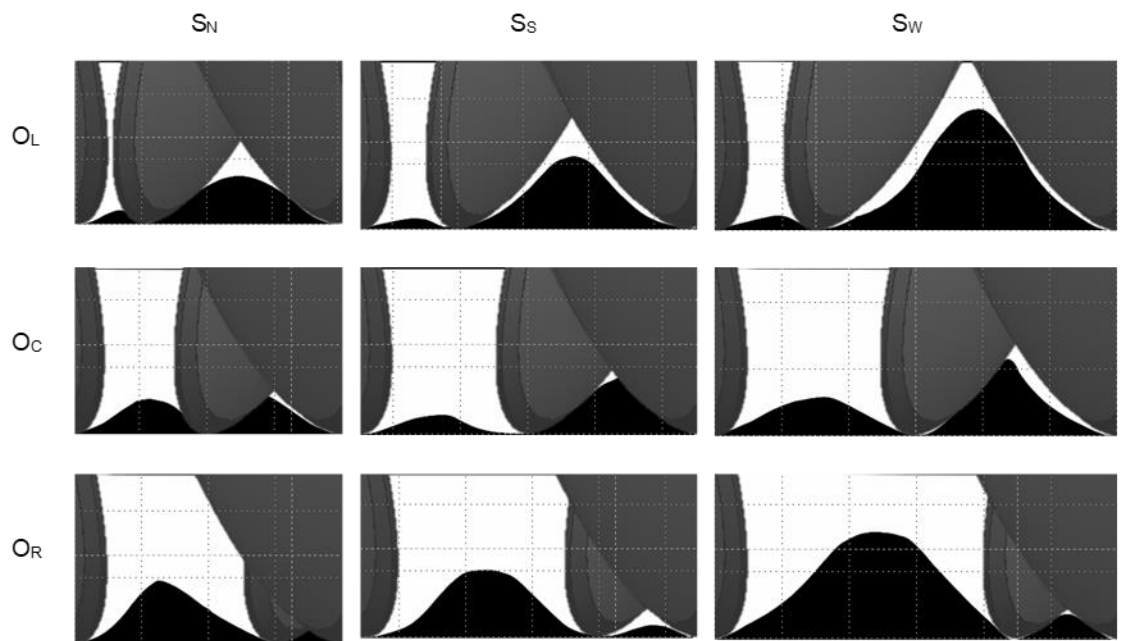
Figure 5.5. Representative furrow profiles and projected disc geometries in the shallow

(a) and deep harrowing (b); columns for different spacing values (S_N: 203 mm; S_S: 254

mm; S_W: 305 mm) and rows for different offset positions (O_L: left; O_C: centre; O_R: right).

The ground symbol in red indicates untilled ridges up to the soil surface.

5.4.2. Ridge height

The ridge height (H) and its variation (ΔH) on the furrow profile of each treatment were quantitatively assessed (Table 5.1). The smaller the H and ΔH were, the better tillage performance was achieved.

In the shallow harrowing, the S_N-O_C arrangement had the lowest H of 24.1 mm. All the other H values ranging from 34.8 to 63.5 mm were more than half of the target tillage depth of 63.5 mm. The S_N resulted in the lowest H at all offsets. The S_S-O_C arrangement had a similar H with that of the S_N-O_L arrangement, which was the highest in the S_N category. The three arrangements with the highest ridges, as expected, had an H of 63.5 mm. The S_N-O_C arrangement had the minimum ΔH of 3 mm, which was the only one less than a quarter of the target tillage depth. The three arrangements with the highest H had ΔH ranged from 47.8 to 53.8 mm, which accounted for more than three-fourths of the target tillage depth.

In the deep harrowing, all the arrangements of spacing-offset, except for S_W-O_L and S_W-O_R, had an H value of less than half of the target tillage depth. This indicated that, generally, more desired soil disturbance conditions were obtained in the deep harrowing as compared to the shallow harrowing. The S_N-O_C resulted in the minimum H of 24.9 mm, which accounted for only 20% of the target tillage depth. As the H increased from 24.9 to 92.7 mm, the ΔH increased from 5.9 to 81.6 mm.

Table 5.1. The ridge height (H) and ridge height variation (ΔH) of the shallow and deep harrowing at different spacing values (S_N: 203 mm; S_S: 254 mm; S_W: 305 mm) and offset positions (O_L: left; O_C: centre; O_R: right)

		Value (mm)	S_N	S_S	S_W
Shallow harrowing	H	O_L	42.7±1.9	63.5±0	63.5±0
		O_C	24.1±1.8	43.2±1.3	51.6±1.9
		O_R	34.8±2.4	44.7±3.7	63.5±0
	ΔH	O_L	35.9±2.5	53.8±1.2	52.6±1.3
		O_C	3.0±0.5	22.9±0.9	21.2±2.5
		O_R	24.1±2.1	34.2±1.9	47.8±0.9
Deep harrowing	H	O_L	38.4±1.1	62.7±1.6	92.7±2.8
		O_C	24.9±1.7	47.2±0.9	54.6±1.4
		O_R	39.4±2.1	53.1±3.4	83.8±3.9
	ΔH	O_L	26.4±1.2	47.3±1.4	81.6±2.9
		O_C	5.9±0.8	31.2±1.1	30.2±1.2
		O_R	31.9±1.9	42.1±2.1	62.2±4.1

5.4.3. Cutting area ratio

The aim of tillage was to have a cutting area ratio (A_Φ) of 100%. The A_Φ was significantly affected by the spacing and offset in the shallow harrowing (Fig. 5.6a). The narrower the discs were spaced, the higher the A_Φ was. The A_Φ of the S_N (75.7%) was significantly higher than that of the S_S (67.6%). The S_W spacing had the lowest A_Φ of 61%, which was significantly different from the other spacing values. The O_C had the highest A_Φ of 76.7% and was significantly higher than the O_R (66.4%), which were both significantly higher than the O_L (61.1%).

The spacing and offset had similar effects on the A_Φ in the deep harrowing as in the shallow harrowing (Fig. 5.6b). However, it was less significant as the depth increased. There were no statistical differences in the A_Φ between the S_N and S_S and between the O_L and O_R in the deep harrowing. The S_N and S_S had a ratio of 84.5% and 83.6% respectively, which were higher than 75.3% of the S_W. The O_C resulted in an A_Φ of 84.3%, which was higher than either 78.8% of the O_L or 80.3% of the O_R.

(a)   (b)
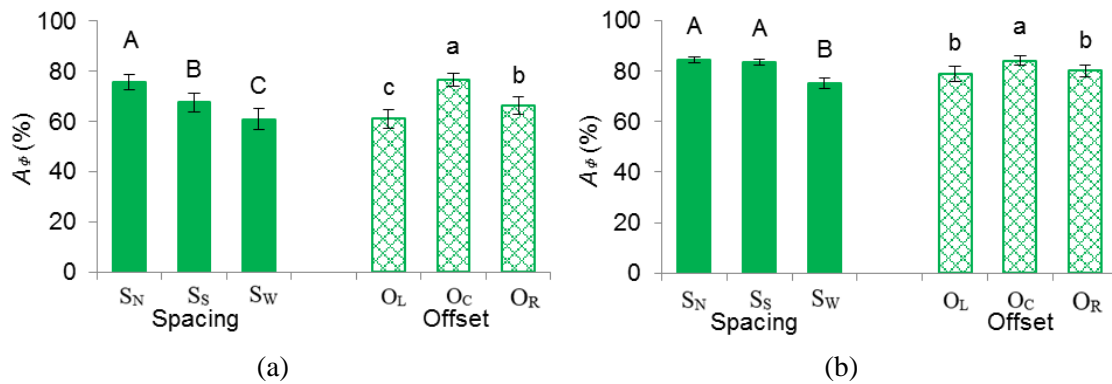
Figure 5.6. Cutting area ratio (A_Φ) of the shallow (a) and deep harrowing (b) as affected by the disc spacing (S_N: 203 mm; S_S: 254 mm; S_W: 305 mm) and offset (O_L: left; O_C: centre; O_R: right). Means followed by different letters are significantly different according to Duncan's multiple range test at the significance level of 0.05; error bars are standard deviations.

5.4.4. Soil loosening efficiency

The significant differences in the soil loosening efficiency (η) were found among different offset positions (Fig. 5.7). As the front disc moved from the left to the right, the η increased from 10 to 15.3 mm^2 N^{-1} and from 18 to 22 mm^2 N^{-1} in the shallow and deep harrowing, respectively. The η of the O_R was significantly higher than that of the other

100

offset positions. The O_C had a 40% higher η than the O_L in the shallow harrowing and the η of the O_R was 22% higher than that of the O_L in the deep harrowing. The three spacing values had similar η with an average value of 13.1 mm^2 N^{-1} in the shallow harrowing. However, in the deep harrowing, the S_W had a η of 23.1 mm^2 N^{-1}, which was significantly higher than that of the S_N and S_S by 29% and 21% respectively.
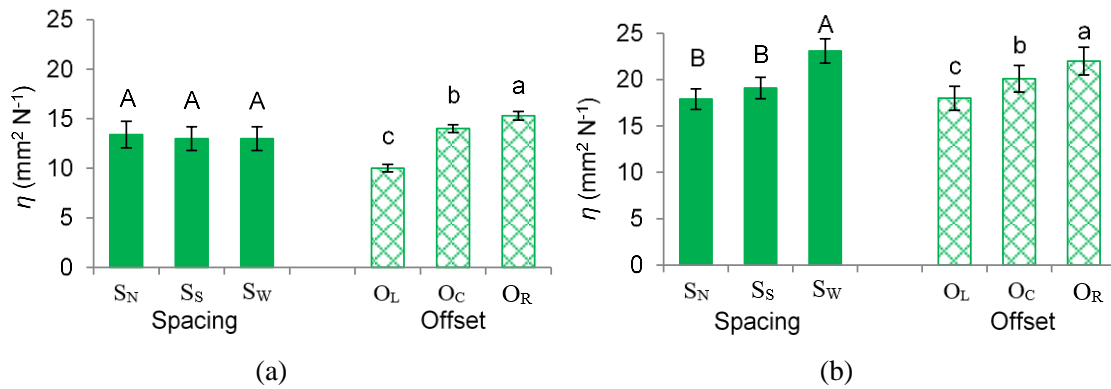
Figure 5.7. Soil loosening efficiency (η) of the shallow (a) and deep harrowing (b) as affected by the disc spacing (S_N: 203 mm; S_S: 254 mm; S_W: 305 mm) and offset (O_L: left; O_C: centre; O_R: right). Means followed by different letters are significantly different according to Duncan's multiple range test at the significance level of 0.05; error bars are standard deviations.

5.4.5. Discussion

Given the fact that the harrowing is followed immediately by seeding (ASABE Standard EP291.3, 2013), the fraction of the area disturbed by the harrowing (area in green) to the cross-sectional area of the layer to be seeded (area within the red box) was defined as seedbed disturbing area ratio (Fig. 5.8a) and was calculated on the soil furrow profiles through image processing in MATLAB. Only deep harrowing scenario with different disc spacings is shown here as an example, where the seedbed disturbing area

ratio was assessed at different seeding depths ranging from 25 to 125 mm with an increment of 25 mm (Fig. 5.8b). For instance, a seedbed disturbing area ratio of 93.8% at a seeding depth of 100 mm and the narrow spacing represented that 93.8% of the seedbed of 100 mm deep was disturbed. A thoroughly disturbed seedbed was obtained at a shallow seeding depth of 25 mm at any spacing value. The seedbed disturbing area ratio increased as the seeding depth decreased and the change was more noticeable at the S_W, where the ratio was minimal among the three spacing values at any given deep seeding depth. For a medium seeding depth of 75 mm, the three spacing settings had similar area ratios of more than 90%.

(a)   (b)
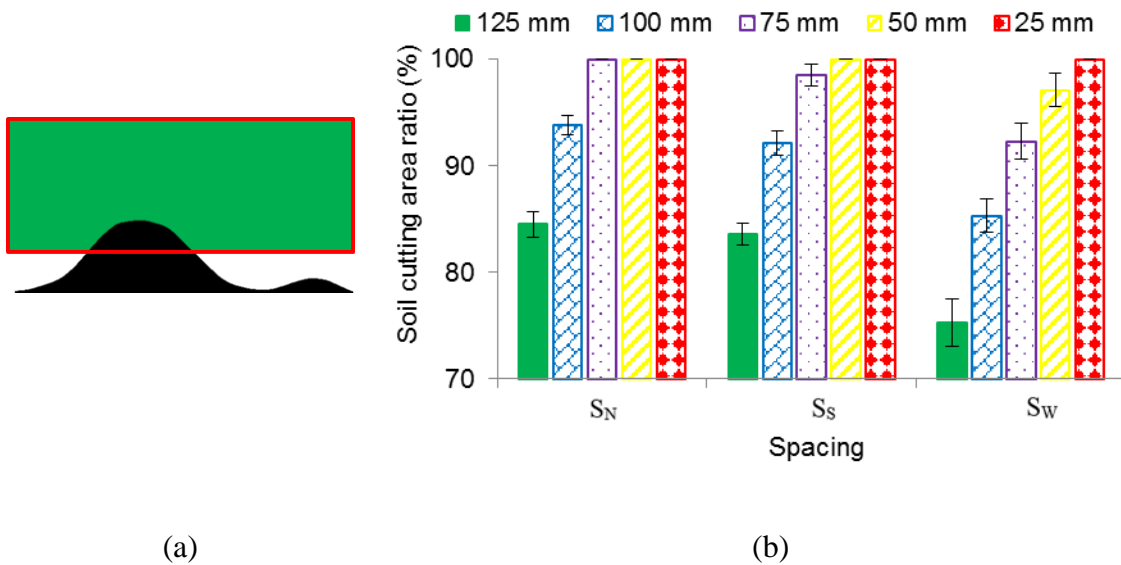
Figure 5.8. Seedbed disturbing area ratio: demonstration (a) and values (b) at different seeding depths for different disc spacings (S_N: 203 mm; S_S: 254 mm; S_W: 305 mm). Error bars are standard deviations.

In general, the furrow profiles demonstrated various levels of irregularity and completeness at different arrangements of the spacing and offset. None of them had a

102

traversed area completely tilled, which can be quantified by either a zero H or an A_Φ value of 100% as might be in the intensive tillage of sweep cultivating. The disc spacing and offset had dissimilar effects on the A_Φ and η. The A_Φ decreased as the spacing increased from 203 to 305 mm; in contrast, the η kept constant and increased in the shallow and deep harrowing, respectively, as the spacing increased from 203 to 305 mm. As for the offset, the O_C was superior to the others in terms of the A_Φ; on the other hand, the O_R stood out with regard to the η. For the shallow harrowing, the optimal disc spacing value was 203 mm and the optimal offset position was the O_C. For the deep harrowing, if a medium seeding depth of 75 mm was required, the 305 mm spacing would be the most cost-effective consideration as demonstrated by the highest η and a soil disturbance ratio of more than 90%. It was speculated that the optimal offset position existed at an intermediate level of the O_C and O_R, i.e., when the front disc sitting between ½ and ¾ of the two rear discs. There were two reasons for the speculation: (a) a more uniform furrow profile would be obtained at an offset between the O_C and O_R as observed in the furrow profiles (Fig. 5.5); (b) the confounding effect of the offset on the A_Φ and η suggested a trade-off offset between the O_C and O_R to achieve an overall optimal performance. Future research was warranted to identify the value of the optimal offset.

The results of this study were compared with limited data available in the literature. The general shape of the furrow profile was in agreement with that reported in Arvidsson et al. (2004) of a disc harrow. The average soil loosening efficiency was in the same magnitude as that of a disc harrow operated at similar disc spacing and tillage depth in Arvidsson et al. (2004). Values of the cutting area ratio measured were close, less than 10% differences, to that calculated based on the projected area of a gang of disc at a disc

angle of 45º in O'Dogherty et al. (1996), which indicated that a reduction of gang angle from 45º (disc plow) to 15º/17º (CDH) was compensated by adding a proceeding disc between two adjacent discs in creating a similar aggressiveness of soil disturbance. The effect of disc spacing on soil cutting area ratio agreed with the analytical investigation of the soil disturbance area based on projected cut geometry in relation to disc spacing of a disc plow (O'Dogherty et al., 1996). Increasing the tillage depth from 63.5 to 127 mm increased the soil loosening efficiency from an average of 13.1 to 20.0 $mm^2 N^{-1}$, which was in agreement with the specific resistance results in Hendrick and Gill (1971) and Al-Ghazal (1989). A mathematical model to predict the draft force of multiple interacting tines found that a tool spacing of 1.4 times of the tillage depth would result in minimum specific resistance (Godwin et al., 1984). However, the disc spacing had no significant effect on the specific draft force in the shallow harrowing and the minimum specific draft force corresponded to a disc spacing of 2.4 times of the tillage depth in the deep harrowing. The discrepancy may be due to the different soil disturbance mechanisms between a tine and disc (Fig. 5.9). No data could be found on the effect of tool offset on the tillage performance of disc implements.

Figure 5.9. A sketch showing different soil disturbance mechanisms of a tine and disc.

The commonly used arrangement of S_S-O_C had the second largest A_Φ of 75.9% and 85.5% in the shallow and deep harrowing, respectively, which were lower than that of 83.0% and 87.0% of the S_N-O_C arrangement. This was inconsistent with the suboptimal H and ΔH values of the S_S-O_C arrangement. The S_N-O_C arrangement outperformed the other arrangements in disturbing soil and creating the most uniform seedbed. From the perspective of efficiency, however, the S_N-O_R and S_W-O_R arrangements had the highest h of 16.0 and 25.4 $mm^2\,N^{-1}$ in the shallow and deep harrowing respectively, which were higher than that of 14.1 and 19.3 $mm^2\,N^{-1}$ of the S_N-O_C arrangement. The S_N-O_C arrangement was not as effective in increasing soil loosening efficiency as in improving soil disturbance uniformity.

The results of A_Φ and η depicted a comprehensive tillage performance. Of practical interest, however, the performance indicators were the thickness of the layer being completely disturbed (D-H), since a considerable tillage depth variation might cause significant variability in soil resistance acting on the seed drills, which generated unwanted vibrations and, consequently, a non-uniform seed placement. For example, the spatial variability of soil mechanical properties in a field resulted in an 8 mm variation in seeding depth in relation to the target depth of 30 mm (Nielsen et al., 2018). It was therefore not recommended to set a seeding depth greater than the value of (D-H) due to a risk of impeding seeding quality and plant growth when using a mechanical seed drill. The information gained in this study was important in the design and use of a CDH. For a particular tillage depth, there were critical disc arrangements, at which the height of untilled ridges equaled to the tillage depth. For example, the S_W-O_L arrangement in this study had furrow ridges extended to the surface of the soil at a tillage depth of 63.5 mm.

These should be avoided when employing a CDH in practice by all means. A tool positioning mechanism for adjusting the relative lateral position of the discs would be beneficial to have in a CDH considering the variability in tillage performance as associated with the disc arrangement. However, it should be borne in mind that a decreased spacing value would increase the costs of manufacture and operation since there would be more discs needed for a given working width. This will also increase the draft force required per unit width of the implement, and in turn the tractor power requirement.

5.5. Conclusions

A three-disc unit was tested at a combination of three spacing settings of narrow (203 mm), standard (254 mm), and wide (305 mm) and three offset positions of left, centre, and right to investigate the effects of the spacing and offset on the tillage performance of a compact disc harrow (CDH). The results showed that the disc spacing and offset had significant effects on the tillage performance, and the effects varied with the tillage depth. At the shallow tillage depth, larger disc spacing resulted in smaller cutting area ratios with negligible changes in the soil loosening efficiency. At the deep tillage depth, increasing in disc spacing resulted in increased cutting area ratios and increased soil loosening efficiencies. As for the effect of the disc offset, the centre offset position had the highest cutting area ratios, while the right offset position had the maximum efficiencies, regardless of the tillage depth. The conventionally adopted standard disc spacing (254 mm) without offset (centre position) would not necessarily guarantee the best tillage performance as compared with other disc arrangements. In terms of area ratios, the arrangement of the narrow disc spacing without offset

outperformed the other arrangements; in terms of efficiencies, the arrangement of the wide disc spacing with the right offset was desired. These were true at both the shallow and deep tillage depths. The results obtained can guide the selection of the disc arrangement of a CDH to optimize the tillage performance under different tillage depths.

5.6. Acknowledgement

5.7. References

Alam, M.M., 1989. Soil Reaction Forces on Agricultural Disc Implements. Ph.D. Thesis, University of Newcastle upon Tyne, UK.

Al-Ghazal, A.A., 1989. An Investigation into the Mechanics of Agricultural Discs. Ph.D. Thesis, Cranfield Institute of Technology, Silsoe, Bedford, UK.

Arvidsson, J., Keller, T., Gustafsson, K., 2004. Specific draft force for mouldboard plough, chisel plough and disc harrow at different water contents. Soil & Tillage Research 79, 221–231.

ASABE Standards. 2013. EP291.3 Terminology and Definitions for Soil Tillage and Soil-Tool Relationships. St. Joseph, Mich.: ASABE.

Atkinson, B.S., Sparkes, D.L., Mooney, S.J., 2009. Effect of seedbed cultivation and soil macrostructure on the establishment of winter wheat (Triticum aestivum). Soil & Tillage Research 103, 291–301.

Celik, A., Altikat, S., Way, T.R., 2013. Strip tillage width effects on sunflower seed emergence and yield. Soil & Tillage Research 131, 20–27.

Celik, A., Ozturk, I., Way, T.R., 2008. A theoretical approach for determining the irregularity of soil tillage depth caused by horizontal axis rotary tillers. Agricultural Engineering International: the CIGR Ejournal. Manuscript PM 08 003. Vol. X.

Chapman, M.L., Johnson, C.E., Schafer, R.L., Gill, W.R., 1988. Some performance characteristics of disc gangs. Journal of Agricultural Engineering Research 39, 1–7.

Gill, W.R., Hendrick, J.G., 1976. The irregularity of soil disturbance depth by circular
and rotating tillage tools. Transactions of the ASAE 19(2), 230–233.

Godwin, R.J., Spoor, G., Soomro, M.S., 1984. The effect of tine arrangement on soil
forces and disturbance. Journal of Agricultural Engineering Research 30, 47–56.

Hakansson, I., Myrbeck, A., Etana, A., 2002. A review of research on seedbed
preparation for small grains in Sweden. Soil & Tillage Research 64, 23–40.

Hang, C., Gao, X., Yuan, M., Huang, Y., Zhu, R., 2018. Discrete element simulations and
experiments of soil disturbance as affected by the tine spacing of subsoiler.
Biosystems Engineering 168, 73–82.

Hasimu, A., Chen, Y., 2014. Soil disturbance and draft force of selected seed openers.
Soil & Tillage Research 140, 48–54.

Hendrick, J.G., Gill, W.R., 1971. Rotary tiller design parameters: Part Ⅱ - depth of
tillage. Transactions of the ASAE 14(4), 675–678.

Kanicki, D., 2014. High Speed Compact Discs Are Not Vertical Tillage Tools? Special
Report: Vertical Tillage. http://www.farm-equipment.com/articles. Accessed 11
September 2018.

Khosravani, A., Zabolestani, M., Sharifi, A., Manesh, A.M., Nejad, M.S., Hemmat, A.,
2004. Evaluation of the possibility of shallow tillage in irrigated wheat. Iranian
Journal of Agricultural Engineering Research 4(17), 29–46.

Knechtges, H.J., Koch, F., Meyer, T., Scheit, S., 2010. Comparison of stubble working
with cultivator or compact disc harrow. Landtechnik 65, 51–53.

Kogut, Z., Sergiel, L., Zurek, G., 2016. The effect of the disc setup angles and working depth on disc harrow working resistance. Biosystems Engineering 151, 328–337.

Lal, R., Reicosky, D.C., Hanson, J.D., 2007. Evolution of the plow over 10,000 years and the rationale for no-till farming. Soil & Tillage Research 93, 1–12.

Mahadi, M.R., Chen, Y., Botha, P., 2017. Instrumented soil bin for testing soil-engaging tools. Applied Engineering in Agriculture 33(3), 357–366.

McKyes, E., 1985. Soil Cutting and Tillage. Elsevier, New York.

Nielsen, S.K., Munkholm, L.J., Lamande, M., Norremark, M., Edwards, G.T.C., Green, O., 2018. Seed drill depth control system for precision seeding. Soil & Tillage Research 144, 174–180.

O'Dogherty, M.J., Godwin, R.J., Hana, M.J., Al-Ghazal, A.A., 1996. A geometrical analysis of inclined and tilted spherical plough discs. Journal of Agricultural Engineering Research 63, 205–218.

Serrano, J.M., Peca, J.O., Pinheiro, A., Carvalho, M., Nunes, M., Ribeiro, L., Santos, F., 2003. The effects of gang angle of offset disc harrows on soil tilth, work rate and fuel consumption. Biosystems Engineering 84(2), 171–176.

Spoor, G., Godwin, R.J., 1978. Experimental Investigation into the deep loosening of soil by rigid tines. Journal of Agricultural Engineering Research 23(3), 243–258.

Tessier, S., 1988. Zero-till Furrow Opener Geometry Effects on Wheat Emergence and Seed Zone Properties. Ph.D. Thesis, Washington State University, Pullman, Washington, USA.

Tessier, S., Papendick, R.I., Saxton, K.E., Hyde, G.M., 1989. Roughness meter to measure seed row geometry and soil disturbance. Transactions of the ASAE 32(6), 1871–1873.

Willatt, S.T., Willis, A.H., 1965. A study of the trough formed by the passage of tines through the soil. Journal of Agricultural Engineering Research 10(1), 1–4.

Zobeck, T.M., Onstad, C.A., 1987. Tillage and rainfall effects on random roughness: A review. Soil & Tillage Research 9(1), 1–20.

Chapter 6: Simulation of the Interaction of Soil-Micropenetrometer Using the Discrete Element Method (DEM) *

6.1. Abstract

Understanding of soil cone index is very important in the fields of agricultural engineering and agronomy, as soil cone index affects the energy requirement of field machines and the development of plant roots. In this study, a discrete element model (DEM) was developed to simulate a micropenetrometer and its interaction with soil using Particle Flow Code in Three Dimensions (PFC^{3D}). Dynamic behaviours of the model were investigated under different container sizes and probe configurations. To calibrate and validate the model, laboratory and field tests were conducted to measure soil cone indices of a loamy fine sand soil using the micropenetrometer. The calibrated value of particle stiffness was 10300 N m^{-1} for the soil. Cone indices simulated using the model were comparable with that from field measurements with relative errors below 15% in both a hard soil condition and a soft soil condition. The results showed that increasing the penetration speed in the model resulted in higher cone index outputs and less computational time. The model allowed monitoring of soil cone indices under different soil bulk densities. The simulation results showed that soil cone indices increased linearly with the increase in bulk density.

6.2. Introduction

Soil mechanical properties such as soil cone index (CI) affect seed emergence, root elongation, and crop growth (Taylor and Ratliff, 1969). Soil CI is also related to the energy requirement of field operations (Dawidowski et al., 1988), and vehicle

trafficability (Dexter and Zoebisch, 2002). In the past two centuries, CI has been studied

intensively using experimental methods and mathematical analyzes (Salgado, 2012).

Most experiments were conducted using the standard size cone penetrometers following

ASABE Standards (2004). Only few studies were carried out using micropenetrometers.

Chi and Tessier (1995) introduced a portable micropenetrometer for assessing soil

compaction of a seedbed. They used sleeve-type probes for the micropenetrometer to

minimize the friction force along the probes. That micropenetrometer is further described

later in this paper.

Measurement of soil CI is time-consuming, and micropenetrometer is not always

commercially available. Therefore, this study took a numerical modelling approach to

simulate a micropenetrometer and its interaction with soil. Experimentally, the friction

force along the rod of a penetrometer is not avoidable and will introduce errors in the

measurement of soil resistance on the cone (Barley et al., 1965; Groenevelt et al., 1984).

Although a sleeve-type micropenetrometer could minimize the friction effect, a sleeve

cannot completely eliminate it, as the relative movement between the sleeve and rod

introduces friction force into the CI measurement. Using the numerical model enables

measurement of soil resistance only to the cone, excluding the effect of the interaction

between the rod and soil.

In the past few years, the discrete element method (DEM) has been used to

simulate cone penetration tests. Huang and Ma (1994) proposed a DEM model of cone

penetration test to simulate the effect of soil loading history on the characteristics of soil

failure mechanism. Calvetti and Nova (2005) calibrated parameters for a DEM model by

conducting a series of biaxial tests and used the calibrated model to simulate cone

penetration tests. Jiang et al. (2006) illustrated the effect of soil-penetrometer interface friction on deep penetration mechanisms by constructing a DEM model. Particle Flow Code in Three Dimensions (PFC^{3D}) (Itasca Consulting Group Inc., Minneapolis, USA) has been regarded as an effective tool to simulate tool penetration into soil. Falagush et al. (2012) studied the effect of relative density, mean effective stresses, and particle shape of soil on the CI by building a model using PFC. Butlanska et al. (2014) used PFC in simulating cone penetration tests in a virtual calibration chamber with Ticino sand by multi-scale analysis.

Most of the previous research focused on the standard size cone penetrometers, two-dimensional DEM modelling, and cohesionless soil. They did not provide much information on micropenetrometers and agricultural soil which were the focus of this study. The specific objectives of the study were to (1) develop a three-dimensional numerical model to simulate the interaction of soil-micropenetrometer using PFC^{3D}; (2) calibrate the model using laboratory measurements and validate the model using field measurements; and (3) apply the model to study soil CI as affected by the penetration speed and soil bulk density.

6.3. Methodology

6.3.1. Description of the micropenetrometer

The micropenetrometer, originally designed by Chi and Tessier (1995), was modified and calibrated in this study (Fig. 6.1a). The micropenetrometer consisted of a frame, a sensor unit for measuring soil resistance, a driving system, and a data acquisition system. The frame had foldable handles and wheels, so that it was portable when it was used in fields. The sensor unit had 11 probes (Fig. 6.1b). Each probe consisted of a rod, a

cone, and a light sleeve tube. The sleeve-type probes were to minimize the effect of friction between rods and soil, which could otherwise be added onto the measured CI. The probes were 165 mm long and 2.75 mm in diameter (sleeves' diameters). The cones had a base diameter of 2.75 mm and a cone angle of 57º. The 11 probes were spaced 10 mm apart and were connected to the sensor compartment through 11 load cells (Capacity: 22 N each). The data acquisition system was built from InstruNet (OMEGA Engineering Inc., Stamford, Connecticut, USA) hardware. Voltage signals of the load cells and the potentiometer were recorded at a rate of 5 Hz.

| (a) | (b) |
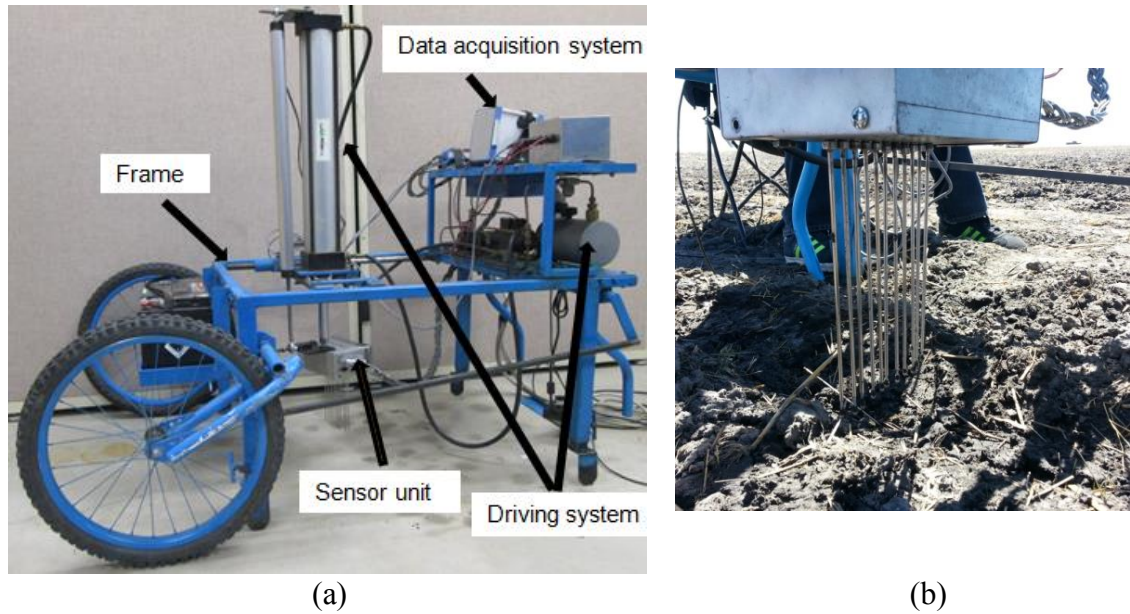
Figure 6.1. Photos of the micropenetrometer: (a) entire unit; (b) eleven probes.

6.3.2. Laboratory tests

For model calibration, laboratory measurements were conducted using a loamy fine sand soil. The soil was taken from the top layer (60 mm) of a field in Manitoba, Canada. The soil was put into aluminum containers (150 mm in diameter and 160 mm in height). Three containers were used as replicates. The soil in the containers was

115

compacted with a modified soil proctor (Fig. 6.2a). On average, the soil dry bulk density in the containers was 1100 kg m^{-3} and the soil moisture content was 26% (dry basis). After compaction, CI of the soil in the containers was measured using the micropenetrometer (Fig. 6.2b). The penetrometer probes were operated at a penetration speed of 3e-4 m s^{-1} (20 mm min^{-1}) and a penetration depth of 60 mm. The data from two side probes were exclusive from calculating the average cone index in order to eliminate any potential edge effects from the container.

(a)   (b)

Figure 6.2. Soil preparation and cone index measurement in the laboratory: (a) container, soil and compacting proctor; (b) penetration test using the micropenetrometer.

6.3.3. Development of soil-micropenetrometer interaction model

A soil-micropenetrometer model was developed using PFC^{3D} to mimic the lab measurement. The model development included construction of a virtual micropenetrometer, generation of soil particles, and execution of penetration test. As the probes were the only parts of the micropenetrometer which interacted with soil, and all the 11 probes were the same, the model micropenetrometer was simplified as a single probe (Fig. 6.3a). The probe was formed using a PFC^{3D} conic wall and a cylindrical wall, representing the cone and the sleeve tube respectively. The geometric parameters were

116

chosen to be the same as the real micropenetrometer. To avoid the frictional effect of the tube, only the vertical force of the conic wall was monitored during the simulation to determine the CI value. Thus, the details about sleeve tube and rod in the real micropenetrometer were not necessary to be included in the model for the model micropenetrometer. The normal stiffness and shear stiffness of the probe in the model were considered to be those of steel, 1e9 N m^{-1} (Mak et al., 2012). The friction coefficient between the probe and soil was assumed to be 0.41, the friction coefficient between soil and tools suggested by Godwin (2007). This value has been used as the input for soil-tool friction in the simulation of soil-tool interaction using PFC^{3D} (e.g., Chen et al., 2013; Li et al., 2016).

Considering the extremely low penetration speed used in the simulation, the number of particles and thus particle size had been limited to achieve a reasonable computational time. From preliminary simulations, the model with a particle size of 2 mm in diameter generated a reasonable CI-depth curve within an acceptable computational duration. Soil particles were generated in a cylindrical container which had a diameter of 20 mm and a height of 80 mm (Fig. 6.3a). The radius of model soil container was chosen based on the distance between two adjacent probes. The container side wall was frictionless to avoid edge effects on the probe. In order to assess the potential edge effects of the container, two larger containers (40 and 80 mm in diameter) were considered with a single probe (Fig. 6.3b, c). Further, in order to assess the effect of neighboring probe interaction in the simulation, two neighboring probes of the probe in the centre were added into the model with a container size of 20 mm (Fig. 6.3d). The containers were filled with soil particles to a height of 70 mm (Fig. 6.3a). The linear

117

contact model and parallel bond model implemented in PFC^{3D} were used to reflect the cohesive behaviour of agricultural soil. The parallel bond can transmit force and moment between particles in tangent and normal directions and thus prevent particles from excessive rotation. This model requires eight micro-properties as inputs, and they are particle normal stiffness: K_n (N m^{-1}), particle shear stiffness: K_s (N m^{-1}), particle friction coefficient: μ (dimensionless), bond normal stiffness: $\overline{K}_n$ (Pa m^{-1}), bond shear stiffness: $\overline{K}_s$ (Pa m^{-1}), bond normal strength: $\overline{\sigma}$ (Pa), bond shear strength: $\overline{\tau}$ (Pa), and bond radius multiplier: $\overline{R}_m$ (dimensionless).

To commence the virtual test, the probe was assigned with the penetration speed of 3e-4 m s^{-1} as in the tests. Once the cone tip reached 60 mm it stopped. As the probe moved down, it interacted with soil particles. The force of the cone in the vertical direction was monitored to be the resistance of the micropenetrometer. The CI was determined by dividing the resistance by the base area of the cone. The two side probes in Figure 6.3d had the same parameters and velocity as the middle one, while the resistance forces acted on them were not recorded as they were only introduced to present the neighboring effect on the middle one. The contact force chains at the final state of the simulation were obtained; and they were, along with the average cone indices, used to evaluate the edge effects of the container and the interaction between neighboring probes. The appropriate container size and probe configuration were selected to calibrate the model parameter.
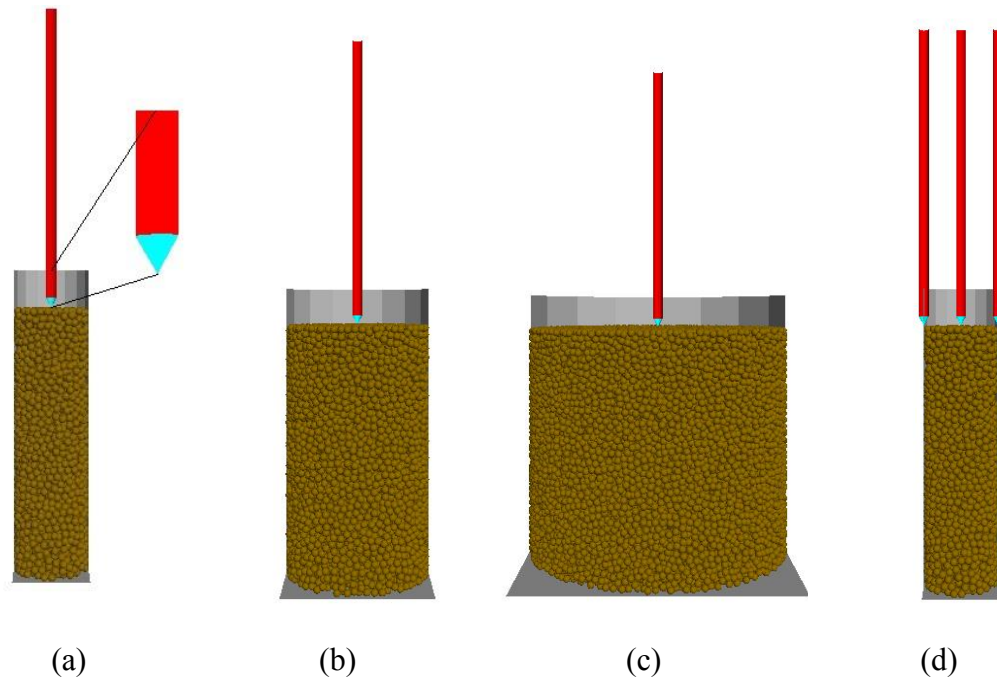
Figure 6.3. Screen captures of soil-micropenetrometer model configurations: (a) a 20 mm container with a single probe (the tip of the probe has been enlarged for better visualization); (b) a 40 mm container with a single probe; (c) an 80 mm container with a single probe; (d) a 20 mm container with three adjacent probes.

6.3.4. Model calibration

Ideally, all the parameters which affected model outputs would need to be calibrated. However, only one parameter can be calibrated. To date, it is not clear on what role of each parameter plays in the model outputs, but all these parameters collectively determine the model outputs which were matched with the behaviour of the material to be simulated in the calibration. In this study, preliminary simulations showed that the predicted CI was most sensitive to the particle stiffness, K_n. Therefore, particle stiffness was chosen to be calibrated. The other parameters were simply taken from Li et al. (2014). This literature was chosen due to a couple of reasons: 1) the soil types used in

the two studies were similar, and 2) Li et al. used a fundamental soil property test (triaxial tests) in matching model outputs and test results, which was considered to be a universal method and independent of model applications. The calibration of K_n was carried out using the laboratory CI data. The model was run with the same penetration speed and depth as that in the lab tests. With a series of assumed K_n values, the model outputs of CI were recorded and compared with the measured values. The final K_n was the one that resulted in the best match between the mean value of the simulated CI and that measured.

6.3.5. Field measurements and model validation

To validate the model, field tests were conducted in the field where the soil was collected for the laboratory tests. To obtain the soil background information of the fields, ten soil cores (50 mm in diameter and 50 mm depth) were taken randomly to determine soil moisture content and dry bulk density. The moisture content (d.b.) was 16.3% for the hard soil and 27.3% for the soft soil. CI measurements were performed in a hard soil condition (a hill top) and a soft soil condition (a low area) of the field. For each soil condition, CI data were taken using the micropenetrometer at three random locations in the same penetration speed and depth as in the laboratory tests. The model was validated by comparing the model outputs CI with field measurements.

6.3.6. Model application

The validated model was used to monitor CI under different penetration speeds and soil bulk densities. Penetration speed is the primary working parameter of the micropenetrometer. The attempts to improve the simulation efficiency were made by altering the penetration speed in the simulation. The decision of the model working parameter was made based on the examination of the relationships between penetration

speed, CI output, and computing time. Soil bulk density is regarded as one of the predominant factors among soil properties which affect soil CI. Soil bulk density can be easily measured in the field using the soil core sampling method, whereas soil CI measurement requires a micropenetrometer which is not always available. The soil bulk density in the simulation can be represented either by constraining soil porosity in particle generation or specifying particle density of soil domain, where the soil porosity reflected sol bulk density from a microstructure perspective while the latter exhibited soil bulk density in the respect of density. In the application of the micropenetrometer that vertically interacted with soil domain, the difference of soil bulk density should be reflected in the change of soil porosity. For model results, the relationship between CI and soil bulk density was obtained, and the relationship can be used to predict CI values using bulk density data.

6.4. Results and discussions

6.4.1. Model behaviours

Simulations were performed using the soil-micropenetrometer model to examine the effects of container size and probe configuration. A computer with an Intel Core i7 CPU with a clock speed of 2.67 GHz was used for all the simulations. The microproperties were assumed to be: $\mu = 0.93$, $\overline{K}_n = \overline{K}_s = $ 1e6 Pa m^{-1}, $\overline{R}_m = 1.0$, $\overline{\tau} = \overline{\sigma} = $ 1e6 Pa. The other parameters were 0.4 for soil porosity, 0.6 for shear damping coefficient, and 0.8 for normal damping coefficient. All these model parameters were derived from Li et al. (2014). The particle stiffness of 1833 kg m^{-3} was determined to have the same bulk density in simulation as that used in the laboratory tests. The particle

normal and shear stiffness were tentatively fixed at 1e4 N m^{-1}, which were to be calibrated later.

The CI-depth curve generally fluctuated around the average value, which is typical for CI results from DEM simulations (Falagush, 2013). The fluctuation may be partly due to the bonds between particles being broken during the course of penetration. A bond broke when external forces, the penetration force in this case, exceeded the strength of the bond, and the interaction between particles became a no-force contact when the bond was broken, resulting in a fluctuation of the force at the soil-micropenetrometer interface. At the end of the penetration, a cutting plane passing through the centre of the container and the probe(s) was obtained and the contact force chains on the plane were plotted in Figure 6.4. The corresponding cone indices for each model configuration in Figure 6.4 were summarized in Table 6.1. The comparisons of the average cone index between the 20 mm single probe container with others were also listed in forms of the relative error.

As can be seen from the screen captures, the stress concentration area due to penetration is generally within a cylinder centred on the probe with a radius of approximately 5 mm. The relatively small stress concentration area and the similar cone index in (a), (b) and (c) implied that the container size did not significantly affect the cone index value. Therefore, it is reasonable to draw the conclusion that the container with a diameter of 20 mm would not cause the edge effect to the penetration. However, potential overlap of the stress concentration area was identified in the case of the model with three probes (Fig. 6.4d), which indicated that two side probes introduced additional stresses on the middle one. This is also evident in the measured cone index, where the

value in the three-probe model was 9.87% higher than that in the single-probe model. Thus, the interaction between adjacent probes with a distance of 10 mm should be taken into consideration when studying the soil-micropenetrometer interaction. Therefore, the 20 mm container with three probes as in Figure 6.4d was determined in this initial model investigation.

(a)   (b)   (c)   (d)
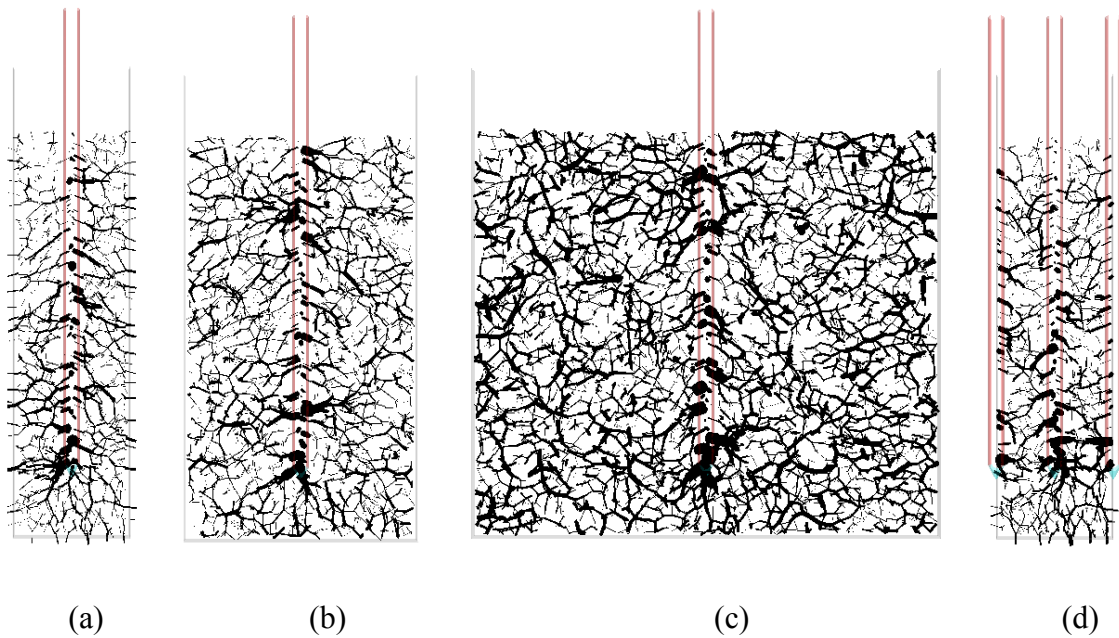
Figure 6.4. Screen captures of the contact force chain on the centre cutting plane of the container showing the physics of soil-micropenetrometer interaction: (a) a 20 mm container with a single probe; (b) a 40 mm container with a single probe; (c) an 80 mm container with a single probe; (d) a 20 mm container with three adjacent probes.

Table 6.1. Comparisons between different model configurations.

Model configuration	Simulated cone index (MPa)	RE[a] (%)
(a) 20 mm + single probe	0.912	N/A
(b) 40 mm + single probe	0.908	0.439
(c) 80 mm + single probe	0.905	0.768
(d) 20 mm + three probes	1.002	9.87

[a] RE = relative error between (a) and others.

6.4.2. Model calibration results

For calibration, the model probe moved down at the same penetration speed as in the lab tests. The value of K_n was adjusted until the simulated average CI matched with the average value measured in the laboratory tests. The agreement between simulation and measurement was evaluated using the relative error (RE). Table 6.2 demonstrates the calibration process. The simulated CI varied from 0.810 to 1.393 MPa with the assumed range of K_n from 3000 to 20000 N m^{-1}. The average value of CI measured in the laboratory tests was 1.014 MPa. When compared this with the simulated CI values from different K_n values, the minimum RE (0.5%) occurred when the K_n was 10300 N m^{-1}, which was the calibrated value of the particle stiffness.

Table 6.2. Particle stiffness calibration results.

Assumed K_n[a] (N m^{-1})	Simulated cone index (MPa)	RE[b] (%)
3000	0.810	20.1
5000	0.909	10.3
8000	0.964	4.93
10000	1.002	1.18
10300	1.019	0.5
11000	1.048	3.35
12000	1.113	9.76
13000	1.136	12.0
14000	1.212	19.5
20000	1.393	37.4

[a] K_n = particle stiffness.

[b] RE = relative error between simulation and measurement.

With the calibrated K_n (10300 N m^{-1}), the simulated CI-depth curve is compared

with the curve from the lab test (Fig. 6.5). A smoothing operator was applied in the

simulation curve to facilitate the comparison. In general, the two curves were

comparable, although the simulation curve showed a more rapid increase at the beginning

and more fluctuation over the course of penetration. This fluctuation also has been found

in other DEM simulations for cone penetration testing (Falagush, 2013). Reducing the

particle size would minimize the fluctuation but at the expense of simulation efficiency.

The rapid increase was mainly attributed to the soil preparation method used in the

model, where a virtual plate was used to compress the soil to achieve the desired

compactness.
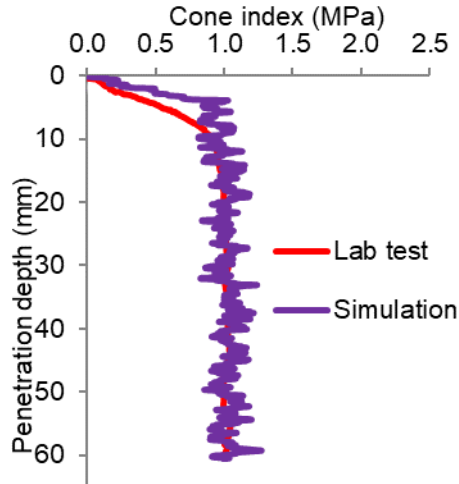
Figure 6.5. The CI-depth curves measured in a laboratory test (average over three replicates) and monitored during simulation using the calibrated particle stiffness.

6.4.3. Model validation results

The average bulk density measured in the field was 1060 kg m^{-3} for the soft soil condition and 1490 kg m^{-3} for the hard soil condition. Cone indices measured in the field were highly variable due to a larger variability in soil condition in the vertical direction compared to the lab soils. Typical CI-depth curves from each probe from field measurements and the average are shown in Figure 6.6. A rapid increasing trend was observed from the depth of 5 to 30 mm, and then the CI gradually increased up to the 50 mm depth. This trend was different with that from the lab tests. For model validation, the measured cone indices were averaged over all probes and all depths for each of the soft and hard soil conditions. The average values are listed in Table 6.3.
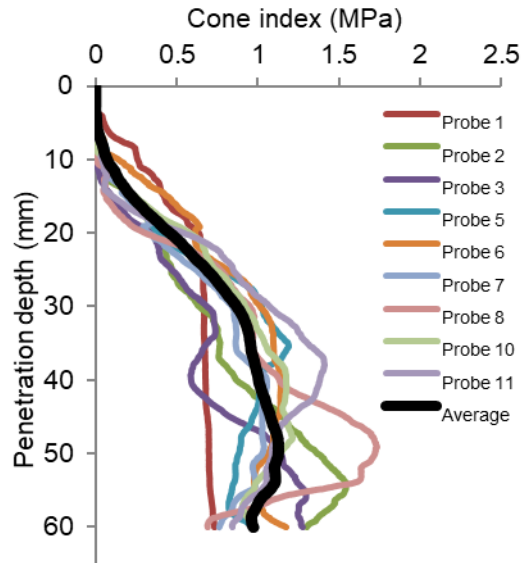
Figure 6.6. Typical CI-depth curves from field tests (a trial from the soft soil condition); data from two probes were missing.

Field measurements were simulated using the calibrated model. The soil domain was prepared in a porosity that resulted in the same bulk density as that measured in the field test. This porosity was derived from the measured dry bulk density for each field and the model particle density. The average CI values simulated are listed in Table 6.3 and they were compared with the averages measured in the field. When compared with those measured, the simulated average CI values were in close agreement, as indicated by the low relative errors of 14.9% for the hard soil condition and 5.5% for the soft soil condition. The discrepancy could be attributed to different conditions (such as moisture content and density variation in the vertical direction) between the lab soil for the model calibration and the field soil for the model validation.

Table 6.3. Simulated average soil cone indices and errors relative to the field measurement data for two soil conditions.

Field condition	Bulk density ($kg\ m^{-3}$)	Measured cone index (MPa)	Simulated cone index (MPa)	RE[a] (%)
Hard soil	1490	1.287	1.479	14.9
Soft soil	1060	0.903	0.853	5.5

[a] RE = relative error between simulation and measurement.

6.4.4. Model application

The validated model was run at various penetration speeds varying from 3e-4 to 3e-1 m s^{-1}. The resultant CI-depth curves are illustrated in Figure 6.7. All the curves had high fluctuations as observed in the model behaviour investigation. However, using smaller particle sizes will reduce the fluctuation of the model results. Higher penetration speed yielded higher CI, and the curve tended to be more fluctuant at a higher speed. The overall trend of the curves was similar to each other among tested speeds, i.e. increasing at the beginning and then keeping statically stable.
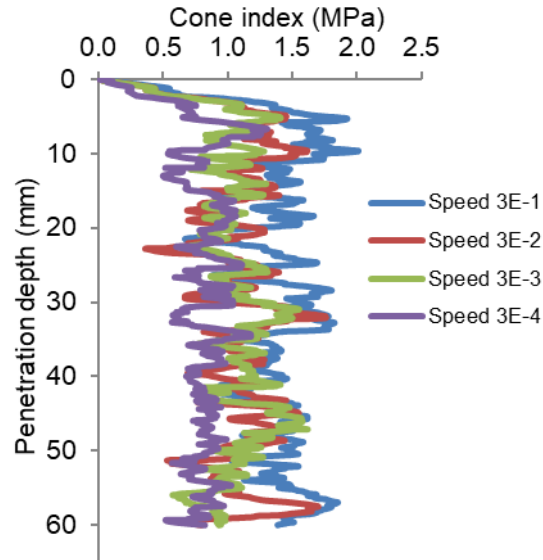
Figure 6.7. Typical simulated CI-depth curves for different penetration speeds (m s^{-1}).

The average CI of each simulation run was obtained from the statically stable section of the CI-depth curve. A summary of the average CI values and computational times is displayed in Table 6.4. The increase in penetration speed from 3e-4 to 3e-1 m s^{-1} resulted in a 37% increase in the average CI and sped up the simulation more than 700 times. A higher penetration speed required significantly less computational time. It is ideal to set the penetration speed in simulation the same as the test to be simulated. However, one may consider using a higher speed in both simulation and test to reduce the computational time, if allowed. Regardless, the penetration speed should be reported together with the simulation results.

Table 6.4. Comparisons between different penetration speeds.

Penetration speed (m s^{-1})	Simulated cone index (MPa)	Computational time[a] (mins)
3e-4	1.019	6080
3e-3	1.174	610
3e-2	1.184	78
3e-1	1.399	8

[a] using a computer with an Intel Core i7 CPU at 2.67 GHz.

The above discussion was limited to only two specific soil conditions, soft and hard that corresponding to bulk densities of 1060 and 1490 kg m^{-3} respectively. In practice, the field condition varied in bulk density, depending on the intensity of tillage and traffic. Simulations were run using the validated model to predict soil cone indices under a wide range of bulk densities. In the simulations, the bulk density of the model particles was varied by altering the particle porosity with a constant particle density of 1833 kg m^{-3}, while the value of particle stiffness calibrated above was used for all simulations. This means that the model results are only applicable to the given soil. The range of bulk density was from 733 to 1558 kg m^{-3} that was a practical range observed in typical fields. Results showed that the simulated average CI was 0.554 MPa at the minimum bulk density of 733 kg m^{-3} and increased to 1.752 MPa at the maximum bulk density of 1558 kg m^{-3} (Fig. 6.8). The relationship between the average CI and bulk density fitted into a linear line with a coefficient of determination (R^2) of 0.97. In comparison with the linear model found by Kumar et al. (2012) through compiling the literature data and by Santos et al. (2012) through statistical analysis, and other models, including power (Hernanz et al., 2000), exponential (Busscher et al., 1997), power-exponential (Upadhyaya et al., 1982), and polynomial (Vasquez et al., 1991), the

considerably high R^2 value obtained in the simulation offered strong confidence of the model to examine the soil property correlation. The relationship obtained can be used to predict cone indices from the bulk densities which are easier to measure.
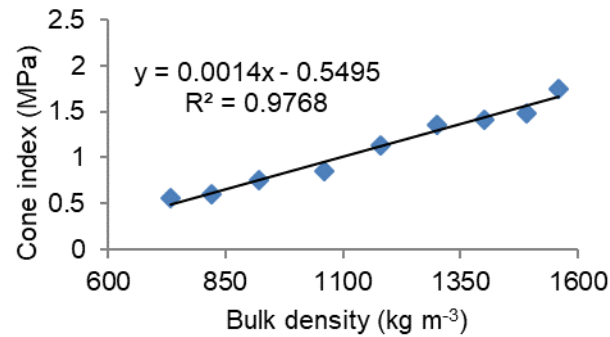
Figure 6.8. Relationship between soil bulk density and the cone index from simulation.

6.5. Conclusions

The soil-micropenetrometer model developed using PFC^{3D} produced similar results as the laboratory measurements, in terms of the variation of cone index over penetration depth. The calibrated particle stiffness was 10300 N m^{-1} for the loamy fine sand soil. The cone index values predicted with the model agreed well with the field measurements, demonstrated by the relative errors under 15% in two soil contrasting conditions (hard and soft soils). Increasing the penetration speed in the model increased the output cone index value and reduced the computational time significantly. The same speed as in the tests was used throughout the model development to better represent the actual physics of soil-micropenetrometer interaction. The model was able to predict soil cone indices for different soil bulk densities. The results showed that cone indices were proportional to the bulk densities, and the two variables had a linear relationship. At this stage of PFC^{3D} development, soil moisture content is not included in the model input

parameters; effects of moisture content can only be addressed indirectly using the parallel bond model implemented in PFC^{3D}. Users of the model should be made aware of this limitation.

6.6. Acknowledgement

6.7. References

ASABE Standards. 2004. S313.3 Soil Cone Penetrometer. St. Joseph, Mich.: ASABE.

Barley, K.P., Farrell, D.A., Greacen, E.L., 1965. The influence of soil strength on the penetration of a loam by plant roots. Australia Journal of Soil Research 3, 69–79.

Busscher, W.J., Bauer, P.J., Camp, C.R., Sojka, R.E., 1997. Correction of cone index for soil water content differences in a coastal plain soil. Soil & Tillage Research 43, 205–217.

Butlanska, J., Arroyo, M., Gens, A., Sullivan, C.O., 2014. Multi-scale analysis of cone penetration test (CPT) in a virtual calibration chamber. Canadian Geotechnical Journal 51(1), 51–66.

Calvetti, F., Nova, R., 2005. Micro-macro relationships from DEM simulated element and in-situ tests. In: Proceedings of the 5th International Conference on Micromechanics of Granular Media. Stuttgart, Germany.

Chen, Y., Munkholm, L.J., Nyord, T., 2013. A discrete element model for soil-sweep interaction in three different soils. Soil & Tillage Research 126, 34–41.

Chi, L., Tessier, S., 1995. A portable micro-penetrometer for measuring seed row compaction. Soil & Tillage Research 34(1), 27–39.

Dawidowski, J.B., Worona, M., Hencel, A., 1988. The determination of plow draft from soil penetration resistance. In: Proceedings of the 11th International Conference on Soil Tillage Research Organization. Edinburgh, Scotland.

Dexter, A.R., Zoebisch, M.A., 2002. Critical limits of soil properties and irreversible soil degradation. In: Lal, R. (Ed.), Encyclopedia of Soil Science. Marcel Dekker, New York.

Falagush, O., McDowell, G., Yu, H.S., 2012. Discrete element modelling of cone penetration tests in granular materials. In: Proceedings of 4th International Conference on Site Characterization. Pernambuco, Brazil.

Falagush, O., 2013. Discrete Element Modelling of Cone Penetration Testing in Granular Materials. Ph.D. Thesis, The University of Nottingham, Nottingham, United Kingdom.

Godwin, R.J., 2007. A review of the effect of implement geometry on soil failure and implement force. Soil & Tillage Research 97, 331–340.

Groenevelt, P.H., Kay, B.D., Grant, C.D., 1984. Physical assessment of a soil with respect to rooting potential. Geoderma 34, 101–114.

Hernanz, J.L., Peixoto, H., Cerisola, C., 2000. An empirical model to predict soil bulk density profiles in field conditions using penetration resistance, moisture content and soil depth. Journal of Terramechanics 37, 167–184.

Huang, A.B., Ma, M.Y., 1994. An analytical study of cone penetration tests in granular material. Canadian Geotechnical Journal 31(1), 91–103.

Jiang, M.J., Yu, H.S., Harris, D., 2006. Discrete element modelling of deep penetration in granular soils. International Journal for Numerical and Analytical Methods in Geomechanics 30(4), 335–361.

Kumar, A., Chen, Y., Sadek, M.A., Rahman, S., 2012. Soil cone index in relation to soil texture, moisture content, and bulk density for no-tillage and conventional tillage. Agricultural Engineering International: CIGR Journal 14(1), 26–37.

Li, B., Chen, Y., Chen, J., 2016. Modelling of soil-claw interaction using the discrete element method (DEM). Soil & Tillage Research 158, 177–185.

Li, B., Liu, F., Mu, J., Chen, J., Han, W., 2014. Distinct element method analysis and field experiment of soil resistance applied on the subsoiler. International Journal of Agricultural and Biological Engineering 7(1), 54–59.

Mak, J., Chen, Y., Sadek, M.A., 2012. Determining parameters of a discrete element model for soil-tool interaction. Soil & Tillage Research 118, 117–122.

Salgado, R., 2012. The mechanics of cone penetration: Contribution from experimental and theoretical studies. In: Proceedings of 4th International Conference on Site Characterization. Pernambuco, Brazil.

Santos, F.L., Jesus, V.A.M.D., Valente, D.S.M., 2012. Modelling of soil penetration resistance using statistical analyzes and artificial neural networks. Acta Scientiarum. Agronomy 34(2), 219–224.

Taylor, H.M., Ratliff, L.F., 1969. Root elongation rates of cotton and peanuts as function of soil strength and soil water content. Soil Science 108(2), 113–119.

Upadhyaya, S.K., Kemble, L.J., Collins, N.E., 1982. Cone index prediction equations for Delaware soils. Paper No. 82-1452-1456. In: ASAE 1982 Annual Conference.

Vasquez, L., Myhre, D.L., Hanlon, E.A., Gallaher, R.N., 1991. Soil penetrometer resistance and bulk density relationships after long-term tillage. Communication of Soil Plant Analysis 22, 2101–2117.

Chapter 7: A Discrete Element Model for the Interaction of a Deep Tillage Tool with Soil Having a Hardpan Layer *

7.1. Abstract

Numerical simulation of soil-tool interactions is a cost-effective method to assess and gain insight into the tool performance as affected by working parameters. In this study, a discrete element model (DEM) was developed to simulate a subsoiler-type tool and its interaction with soil to address the stratified soil layers in agricultural fields using the Particle Flow Code in Three Dimensions (PFC^{3D}). Sensitivity analysis was performed to determine the most critical set of model parameters which affected the soil dynamic behaviours. With test data, this set of model parameters was calibrated using a systematic scheme that featured response surface optimization and inverse solution technique to minimize the discrepancy between simulations and measurements. The model was validated and then utilized to investigate the effects and the optimal value of the working depth. The results showed that the particle stiffness and bond stiffness were the most influential model parameters and the calibrated values were 6.43e4 N m^{-1} and 2.6e6 Pa m^{-1}, respectively. The calibrated model was capable of predicting soil cutting resistance and soil disturbance characteristics with relative errors ranging from 2.63 to 10.2%. Simulation results indicated that the shallow tillage, where the subsoiler-type tool works at either 5 or 20 mm deeper than the hardpan layer among other depths examined, could achieve the best performance in terms of breaking the hardpan and improving soil loosening efficiency. The proposed model can facilitate the investigation of interactions between soil engaging tools and heterogeneous soil.

7.2. Introduction

With the successive use of tillage implements at the same depth, there is a growing concern about hardpan formation and soil compaction. Several deep tillage implements have commonly been used to disrupt hardpans without significantly disturbing the topsoil and the surface residue for soil conservation (Hamza and Anderson, 2005). Other benefits of deep tillage include improvements in water infiltration (Chamen, 2011), drainage (Said, 2003), root penetration (Bateman and Chanasyk, 2001), crop growth (Ellington, 1996), and ultimately crop yield (Hamza and Anderson, 2003). The major concern with deep tillage is high energy consumption due to the high draft force requirement of deep tillage implements (Manuwa, 2009). Therefore, reducing the draft force requirement has been the focus of tool design (Raper and Bergtold, 2007). Soil disturbance characteristics also serve as performance indicators of a deep tillage implement (Lacey et al., 2001). An ideal tool would loosen most of the subsoil and leave most of the soil surface undisturbed with minimum draft force requirement.

The soil heterogeneity in terms of bulk density in the vertical direction can be caused by field traffic or repeated plowing, for example hardpans (Brady and Weil, 2007). The soil profile with a hardpan typically shows a three-layer sandwich structure. The topmost layer has relatively low bulk density mainly due to annual plowing and secondary shallow tillage. The hardpan layer just below the depth of plowing has a greater bulk density than the top layer. The subsoil layer below the hardpan has a slightly decreased bulk density as this layer is typically unaffected by normal tillage implements and field traffic. For example, in a clay soil field with plowing at a depth of 200 mm, the top layer, hardpan, and subsoil layer were found at 0-230, 230-330, and 330-600 mm

138

with the average bulk density of 1.25, 1.5, and 1.35 Mg m^{-3} respectively (Chen and Tessier, 1997). However, soil characteristics, such as the thickness and bulk density of different layers, vary from field to field and within a field due to different tillage practices, soil texture and properties, and agronomic activities (Raper et al., 2000a, 2000b). Given the vertical location of a hardpan, the information regarding the working depth of a deep tillage implement that leads to optimal performance is lacking in the literature. If deep tillage depth is greater than the hardpan depth, unnecessary energy may be consumed. In some instances, unnecessarily deep tilling may even hinder crop production due to the re-compaction effect of subsequent field operations (Raper et al., 2000c). If the deep tillage depth is set the same as the depth of hardpan, there is a risk of incomplete disruption of the hardpan. Therefore, there is a need to determine the optimal depth at which a deep tillage implement needs to operate in order to achieve a relatively high soil loosening efficiency. This research aimed to address this need by studying the interaction of a subsoiler-type tool with heterogeneous soil.

The existing research on soil-tool interaction can be grouped into three categories: experimental, analytical, and numerical methods. Experimental methods are time-consuming and expensive while analytical methods are limited by soil failure assumptions and simple tool geometry. Numerical methods, on the other hand, are capable of examining complex tool geometries and more soil dynamic attributes, such as soil pressure and stress distribution. In recent years, the discrete element method (DEM) has been used to simulate soil-subsoiler interactions. Van der Linde (2007) evaluated the ability of the DEM to model a vibrating subsoiler and investigated the cause of the draft force reduction with the aid of the DEM model. Tanaka et al. (2007) developed a

139

modified DEM model to predict soil loosening and cracking generation caused by a vibrating subsoiler. Li et al. (2014) proposed a subsoiler model developed using the DEM, which was able to predict draft force at three different working depths with relative errors less than 20%. However, the heterogeneity in soil structure and the regime of hardpan breaking, which are the predominant features of deep tillage, were absent in previous DEM studies.

In this study, the DEM that implemented in a commercial software, Particle Flow Code in Three Dimensions (PFC^{3D}) (Itasca Consulting Group Inc., Minneapolis, USA), was used to simulate a subsoiler-type tool and its interaction with soil. With this method, the accuracy of the simulation largely depends on the calibration of model parameters. Traditionally, calibrations were done using fundamental soil mechanical tests, such as the triaxial test, angle of repose, cone penetration test, and direct shear test (Nandanwar, 2015; Ucgul et al., 2014; Sadek et al., 2011). The reliability of these calibrations is questionable, as soil under the impact of soil-engaging tools may have different failures than those in soil mechanical tests. For this reason, Sadek and Chen (2015) utilized a simple blade to calibrate the model parameters and used the calibrated model parameters to model other soil-engaging tools with complex geometries. This is considered a better approach as soil failure under a soil-engaging tool would be more similar to a blade than failure during a mechanical test. However, the best approach to increase calibration reliability would be to use the same soil-engaging tool for calibration, which was implemented in this study. Furthermore, the accuracy of model calibration was improved by accounting for more model parameters when calibrating; whereas only one parameter was calibrated in most previous studies.

The objectives of the study were to (1) construct a numerical model to simulate the interactions between a subsoiler-type tool and heterogeneous soil, (2) calibrate the most sensitive model parameters using a combination of the optimization approach and the inverse solution technique, and (3) validate and apply the model to investigate the effect of working depth on tool performance.

7.3. Methodology

7.3.1. Tillage tool

A subsoiler-type tool (John Deere PS1001, Deere & Co., Moline, Illinois, USA) was modelled and tested in this study. The tool consisted of a straight vertical shank, a sloped point, and a rectangular cutting share bolted to the point. The main geometrical parameters are labeled in Fig. 7.1 and their values are also given.

(a)   (b)
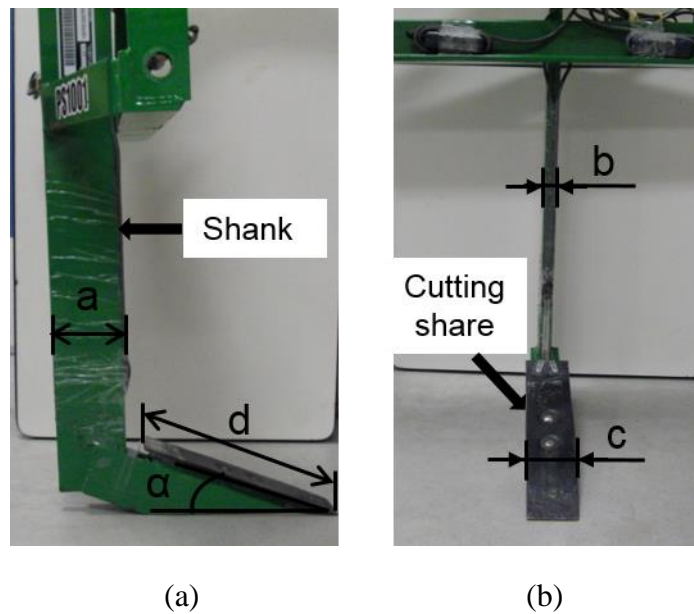
Figure 7.1. The side view (a) and front view (b) of subsoiler-type tool and its geometrical parameters; a = 101 mm, shank thickness; b = 20 mm, shank width; c = 68 mm, share width; d = 306 mm, share length; α = 22.5º, share rake angle.

7.3.2. Model development

7.3.2.1. Soil-tool interaction model

A soil-tool model was developed using the basic PFC^{3D} elements: walls and balls. Seven walls were used to form a model soil container having a rectangular top and a trapezoid-shaped bottom (Fig. 7.2). The soil container shape was designed to reduce the number of particles in the model and thus increase computation efficiency. The use of this shape was justified by the wedge model in McKyes and Ali (1977), where the cross-sectional shape of the soil cut by a narrow tool is a straight-sided trapezoid. The isosceles trapezoid cross section had a long base of 600 mm, a height of 300 mm, and a short base of 100 mm. The length of the model soil container was one meter. Balls with a diameter of 10 mm were used to form the soil particle assembly. The parallel bond model implemented in PFC was used to model the contacts between particles to mimic the cohesive behaviour of agricultural soil. Model parameters were initially adopted from Sadek and Chen (2015) and were calibrated later as will be described in the model calibration section. Major model parameters are listed in Table 7.1. Particles were generated and allowed to settle in the container. Then the particles above the trapezoidal container surface were deleted to create a smooth soil surface for the precise setting of working depth of the tool. The default time step is automatically updated based on the stiffnesses and masses of all objects in the model during the simulation. A maximum time step of 2.28e-5 s was calculated based on the particle size and the time step determination equation in Ucgul et al. (2014). The maximum time step was used whenever the default time step exceeded it to avoid unrealistic unbalanced forces generation, which may result in model instabilities. The soil domain was divided into three layers: a top layer, a hardpan, and a subsoil layer. To simulate the heterogeneity of soil, different layers had

142

different bulk densities by assigning different particle densities. The model tool was an

imported CAD drawing of the John Deere subsoiler (Fig. 7.2). The tool was initially

placed at a desired working depth, and was later assigned a desired travel speed.
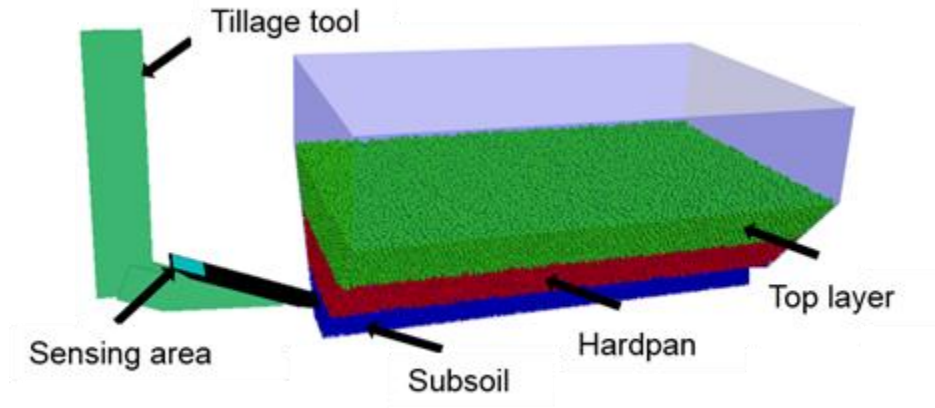
Figure 7.2. Soil-tool model showing different soil layers and pressure sensing area on the

cutting share of the subsoiler-type tool.

Table 7.1. Major parameters of the subsoiler model

Parameter	Unit	Value
Wall stiffness, K_w	N m^{-1}	1e8
Wall friction, μ_w	Dimensionless	0.5
Particle stiffness, K	N m^{-1}	To be calibrated
Particle friction, μ_p	Dimensionless	0.5
Particle density, ρ_p	kg m^{-3}	To be calculated
Bond radius multiplier, R_m	Dimensionless	0.5
Bond stiffness, K_{pb}	Pa m^{-1}	To be calibrated
Bond strength, σ	Pa	2e4
Viscous damping coefficient, ω	Dimensionless	1.0
Local damping coefficient, θ	Dimensionless	0.5

7.3.2.2. Monitoring of soil dynamic properties

Soil cutting pressure (P) on the tool share was examined by monitoring the pressure on a square wall (60 by 60 mm) located on the cutting share (Fig. 7.2). During the simulation, the normal force of the square wall was recorded and was converted to pressure by dividing the wall area. Draft force (F_d) and vertical force (F_v) of the tool were also monitored during the simulations. The typical curves of these outputs are illustrated in Fig. 7.3a. The pressure started to increase about 0.3 s later than that of draft and vertical forces since the sensing area did not interact with the soil within the initial period. The sharp increase near the end of the curves was due to the effect of the soil bin wall at the end. The middle stable section was long enough for the simulation to reach the steady state. The averages over the stable section of the curves were used as the simulated values.

Soil disturbance characteristics resulting from the tool were monitored using the soil displacement contours. In PFC, particles have non-zero displacements at all times, which were referred to as "noise" displacement. The average noise displacement of all particles was recorded before running the tool. During the deep tillage operation, a cutting plane of the soil cross-section was taken at the shank's rear edge. Using the noise displacement as the separation point to draw the displacement contour, particles disturbed by the model tool formed a distinct area (Fig. 7.3b). The width of disturbed area at the soil surface (W) and the disturbed area (A) were characterized through image processing in MATLAB. The monitoring was performed on four cutting planes taken within the stable section of the model soil bin and the average values of A and W were used.

(a)   (b)
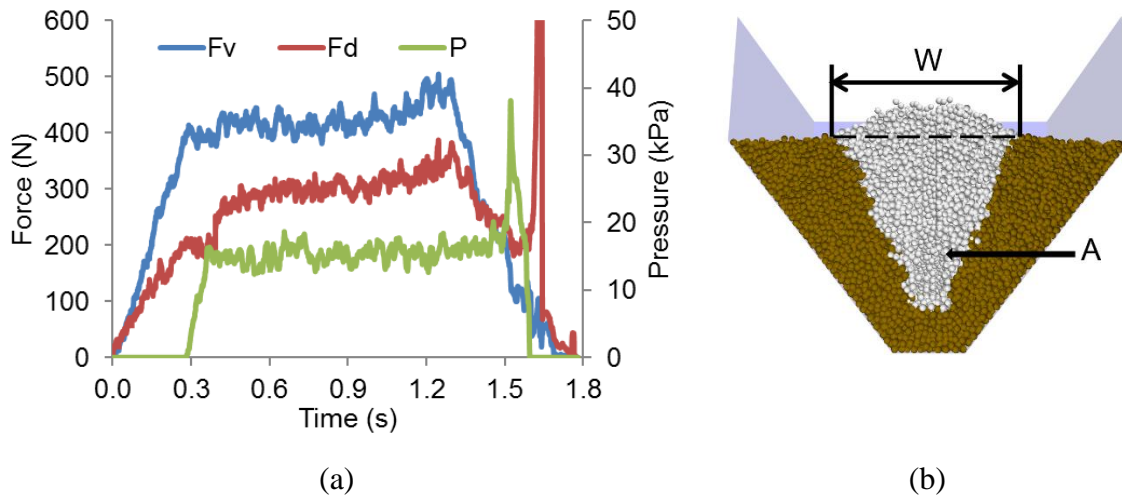
Figure 7.3. Monitoring model outputs: (a) typical draft force (F_d), vertical force (F_v), and soil cutting pressure (P) curves; (b) typical soil displacement contour showing the width of the disturbed area at the soil surface (W) and soil disturbance area (A).

7.3.3. Lab test

A laboratory test was conducted to calibrate and validate the soil-tool model. The test was carried out in an indoor soil bin located in the Soil Dynamics and Machinery Laboratory at the University of Manitoba, Winnipeg, Manitoba, Canada. The soil was sandy loam (70% sand, 16% silt, and 14% clay) with a plastic limit of 27.7%.

7.3.3.1. Preparation of layered soil and test of the tool

To mimic heterogeneous field soil conditions with a hardpan, a three-layer structure (topsoil layer, hardpan, and subsoil layer) was prepared in the soil bin. First, the soil was completely moved to spare ends of the soil bin, after which layers of approximately 50 mm thickness were compacted sequentially. Compression was done with passes of a water-filled roller and a vibratory plate compactor. The hardpan layer received more passes than the other layers. Chalk powder was smeared on the surface of the hardpan and the subsoil layer. For tests, the subsoiler-type tool with its original

145

toolbar frame was mounted on the soil bin carriage through a plate dynamometer (Fig.

7.4). The tool was run at a working depth of 240 mm with a travel speed of 0.83 m s^{-1} (3

km h^{-1}), which was a typical setting for operating this tool in Western Canada.

Figure 7.4. Lab test setup showing the subsoiler-type tool mounted on the tool carriage

through a dynamometer.

7.3.3.2. Measurements

After soil preparation and before the test, a cone penetrometer (Model CP20,

Agridy Rimik pty. Ltd. Toowoomba, Australia) was used to measure the soil cone index

to a depth of 350 mm. A cross-section of the soil bin was exposed to measure bulk

density of the three layers separated by the chalk powder (Fig. 7.5a). Soil cores (50 mm

in diameter and 100 mm in length) were taken horizontally from each layer. Soil cores

were weighed, oven-dried for 24 h at 105 ºC, and weighed again to determine the dry

bulk density and moisture content.

As the tool travelled, the draft force and vertical force of the tool were measured using the dynamometer and a data acquisition system. To measure the soil cutting pressure of the tool, two FlexiForce film pressure sensors (Tekscan Inc., South Boston, Massachusetts, USA) were installed side-by-side on the cutting share surface (Fig. 7.5b) within the range of the sensing wall which was used in the simulation. The pressure signal was remotely recorded using a computer.

Soil disturbance characteristics were measured following the tillage operation. After the loose soil was carefully removed from the furrow, a metal wire was deformed along the furrow profile (Fig. 7.5c). The curved wire was then traced on a paper (Fig. 7.5d). The width of disturbed area at the soil surface (W) was recorded from the paper and the soil disturbance area (A) was analyzed in MATLAB. Four measurements were performed at random locations along the tool path.
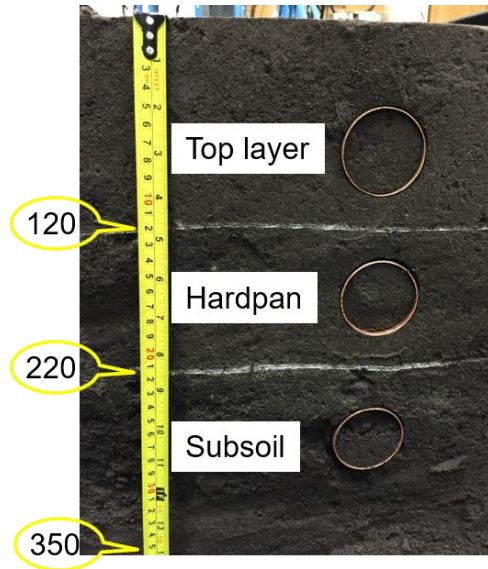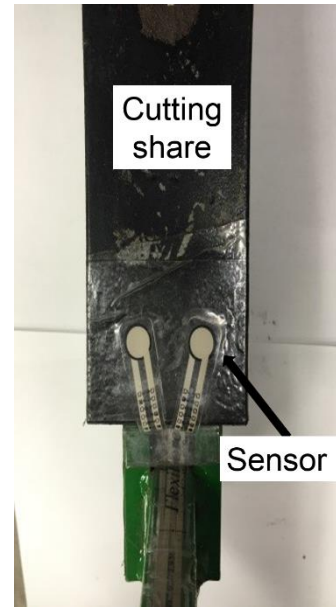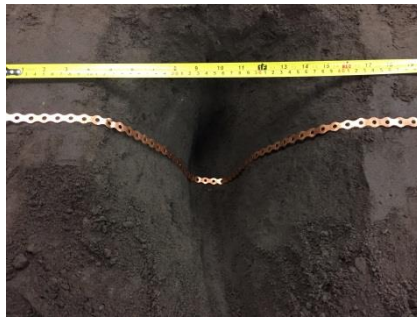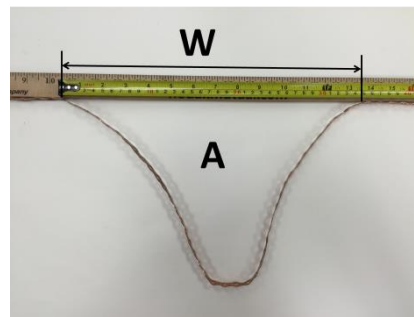
Figure 7.5. Lab test measurements: (a) Soil cross-section for soil core sampling; (b) sensors on the cutting share of the subsoiler-type tool; (c) and (d) a deformable wire for soil disturbance characteristics measurements (W = width of disturbed soil at the soil surface; A = soil disturbance area).

7.3.4. Model calibration and validation

The thickness and bulk density of each soil layer in the simulation was adjusted to the same as the lab test. The model tool was placed at a working depth of 240 mm and

was assigned a travel speed of 3 km h^{-1}, as in the lab test. The working depth enabled the tool to fully disrupt the hardpan that was located between 120 to 220 mm. The model parameters were calibrated using the measured soil cutting pressure (P) and width of disturbed area at the soil surface (W). Regression analysis was conducted to establish the relationships between model parameters and outputs. Then, an objective function was constructed to calculate the average relative error as follows:

$$Z = (\frac{|P_m - P_s|}{P_m} + \frac{|W_m - W_s|}{W_m}) \times \frac{1}{2} \times 100\% \qquad (7.1)$$

where

Z = average relative error between the measurement and simulation (%),

P = soil cutting pressure (Pa),

W = soil disturbance width at the soil surface (m),

subscripts m and s stand for measured and simulated values, respectively.

The optimization of the objective function was conducted in MATLAB to find the optimal model parameters which resulted in a minimum value of Z. A solver function called fmincon was selected based on the nature of the optimization problem. The Sequential Quadratic Programming (SQP) method (Nocedal and Wright, 2006) was utilized with several different initial points for optimization to approach the global optima.

The soil-tool model was validated using the data of draft (F_d) and vertical forces (F_v), and soil disturbance area (A). The calibrated model parameters were used as the

model inputs to predict F_d, F_v, and A. The predicted results were compared with the measured values.

7.3.5. Model applications

The validated model was then used to examine the effects of working depth (from 200 to 280 mm at 5 mm intervals) on the tool performance including draft force, vertical force, soil disturbance area, soil loosening efficiency, and hardpan loosening. The soil loosening efficiency was calculated as the ratio of soil disturbance area and draft force (McKyes, 1985). A measuring sphere with a diameter of the hardpan thickness was placed in the centre of the soil bin and within the hardpan (Fig. 7.6) to measure the soil porosity and stress of the hardpan. The measurement logic implemented in PFC^{3D} returns average values computed over particles that lie in or intersect the measuring sphere. The stress was derived from the contact force and particle displacement at each discrete contact, which indicated the soil behaviour on a microscale. In addition, the relationship between soil disturbance area and parallel bond quantity was identified to facilitate model monitoring and simplifying model applications.
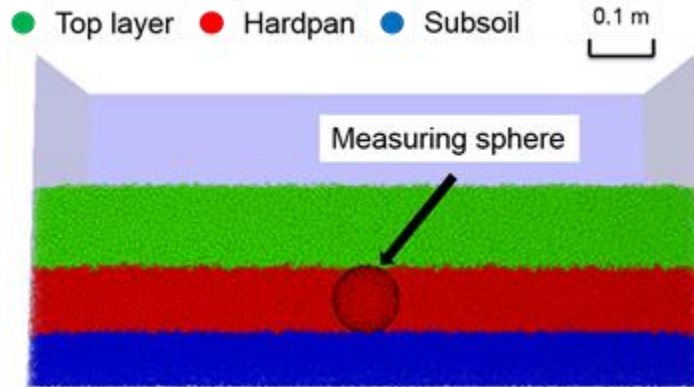
Figure 7.6. A measuring sphere for monitoring soil porosity and average stress within the hardpan.

7.4. Results and discussions

7.4.1. Lab test results

The cone index results showed the lowest penetration resistance in the top layer, the highest resistance in the centre and in-between resistance below (Fig. 7.7). The average cone index and dry bulk density for each of three layers also demonstrated the three distinctive layers of the soil profile (Table 7.2). The average soil moisture content was 23% (d.b.). The tool experienced an average F_d and F_v of 380 and 539 N, respectively. The vertical force on the tool pointed downward. The P on the cutting plate surface was 21.4 kPa. The soil disturbance cross section had an average W of 0.329 m and an average A of 0.0375 m^2.
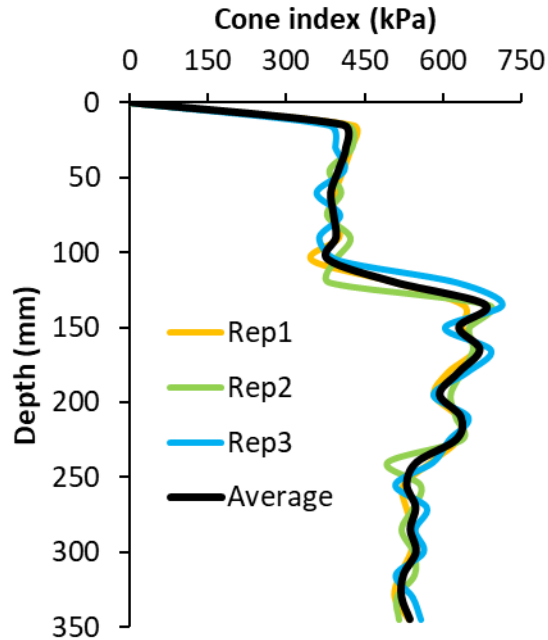
Figure 7.7. Variation of cone indices for different penetration depths at different soil

layers.

Table 7.2. Some soil physical and mechanical properties

Soil layers	Thickness (mm)	Cone index (kPa)	Dry bulk density (kg m^{-3})
Top layer	120	364	1210
Hardpan	100	637	1428
Subsoil	130	536	1345

7.4.2. Model behaviour as affected by model parameters

Preliminary simulations of the soil-subsoiler model showed that the model

behaviour was mostly influenced by particle stiffness (K) and parallel bond stiffness

(K_{pb}). This can be demonstrated by the top view screenshots from two sets of contrasting

model parameters. The number and distribution of the parallel bonds were hardly

changed when both particle stiffness and bond stiffness were low ($K = 1e3$ N m^{-1}, $K_{pb} =$

1e5 Pa m^{-1}) (Fig. 7.8a). In contrast, the tool was aggressive in reducing the number of

parallel bonds along its pass if the value of the model parameters was increased ($K = 2e5$ N m^{-1}, $K_{pb} = 1e8$ Pa m^{-1}) (Fig. 7.8b). The stress in the bond is a product of the bond stiffness and the relative displacement between two particles which are connected by the parallel bond (Itasca, 2016). If the calculated stress exceeded the bond strength, the parallel bond between particles broke and did not play any further role in the soil-tool interaction. In the scenario of high particle stiffness with high bond stiffness, the stress was extremely high and easily led to the breakage of parallel bonds. In contrast, low stress was found for the combination of low particle stiffness and low bond stiffness; therefore, most of the parallel bonds remained intact. It was also reasonable to speculate that soil failure pattern and critical depth were different between the two models. The compressive failure was dominant in Fig. 7.8a and the share was under its critical depth; whereas Fig. 7.8b had a brittle failure and the share was above its critical depth. However, the effects of model parameters on soil failure mode and critical depth would need to be further examined before any conclusion can be made. Based on these observations, the K and K_{pb} were calibrated and the results are described in the following section.

(a)	(b)
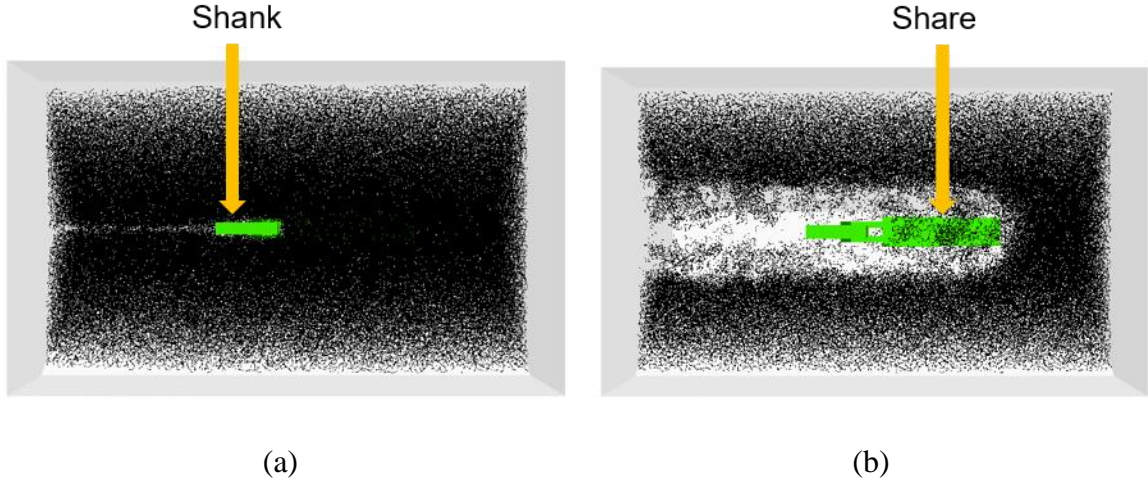
Figure 7.8. Top views of parallel bond distribution from simulations with two contrasting set of model parameters: (a) particle stiffness = 1e3 N m^{-1}, bond stiffness = 1e5 Pa m^{-1}; (b) particle stiffness = 2e5 N m^{-1}, bond stiffness = 1e8 Pa m^{-1}.

7.4.3. Calibrated particle stiffness and bond stiffness

Five values of particle stiffness K for model inputs were 2e3, 6.3e3, 2e4, 5e4, and 1e5 N m^{-1} and each of them was combined with six values of bond stiffness K_{pb} of 5e5, 1.26e6, 3.16e6, 8e6, 2e7, 5e7 Pa m^{-1}. The other parameters, including friction coefficient, parallel bond strength, and damping ratios, were kept as in Sadek and Chen (2015), who also used the same soil in their tests with similar soil conditions. Figure 7.9 (a) and (b) plot the model response points to different combinations of K and K_{pb} on a semi-log scale, in terms of P and W, respectively. The polynomial surfaces can be described by following equations:

$$P = -33.2 + 7.67(logK) + 11.1(logK_{pb}) - 0.314(logK)(logK_{pb}) - 1.07(logK_{pb})^2 \qquad (7.2)$$

$$W = -14.7 - 1.27(logK) + 8.23(logK_{pb}) + 0.12(logK)^2 + 0.225(logK)(logK_{pb}) -$$
$$1.39(logK_{pb})^2 - 0.019(logK)^2(logK_{pb}) - 0.00436(logK)(logK_{pb})^2 + 0.0734(logK_{pb})^3 \quad (7.3)$$

The root mean squared errors (RMSE) were 1.26 kPa and 0.0191 m for predicted P and W respectively. The coefficients of determination (R^2) were 0.95 and 0.94 for equations (7.2) and (7.3), respectively, which indicated a high degree of accuracy of the surrogate models. The results of analysis of variance (ANOVA) confirmed that the regression models were significant ($P < 0.05$). Substituting equations (7.2) and (7.3) into the objective function (eq. 7.1) and using the measured average values ($P_m=21.4 \ kPa$; $W_m=0.329 \ m$), the K and K_{pb} that yielded the minimal relative error were 6.43e4 m^{-1} and 2.62e6 Pa m^{-1}, respectively.

(a)   (b)
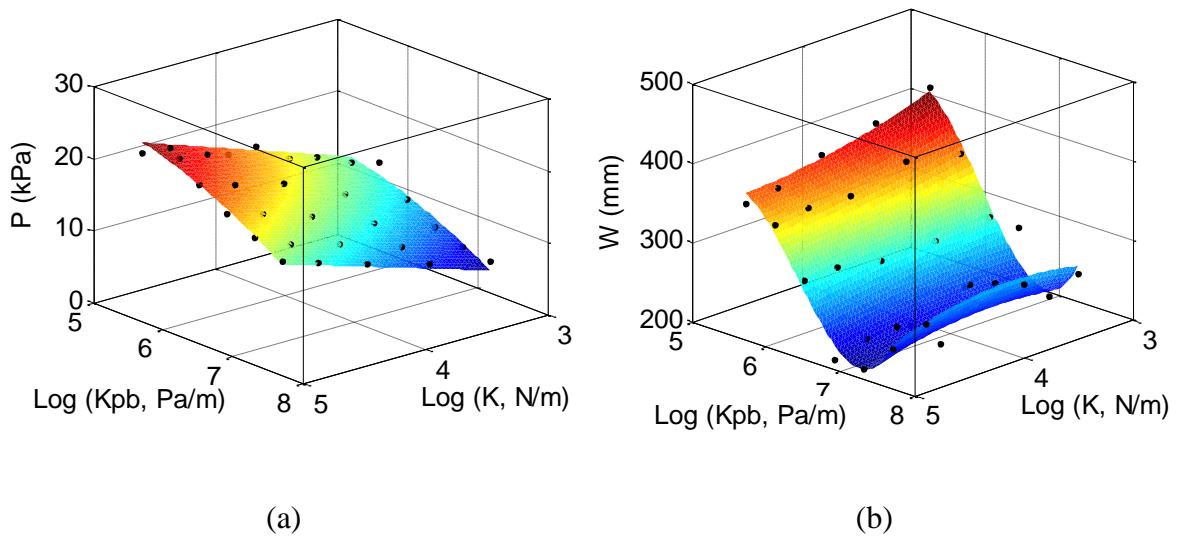
Figure 7.9. Response surface of (a) soil cutting pressure (P) and (b) width of the disturbed area at the soil surface (W) with respect to particle stiffness (K) and bond stiffness (K_{pb}) on a semi-log scale.

7.4.4. Comparisons of model predictions and measurements

With the calibrated values of K and K_{pb}, the soil-tool model was used to predict draft and vertical forces as well as soil disturbance area. The prediction results were compared with the measurements from the soil bin test, and the agreement was assessed

by the relative errors (Table 7.3). The highest relative error was 10.2% for the vertical

force prediction. This indicated that the model was reasonably accurate in predicting the

soil dynamics properties of the tillage tool.

Table 7.3. Comparison between simulation outputs and the soil bin measurements.

Dynamic soil characteristics	Draft force, F_d (N)	Vertical force, F_v (N)	Soil disturbance area, A (m^2)
Simulation	390	484	0.0394
Measurement	380	539	0.0375
Relative error	2.63%	10.2%	5.07%

7.4.5. Effects of working depth on the tool performance

7.4.5.1. Draft force and soil disturbance area

The calibrated and validated soil-tool model was used to examine the effect of

tillage depth (ranging from 200 to 280 mm) on the draft force (F_d) and soil disturbance

area (A). The F_d increased from 303 to 480 N when the depth increased from 200 to 280

mm (Fig. 7.10a). The increasing trend could be described by a linear function with

R^2=0.99. The linear increasing relationship between draft force and working depth agreed

with the draft force prediction model in Godwin and O'Dogherty (2007). Raper et al.

(2000c) also reported that the deep tillage conducted to a depth of 330 mm doubled the

draft force as compared with the shallow tillage conducted to a depth of 180 mm. It was

interesting to notice that the A also increased linearly with the working depth (Fig.

7.10b). According to the wedge model in McKyes and Ali (1977), in the homogeneous

soil, the area of disturbance would increase in a quadratic fashion as the working depth

increased linearly. However, the soil heterogeneity possibly diluted the effect of working

depth on the A in the simulation. Specifically, the hardpan with a high particle density

tended to be more stable as the impact stress of the tool propagated in the soil, which not only restricted the expanding of the disturbed area in the hardpan but also limited the stress propagation from the tool point to the top soil layer. The dilution phenomenon became more noteworthy as the working depth increased, where the tool point moved away from the hardpan.

The model was also used to predict the number of broken parallel bonds (n), as it reflected the degree of particle disturbance from a microscopic perspective. The results showed that the parallel bond breakage quantity also had a generally increasing linear trend with respect to the working depth of the tool (Fig. 7.10c). As noticed in the model development, the function for monitoring A was not readily available in PFC^{3D}; while there was a built-in function for monitoring the number of broken parallel bonds between particles. The relationship of the two variables could be described using the following linear regression equation with R^2=0.94. The equation provides an alternative method to obtain the *A*.

$$A = 4.3811n-43107 \tag{7.4}$$
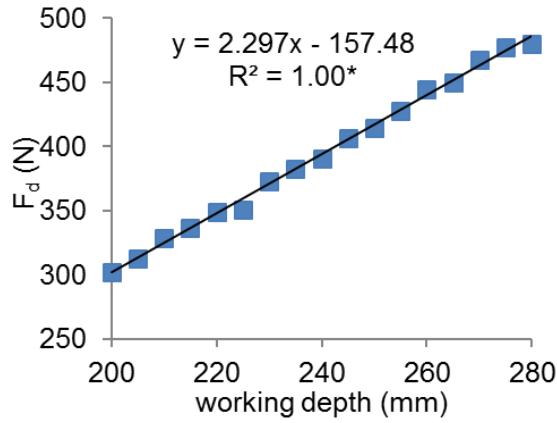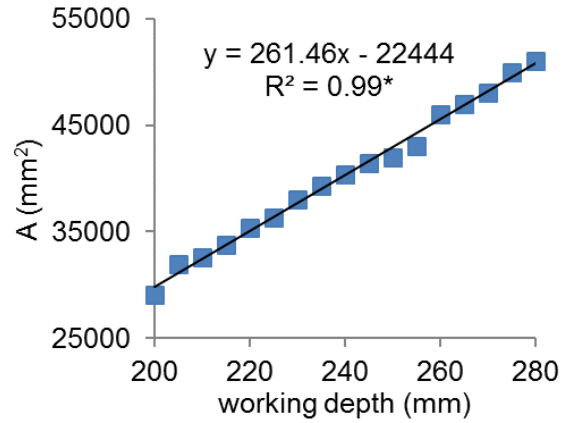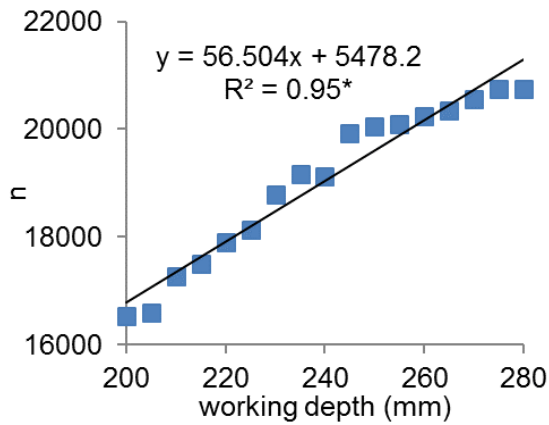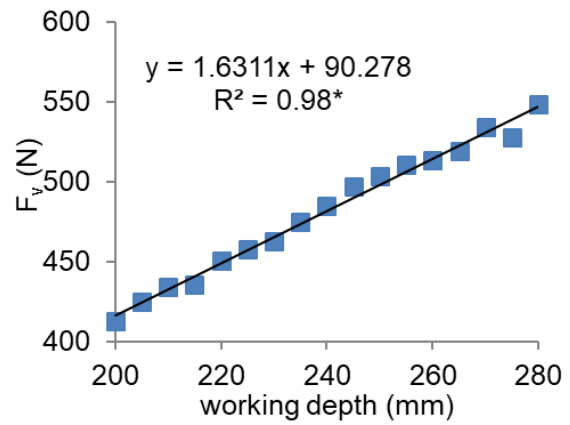
Figure 7.10. The predicted draft force (F_d), soil disturbance area (A), parallel bond breakage quantity (n), and vertical force (F_v) at different working depths.

7.4.5.2. Soil loosening efficiency

While reducing draft force is important, a maximum soil disturbance area may also be desired in deep tillage operations to improve the soil structure. Therefore, soil loosening efficiency was calculated as the ratio of A and F_d (McKyes, 1985) to reflect the overall performance of the deep tillage. To deal with field conditions where the hardpan

is located at different depths, a relative working depth was defined by subtracting the depth of hardpan bottom from the tool working depth. The soil loosening efficiency was examined as affected by the relative working depth. Simulation results showed that the soil loosening efficiency varied within a small range of that from 96 to 106 mm^2 N^{-1} (Fig. 7.11). The curve had a generally increasing trend, meaning soil loosening efficiency increased with the working depth.
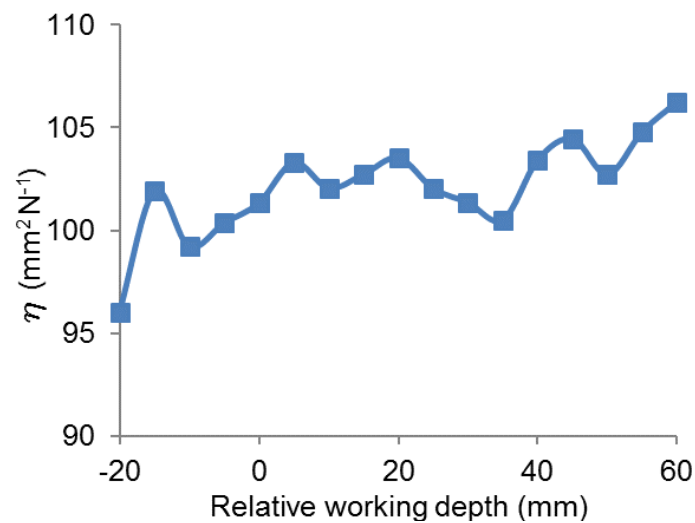
Figure 7.11. The soil loosening efficiency (η) at different relative working depths.

Five peaks of soil loosening efficiency were observed in Fig. 7.11, which corresponding to the relative working depths of -15, 5, 20, 45, and 60 mm. This was an interesting phenomenon, and soil dynamic behaviours corresponding to these peaks were further examined. A clip box was used to cut the model soil bin longitudinally to examine the soil particle disturbance and parallel bond distribution around the tool (Fig. 7.12). The soil dynamic behaviours of 5 and 45 mm were similar to that of 20 and 60 mm respectively. Therefore, the screenshots from -15, 20, 60 mm are shown in Fig. 7.12 for the sake of conciseness. The general characteristics of soil fracture and deformation were

159

similar to the experimental observations reported by Araya and Gao (1995). For the peak efficiency at a relative working depth of -15 mm (Fig. 7.12a), a thin sheet of the hardpan on the bottom was left undisturbed. Most of the parallel bonds within the upper part of the hardpan were broken due to the direct contact with the tool cutting share, which indicated fine soil aggregates were produced in the compacted hardpan layer. For the peak at the relative working depth of 20 mm, the tool was able to fully disrupt the hardpan through shattering and upheaving (Fig. 7.12b). The parallel bonds were broken continuously and uniformly over the depth of the hardpan. For the peak at a relative working depth of 60 mm, the shattering action occurred in the subsoil layer beneath the hardpan and the hardpan was mainly upheaved as demonstrated by the similar parallel bond distributions in the top layer and the hardpan (Fig. 7.12c). The major difference between relative working depths of 20 and 60 mm is the former resulted in finer and more uniform soil aggregates in the hardpan layer. Comparing the soil dynamic behaviours among the peaks, the relative working depth (-15 mm) corresponding to the first peaks would have risks of not completely breaking the hardpan, which was undesired. The relative working depths (5 and 20 mm) at the second and third peaks would ensure that the entire layer of the hardpan is loosened, and they also had relatively higher soil loosening efficiency than at the first peak. Although the relative working depths (45 and 60 mm) at the last two peaks had a 1% and 2% increase in the efficiency, they were at the expense of a 28% and 23% increase in the draft force as compared with that at the second and third peaks respectively. In summary, the relative working depths of 5 mm and 20 mm are recommended. Beyond 20 mm depth, the deep tillage would require high power due to its high draft force.
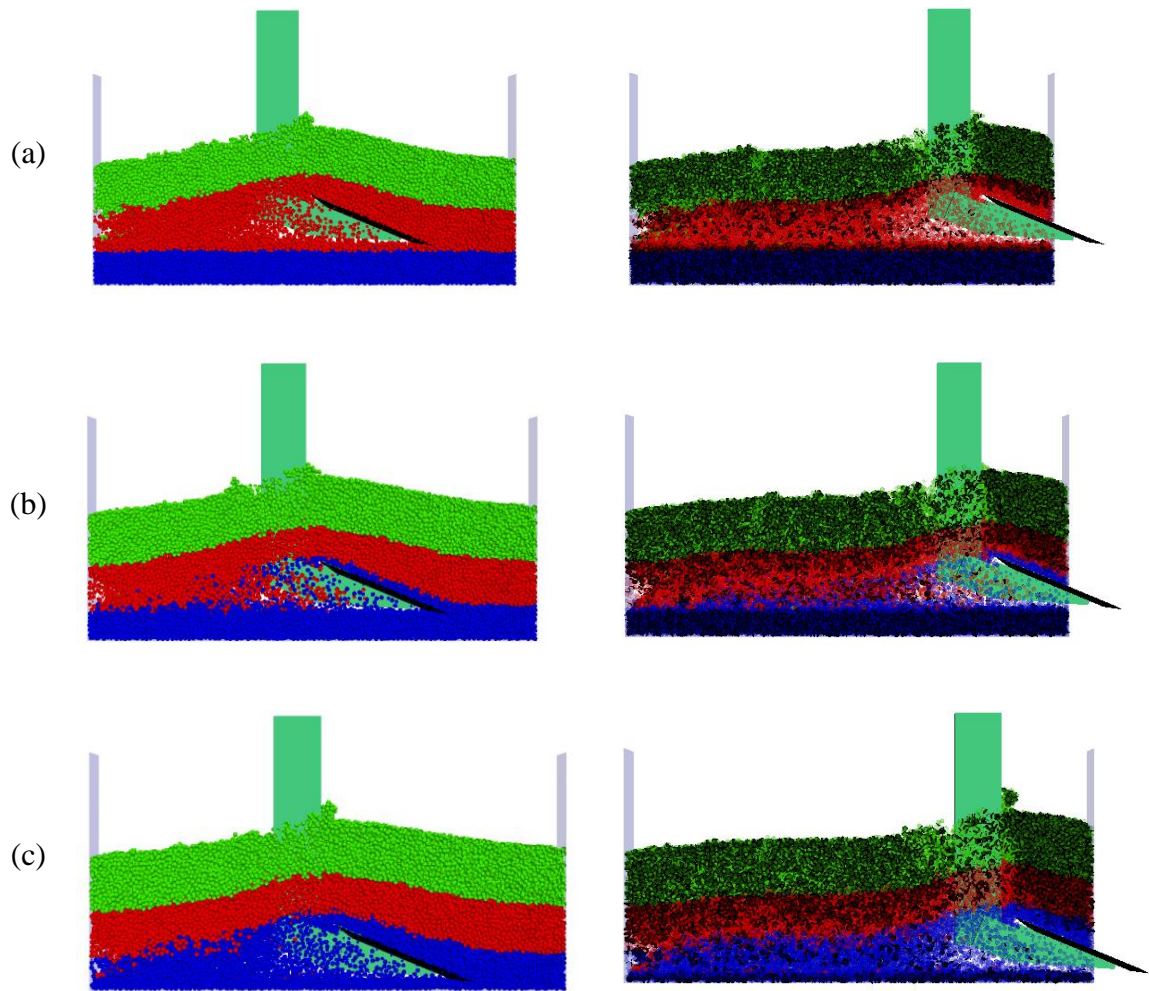
Figure 7.12. The soil particle disturbance and parallel bond field at different working depths of (a) -15 mm; (b) 20 mm; and (c) 60 mm that relative to the bottom of the hardpan layer.

7.4.5.3. Hardpan loosening

The soil porosity and average stress of the hardpan monitored by the measuring sphere are plotted versus the tillage time to investigate the soil loosening specifically within the hardpan (Fig. 7.13). The results of 5 and 45 mm are not shown here due to their similarity with that of 20 and 60 mm respectively. Generally speaking, all the curves presented a single peak trend with different peak values at different time points. The

stress started to accumulate once the tool interacted with the soil. The average stress increased to a peak where the parallel bonds started to break as reflected by the initial increase in the soil porosity. Then, the soil porosity increased as a result of the loosening of the hardpan. After that, the average stress dropped to the minimum value when the hardpan had the maximum soil porosity. Finally, the soil porosity gradually decreased to a stable value as the soil settled down. This stable value was higher than the initial value of soil porosity, which indicated the hardpan was more or less loosened by the tool. The relative working depth of 20 mm created the maximum stress and consequently the maximum soil porosity within the hardpan, which suggested a more pulverized hardpan was achieved. All those quantitative observations were consistent with the qualitative behaviours in Fig. 7.12. Therefore, the relative working depths of 5 and 20 mm were recommended for the simulated soil condition and tool geometry to effectively break and loose the hardpan.
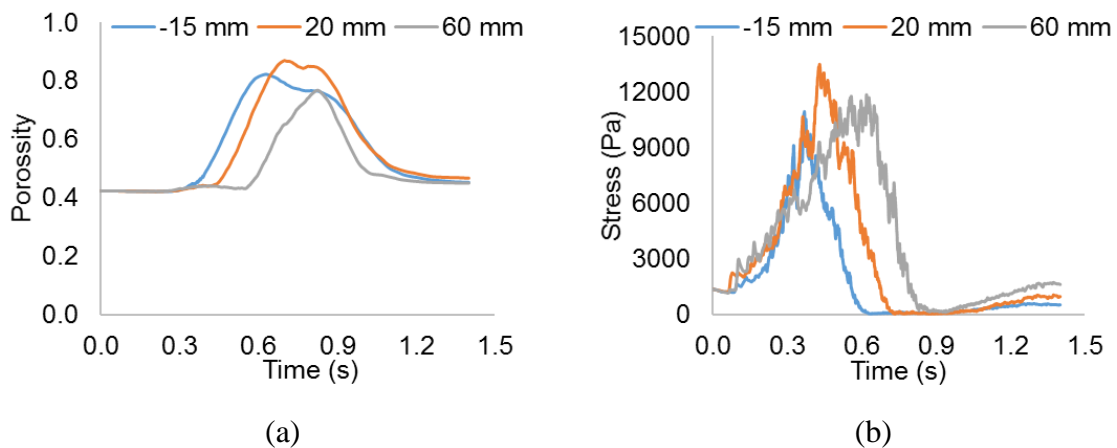
Figure 7.13. The variation of soil porosity (a) and average stress (b) of the hardpan at three different relative working depths.

7.5. Conclusions

The model developed using PFC^{3D} could simulate soil-tool interactions in full scale. It was feasible to use the layered soil structure in the model to reflect a realistic field condition with a hardpan. The calibrated model parameters were 6.43e4 N m^{-1} for particle stiffness and 2.62e6 Pa m^{-1} for bond stiffness, which were obtained through optimizing response surfaces of model outputs as functions of model parameters. The model results of draft force, vertical force, and soil disturbance agreed well with the laboratory measurements as demonstrated by relative errors less than 15%. The simulated draft force, vertical force, and soil disturbance area had positive linear relationships with the working depth. The soil disturbance area could be predicted using the bond breakage information which was readily accessible to PFC users. The relationship between the two parameters was highly linear. Based on the simulated soil loosening efficiency and soil dynamic behaviour, the shallow tillage, such as a working depth of 20 mm deeper than the hardpan, was recommended for the simulated soil condition and tool geometry. Results from this study demonstrated that the soil-tool model managed to incorporate soil heterogeneity and examine macro- and micro- soil dynamic properties in deep tillage. However, the model was calibrated and validated only for the given sandy loam soil. It is recommended that the procedures of calibration and validation proposed in this study should be followed when applying the model to other types of soils.

7.6. Acknowledgement

7.7. References

Araya, K., Gao, R., 1995. A non-linear three-dimensional finite element analysis of subsoiler cutting with pressurized air injection. Journal of Agricultural Engineering Research 61, 115–128.

Bateman, J.C., Chanasyk, D.S., 2001. Effects of deep ripping and organic matter amendments on Ap horizons of soil reconstructed after coal strip-mining. Canadian Journal of Soil Science 8, 113–120.

Brady, N.C., Weil, R., 2007. The Nature and Properties of Soils. Pearson, London.

Chamen, W.C.T., 2011. The Effects of Low and Controlled Traffic Systems on Soil Physical Properties Yields and the Profitability of Cereal Crops on a Range of Soil Types. Ph.D. Thesis, Cranfield University, Bedfordshire, UK.

Chen, Y., Tessier, S., 1997. Techniques to diagnose plow and disk pans. Canadian Agricultural Engineering 39, 143–147.

Ellington, A., 1996. Deep tillage research in Western Australia. In: Perry, M.W. (Ed.), A review of deep tillage research in Western Australia, Technical Report No. 13, Department of Agriculture Western Australia. pp. 100–108.

Godwin, R.J., O'Dogherty, M.J., 2007. Integrated soil tillage force prediction models. Journal of Terramechanics 44, 3–14.

Hamza, M.A., Anderson, W.K., 2003. Responses of soil properties and grain yields to deep ripping and gypsum application in a compacted loamy sand soil contrasted with a sandy clay loam soil in Western Australia. Australia Journal of Agriculture Research 54, 273–282.

164

Hamza, M.A., Anderson, W.K., 2005. Soil compaction in cropping systems: a review of the nature, causes and possible solutions. Soil & Tillage Research 82, 121–145.

Itasca, 2016. Particle flow code in three dimensions (PFC^{3D}). Theory and Background. Itasca Consulting Group Inc., Minneapolis, Minnesota, USA.

Lacey, S.T., Brennan, P.D., Parekh, J., 2001. Deep may not be meaningful: cost and effectiveness of various ripping tine configurations in a plantation cultivation trail in Eastern Australia. New Forests 21, 231–248.

Li, B., Liu, F., Mu, J.Y., Chen, J., Han, W.T., 2014. Distinct element method analysis and field experiment of soil resistance applied on the subsoiler. International Journal of Agricultural and Biological Engineering 7(1), 54–59.

Manuwa, S.I., 2009. Performance evaluation of tillage tines operating under different depths in a sandy clay loam soil. Soil & Tillage Research 103, 399–405.

McKyes, E., Ali, O.S., 1977. The cutting of soil by narrow blades. Journal of Terramechanics 14(2), 43–58.

McKyes, E., 1985. Soil Cutting and Tillage. Elsevier, New York.

Nandanwar, M., 2015. Simulation of Triaxial Compression Test for Sandy Loam Soil Using PFC3D. M.Sc. Thesis, University of Manitoba, Winnipeg, Manitoba, Canada.

Nocedal, J., Wright, S.J., 2006. Numerical Optimization, Springer Series in Operations Research. Springer, Berlin.

Raper, R.L., Schwab, E.B., Dabney, S.M., 2000a. Spatial variation of the depth of root-restricting layers in Northern Mississippi soils. In: Second International

Conference in Geospatial Information in Agriculture and Forestry, Lake Buena Vista, Florida, USA.

Raper, R.L., Schwab, E.B., Dabney, S.M., 2000b. Site-specific measurement of site-specific compaction in the Southeastern United States. In: Proceeding of the 15th ISTRO Conference, Ft. Worth, Texas, USA. July 3–7.

Raper, R.L., Reeve, D.W., Burmester, C.H., Schwab, E.B., 2000c. Tillage depth, tillage timing, and cover crop effects on cotton yield, soil strength, and tillage energy requirements. Applied Engineering in Agriculture 16(4), 373–385.

Raper, R.L., Reeves, D.W., Shaw, J.N., Van Santen, E., Mask, P.L., 2005a. Using site-specific subsoiling to minimize draft and optimize corn yields. Transactions of the ASABE 48, 2047–2052.

Raper, R.L., Schwab, E.B., Balkcom, K.S., Burmester, C.H., Reeves, D.W., 2005b. Effect of annual, biennial, and triennial in-row subsoiling on soil compaction and cotton yield in Southeastern U.S. silt loam soils. Applied Engineering in Agriculture 21(3), 337–343.

Raper, R.L., Bergtold, J.S., 2007. In-row subsoiling: a review and suggestions for reducing cost of this conservation tillage operation. Applied Engineering in Agriculture 23(4), 463–471.

Sadek, M.A., Chen, Y., Liu, J., 2011. Simulating shear behaviour of a sandy soil under different soil conditions. Journal of Terramechanics 48(6), 451–458.

Sadek, M.A., Chen, Y., 2015. Feasibility of using PFC3D to simulate soil flow resulting from a simple soil-engaging tool. Transactions of the ASABE 58(4), 987–996.

Said, H.M., 2003. Effect of tillage implements on the state of compaction in different

    soils. Egypt Journal of Soil Science 43, 91–107.

Tanaka, H., Oida, A., Daikoku, M., Inooku, K., Sumikawa, O., Nagasaki, Y., Miyazaki.

    M., 2007. DEM simulation of soil loosening process caused by a vibrating

    subsoiler. Agricultural Engineering International: the CIGR Ejournal Vol. IX,

    Manuscript PM 05 010.

Ucgul, M., Fielke, J.M., Saunders, C., 2014. Three-dimensional discrete element

    modelling of tillage: determination of a suitable contact model and parameters for

    a cohesionless soil. Biosystems Engineering 121, 105–117.

Van der Linde, J., 2007. Discrete Element Modelling of a Vibratory Subsoiler. M.Sc.

    Thesis, University of Stellenbosch, Matieland, South Africa.

Chapter 8: Simulation of Straw Movement by Discrete Element Modelling of Straw-Sweep-Soil Interactions *

*Published in Biosystems Engineering (in press).

8.1. Abstract

Understanding residue and soil behaviour under the impact of tillage tools is critical for designing tools for conservation tillage. In this study, a soil-tool-residue interactions model was developed for a sweep and oat straws using the discrete element method (DEM). Soil, sweep, and straw was modelled using spherical particles, walls, and clumps, respectively. A virtual field consisting of two layers, including a soil layer and a top straw layer, was constructed. Some model parameters were adopted from the literature and other parameters were measured from oat straws collected in a field. Dynamic attributes including soil moving area, straw moving area, residue cover, kinetic energy, straw velocity, acceleration, displacement, and moving trajectory were monitored. Comparing the simulated values of soil and straw moving areas with those calculated from analytical models in the literature, the calibrated model parameters of ball stiffness and clump stiffness were 8,730 and 332 N m^{-1}, respectively. The average forward displacement of oat straws was 189 mm, which had a relative error of 9.2% as compared with the literature data. Increasing the travel speed of the sweep increased the residue cover reduction and straw displacements. The kinematic attributes along with trajectory clearly demonstrated three stages of the straw movement, i.e., forced, projectile, and overturning movements. The proposed discrete element model can be applied to simulate other tillage implements in dealing with crop residues.

8.2. Introduction

In the past few decades, soil-tool interaction research has been the main focus of the area of soil dynamics and agricultural machinery. As conservation tillage, where 30 to 100% of crop residue is left on the soil surface, has gained popularity, crop residue has become a critical component of the soil dynamic system. A soil-engaging tool working in conservation tillage fields forms a soil-tool-residue interactions system. Specific interactions in the soil-tool-residue system include interactions between soil particles, soil and tool, residue and tool, residue particles, as well as soil and residue, which all have a complicated, random, and dynamic nature. Dynamic characteristics of the interactions mainly include contact forces (e.g. tool draft force, vertical, and lateral forces) and displacement (e.g. soil and residue movement. A comprehensive understanding of these dynamic characteristics is a prerequisite for designing high-performance soil-engaging tools. However, the complexity, stochasticity, and dynamics of the interactions hampered the progress on soil-tool-residue interactions research.

Investigation on the soil-tool-residue interactions has been carried out mainly through two approaches: experimental studies and modelling methods. Experimental studies have generated large amounts of data on soil and residue dynamics as affected by the soil and residue conditions, tool types, and their design and operational parameters. The soil cutting forces and straw burial rate increased as the disc working depth and speed increased (Mari et al., 2014). The forward displacements of soil and straw were reduced by 70% and 80% respectively, if the working speed of a sweep was reduced from 10 to 5 km h^{-1} (Liu et al., 2010). The straw displacement was not sensitive to standing stubble of oat, whereas the standing stubble significantly reduced soil displacement (Liu

et al., 2007). A rotary blade that was tested in a soil bin with wheat straws resulted in a greater level of straw movement than soil movement (Fang et al., 2016). The effect of working speed was more dominant than the tool geometry on soil throw width and residue cover of a fluted coulter (Zeng and Chen, 2018a). A comparative experiment of different tine and share types showed that tillage tools with greater working depths had a higher degree of soil disturbance and residue incorporation (Arvidsson and Hillerstrom, 2010).

The modelling approach of soil and residue dynamics has progressed from analytical modelling to numerical simulation. A steady-state analytical model for a single tillage sweep predicted the amount of soil and straw moving with a relative error less than 22% and 12%, respectively (Liu et al., 2008), even though the model was unable to provide other information, such as straw moving distance and redistribution pattern. The analytical modelling is based on assumed soil failure patterns, which hinders the applicability of the models to complex tool geometries. The discrete element method (DEM), an innovative and rapidly developing numerical method, has been successfully applied to soil-tool interactions in agriculture (e.g., Sadek and Chen, 2015; Zeng et al., 2017). However, little research has been done to incorporate crop residue into the discrete element models.

There have been some discrete element models of crop residues, but they were not for applications of soil-engaging tools. Rice straw was modelled as a rigid bar by connecting DEM spheres in a row to study its motion in the variable-amplitude screen box of a combine harvester (Ma et al., 2015). A bendable DEM straw model was proposed and validated to examine the influencing factors of the grain-straw separation in

a combine harvester (Lenaerts et al., 2014). A bending model for crop stems was developed in DEM to investigate the effects of plastic deformation and damage on the bending behaviour of individual crop stems (Leblicq et al., 2016b). Similarly, the compression behaviour of crop stems in harvesting machines was simulated in DEM by incorporating the effects of plastic deformation and damage (Leblicq et al., 2016a). Recently, chaffs and bent straws, other than straight straws, were integrated into a grain cleaning model to improve the modelling accuracy of the separation process (Korn and Herlitzius, 2017). In summary, limited research has been conducted on integrating crop residue into soil-tool interaction models.

In this study, a residue type of oat straw and a soil-engaging tool of sweep were simulated using a commercial DEM software, Particle Flow Code in Three Dimensions (PFC^{3D}) (Itasca Consulting Group Inc., Minneapolis, USA). The objectives of the study were to (1) develop a straw-sweep-soil interaction model using the PFC^{3D} to simulate straw movement, (2) calibrate and validate the discrete element model using analytical models and experimental data in the literature, (3) use the validated model to understand straw dynamics and predict straw movement under different working speeds and initial residue covers.

8.3. Methodology

8.3.1. Straw-sweep-soil model

A straw-sweep-soil model was developed using the basic PFC^{3D} elements: clumps, walls, and balls (Itasca, 2018). A clump consisting of a string of overlapped spheres was used to represent the cylindrical shape of an oat straw (Fig. 8.1). A 50% overlapping ratio between adjacent spheres was used as a trade-off between surface

resolution and computation efficiency. The straw in the model was assumed as a rigid body, which was also the case in similar studies, e.g., Chandio (2013) and Barker and Plouffe (2017), primarily because the straw deformation had negligible effects on straw movement. The clump could translate and rotate under applied forces and its motion obeyed the Newton's Second Law of motion. Oat straws were collected in a field in Manitoba and 10 pieces of 175 mm straws were randomly measured to have a diameter of 4.5±0.4 mm and a weight of 0.174±0.018 g. The clump was assigned a diameter of 4.5 mm and a density of 68 kg m^{-3} to have a weight of 0.174 g.

A sweep (Model 50-12K, Ralph McKay Industries Inc., Regina, Canada) and its shank were scanned using a 3D laser scanner (Shape Grabber Series, Ottawa, Canada) and their STL files were imported into the model. The sweep was 325 mm in width and 250 mm in length. PFC walls were used to represent tool geometry and also to form a virtual soil bin (Fig. 8.1). Given the symmetric geometry of the model, a half-width bin was used to reduce computing time without sacrificing simulation resolution (Falagush, 2014). Readers should note that the straw wrapping around the tine is ignored in this study. The bin was 2000 mm long, 120 mm deep, and 500 mm wide. The model sweep was positioned as its symmetry plane coincided with the side plane of the half-width bin. The model sweep was run at a working depth of 100 mm and a travel speed of 5 km h^{-1} for all simulations.

Balls with a diameter of 10 mm were used to form the soil particle assembly. Balls were generated to fill the central 1000 mm of the bin in length (Fig. 8.1), where model measurements were taken place. Larger balls of a diameter of 20 mm were generated in two end sections to further reduce the computing time. The clumps with a

172

uniform length of 150 mm were randomly distributed on the top of the central section of

the bin, in which the straw behaviours were negligibly affected by the particle size in the

end sections in preliminary simulations.
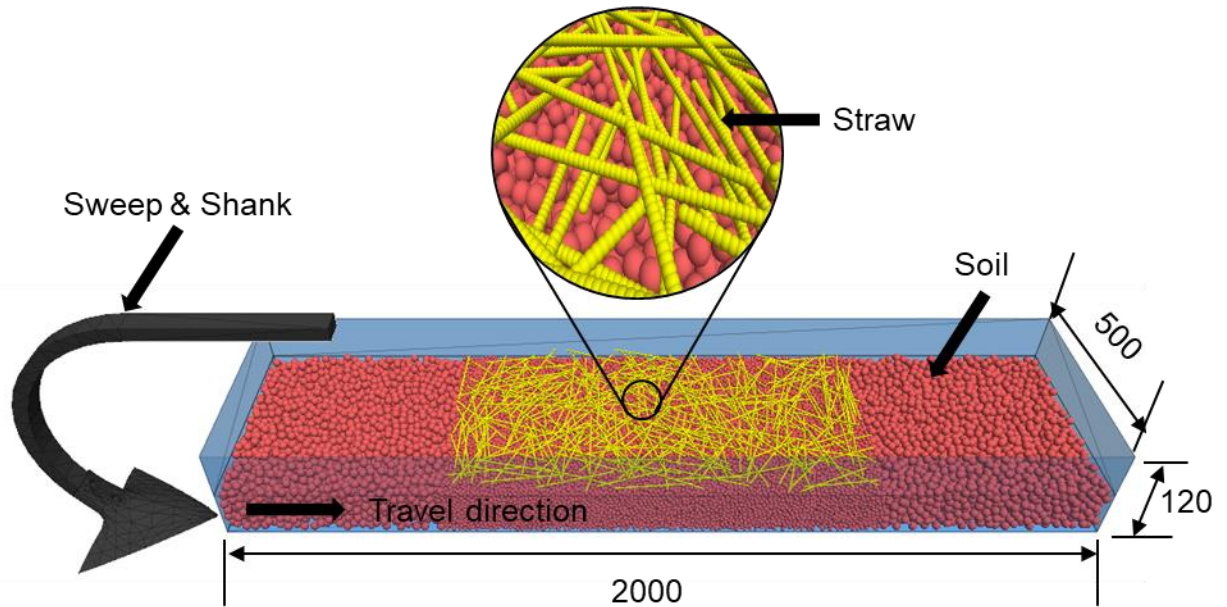
Figure 8.1. Straw-sweep-soil model with an enlarged image of straws. All dimensions in

mm.

The interactions between soil, straw, and sweep were described using two PFC^{3D}

built-in contact models. The interaction of soil-soil was specified as the parallel bond

contact to account for the cohesiveness of agricultural soil (Sadek and Chen, 2015). All

the other interactions including these between straw-straw, soil-straw, soil-sweep, and

straw-sweep were specified as the linear contact model. The linear contact model could

be described as linear elastic law with viscous dashpots, and the parallel bond model was

a linear model with parallel bonding for bonded-particle material. The detailed

mechanism of the contact models can be found in Itasca (2018). Each contact model had

a set of micro-parameters that governed the macroscopic behaviours of the interaction system. The model micro-parameters are described in the following sections.

8.3.2. Simulations of soil and straw dynamics

As the model sweep advanced in the soil bin, it caused soil particles to flow around the sweep. Meanwhile, the interaction between soil and between straws resulted in straw movement and mixing with soil. These phenomena were quantified by several dynamic attributes at the systemic and individual levels. The systemic attributes included soil moving area, straw moving area, residue cover, and straw kinetic energy. The individual-level attributes included the velocity, acceleration, displacement, and trajectory of a straw.

8.3.2.1. Monitoring soil and straw moving areas

During tillage, soil and straw moving zones were formed near the sweep (Fig. 8.2). Soil moving area (A_{soil}) and straw moving area (A_{straw}) were defined as the moving areas above the sweep and ahead of the rear edge of the sweep as per Liu et al. (2008), which were also referred to as the surface area of steady-state movement of soil and straw. Both the A_{soil} and A_{straw} were monitored using their velocity contours. In PFC, particles had non-zero velocities at all times, which were referred to as "noise velocities". For monitoring the soil moving area, the average noise velocities of all soil particles were recorded before running the sweep. When the sweep travelled to the central region of the soil bin, screenshots of the soil were taken from the top view. Using the noise velocity as the separation point to draw the velocity contour of the soil, one could differentiate the soil moving area with the rest of soil particles (Fig. 8.2a). Applying the same procedure to the clumps, the straw moving area was differentiated (Fig. 8.2b). Velocity contours

174

were taken at three random locations within the central region, where the soil and straw reached their steady-state movements. The velocity contours were imported into MATLAB to determine the values of the moving areas through image processing.
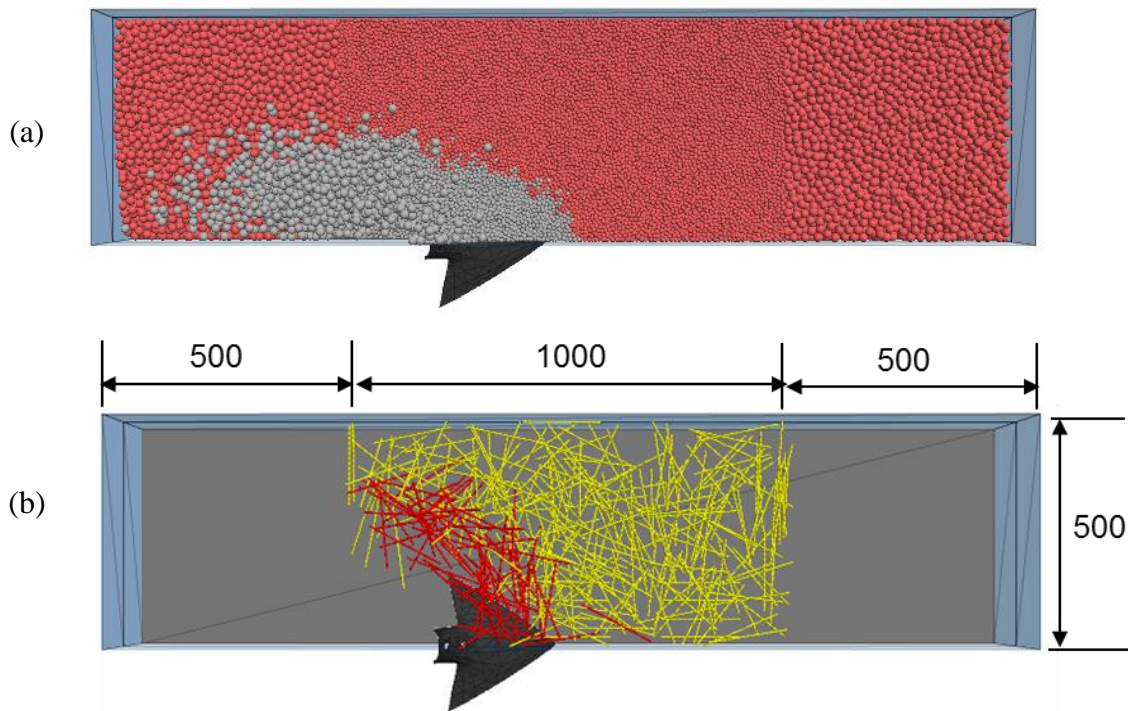
Figure 8.2. Monitoring soil and straw moving areas: (a) particle velocity contour showing disturbed soil particles (shank and straws are invisible); (b) clump velocity contour showing disturbed straws (shank and soil are invisible). All dimensions are in mm.

8.3.2.2. Monitoring straw forward and lateral displacements

Straw forward and lateral displacements were monitored using straw tracers. Figure 8.3 shows that four straw tracers were placed on the soil surface, and they were orientated along the travel direction. Numbers of straw tracers could be varied, and the orientation of straw tracers could also be varied, depending on the application. To monitor the straw displacements, the coordinates of the tracers before and after sweep

175

passing were recorded, and the difference in a direction was calculated as the straw displacement in the respective direction.
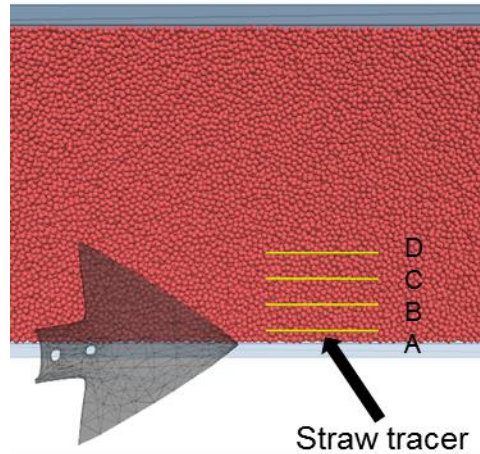
Figure 8.3. Straw tracers placed along the travel direction and across the width of the sweep (in transparency) for monitoring straw displacements (shank and surface straws are invisible).

8.3.2.3. Monitoring residue cover

The percentage of residue cover was monitored from the top view of the surface straws. Screenshots of the 1-metre long central region of the soil bin were taken before and after the tillage (Fig. 8.4). The screenshots were then analyzed in MATLAB using the image thresholding method to determine the percentage of residue cover (Zeng and Chen, 2018b)
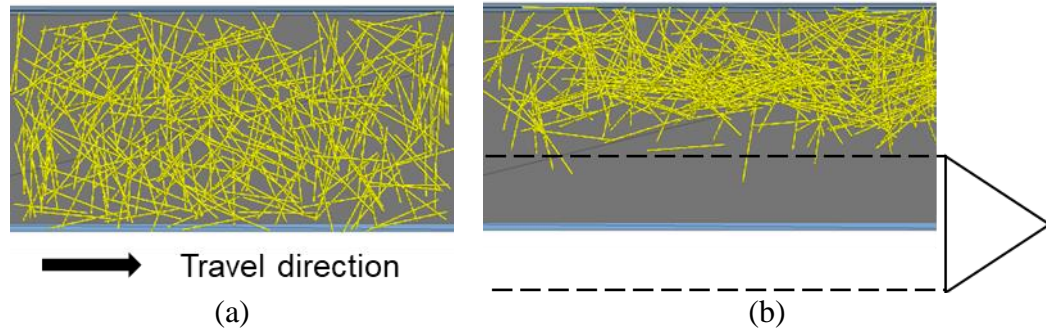
Figure 8.4. Surface straws for monitoring residue cover before (a) and after (b) the tillage (soil is invisible).

8.3.2.4. Monitoring other straw dynamic attributes

The straw kinetic energy on the whole and kinematic characteristics of individual straw including translational and rotational velocity and associated acceleration were recorded using built-in functions of the PFC^{3D}. The kinetic energy of all clumps accounted for the translational and rotational energies of each and every clump. The straw kinetic energy was calculated as following:

$$E_k = \frac{1}{2} \sum_N (m_i V_i^2 + I_i \omega_i \times \omega_i) \tag{8.1}$$

where

E_k = straw kinetic energy (J),

N = the number of clumps (dimensionless),

m_i = inertial mass (kg),

V_i = translational velocities of clump i (m s^{-1}),

I_i = inertial tensor (kg m^2),

ω_i = rotational velocities of clump i (rad s^{-1}).

The motion of a straw was determined by the resultant force and moment acting upon it and could be described in terms of the translational motion of a point in the straw and the rotational motion of the entire straw. The translational motion of the centre of mass was described in terms of its velocity and acceleration. Similarly, the rotational motion of the straw was described in terms of its angular velocity and angular acceleration. Also, the motion of the straw tracers was qualitatively assessed using their trajectories.

8.3.3. Model parameters and calibration

Sensitivity analysis was performed on model micro-parameters, and it was found that soil particle stiffness and straw clump stiffness were the critical micro-parameters that affected soil and straw dynamics. Therefore, they were calibrated and all other micro-parameters were determined as follows. The micro-parameters of balls and walls were adopted from Mak and Chen (2014), in which the model was calibrated and validated for the same sweep working in a loamy sand soil. The micro-parameters of the side walls were chosen the same as the soil particle, similar to the model of Falagush (2014). A friction coefficient of 0.35 for straw was measured using a torsional ring shear test of oat straw samples (ASTM D6467). Normal stiffness and shear stiffness were assumed equal as in previous studies (e.g., Asaf et al., 2007 and Mak et al., 2012). A local damping coefficient of 0.05 was found to be appropriate for system energy dissipation in preliminary simulations. The default timestep was automatically calculated and used throughout the simulation. All those model micro-parameters are summarized in Table 8.1.

Table 8.1. Major parameters of the soil-sweep-straw model

Micro-parameters	Value	Sources
Wall stiffness, N m^{-1}	1e8	Mak and Chen (2014)
Wall friction	0.5	Mak and Chen (2014)
Ball stiffness, N m^{-1}	To be calibrated	
Ball friction	0.36	Mak and Chen (2014)
Sidewall stiffness, N m^{-1}	= ball stiffness	Falagush (2014)
Sidewall friction	0.36	Falagush (2014)
Ball density, kg m^{-3}	2650	Mak and Chen (2014)
Bond radius multiplier	0.5	Mak and Chen (2014)
Bond stiffness, Pa m^{-1}	4.95e7	Mak and Chen (2014)
Bond normal strength, Pa	3.82e4	Mak and Chen (2014)
Bond shear strength, Pa	1.39e4	Mak and Chen (2014)
Clump stiffness, N m^{-1}	To be calibrated	
Clump friction	0.35	Measured
Clump density, kg m^{-3}	68	Measured
Viscous damping coefficient	0	Mak and Chen (2014)
Local damping coefficient	0.05	Selected
Integration timestep, s	~3e-6	Default

The model outputs in the calibration were chosen to be A_{soil} and A_{straw}, two dynamic attributes at the system level. Their values were greatly varied as altering the soil particle stiffness (K_b) and straw clump stiffness (K_c). Regression analysis was conducted to establish the relationships between the micro-parameters (K_b and K_c) and the outputs (A_{soil} and A_{straw}). The calibration method of Zeng et al. (2017) was used for the model, which integrated response surface optimization and inverse solution technique for minimizing the discrepancy between model results and 'true values'. The true values of the A_{soil} and A_{straw} were determined from the steady-state movement models of Liu et al. (2008), which mathematically described the soil and straw movement zones as

disturbed by a sweep and being successfully validated by an indoor soil bin experiment. The discrepancy between the simulation and the true values was expressed as following:

$$E = \left(\frac{|(A_{soil})_t - (A_{soil})_s|}{(A_{soil})_t} + \frac{|(A_{straw})_t - (A_{straw})_s|}{(A_{straw})_t} \right) \qquad (8.2)$$

where

E = relative error between the true value and simulation,

A_{soil} = soil disturbance area (m^2),

A_{straw} = straw disturbance area (m^2),

subscript t stands for the true values and s stands for simulated values.

The optimization of the above function was conducted in MATLAB to search for the optimal model micro-parameters which would result in a minimum value of E. This set of micro-parameters (K_b and K_c) was recorded as the calibrated values of the model.

8.3.4. Model validation

The straw forward displacement data from an experiment conducted by Liu et al. (2007) were used to validate the model. The straw forward displacement was a dynamic attribute at the individual level, which differed from that used in the model calibration exercise, and was therefore considered to offer more credibility to the model validation result. As in the experiment, four straw tracers were used in the model simulations. The tracers were equally spaced on the soil surface across the width of the sweep, labeled as tracer A, B, C, and D, from the centre to the side, as shown in Figure 8.3. The other conditions of the simulations, including the amount of surface straws, soil bulk density,

180

working speed and depth were set the same as in the experiment. The model performance was evaluated by comparing the simulated straw forward displacement against the experimental data.

8.3.5. Model applications

The model was used to conduct a virtual test to investigate the effects of working speed on straw dynamic attributes under different amounts of initial surface residue. The type of the sweep studied is typically used at field speeds ranging from 5 to 11 km h^{-1} (ASABE D497.7). Therefore, three speeds of 5, 8, and 11 km h^{-1} were selected, and named as low (S_L), medium (S_M), and high (S_H) speeds, respectively. A typical oat field of conservation tillage has residue amount ranging from 80 to 220 g m^{-2} (Sloneker and Moldenhauer, 1977). Thus, three residue masses of 80, 150, and 220 g m^{-2} were used and named as low (R_L), medium (R_M), and high (R_H) levels of surface residue, respectively. The dynamic attributes monitored in the virtual test included residue cover and straw forward and lateral displacements. Using the validated model as a case study, several straw dynamic attributes including kinetic energy, trajectory, translational velocity and acceleration, as well as angular velocity and acceleration were monitored to examine the availability of the discrete element model to gain an in-depth understanding of the interaction system. These model dynamic attributes are difficult to measure in a physical test, if not impossible.

8.4. Results and discussions

8.4.1. Calibrated model micro-parameters

Five values of soil ball stiffness K_b for model inputs were 1e3, 3e3, 1e4, 3e4, and 1e5 N m^{-1}, and each of them was combined with five values of straw clump stiffness K_c

of 1e2, 3e2, 1e3, 3e3, and 1e4 N m^{-1}, which resulted in a total of 25 simulation runs. All other model micro-parameters were kept constant as in Table 1. The model outputs of A_{soil} and A_{straw} were plotted versus the K_b and K_c on a log scale (Fig. 8.5). The A_{soil} slightly decreased as the K_c increased, while the A_{soil} was significantly affected by the K_b in a directly proportional relationship. For the straw, its moving area increased as the K_b and K_c increased and the effect of K_c was more remarkable than that of K_b. Comparing the two areas, the A_{straw} was greater than A_{soil} at any combination of model micro-parameters, which was mainly due to the interaction among straw pieces. This agreed with the experimental results of Eltom et al. (2015) that the straw displacement was significantly larger than soil displacement. The difference between A_{soil} and A_{straw} became greater as the K_c increased, which reflected a higher level of interaction among surface straws.

(a)   (b)
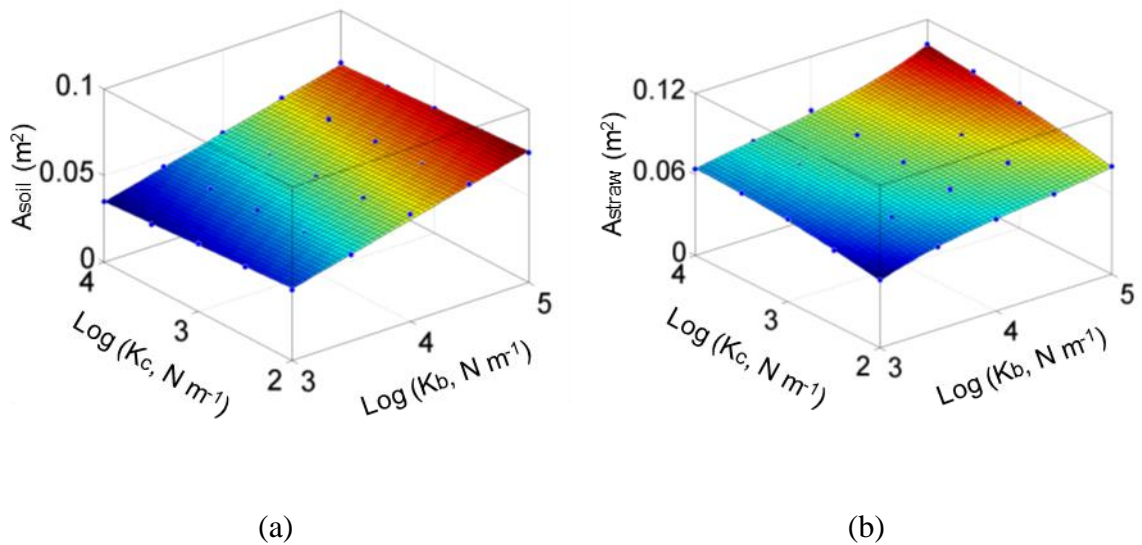
Figure 8.5. Response surface of (a) soil moving area (A_{soil}) and (b) straw moving area (A_{straw}) with respect to ball stiffness (K_b) and clump stiffness (K_c) on a semi-log scale.

The response surfaces of A_{soil} and A_{straw} can be described by the following polynomial equations:

$$A_{soil} = -0.00252 + 0.017(logK_b) - 0.00336(logK_c) \qquad (8.3)$$

$$A_{straw} = -0.4693 + 0.3092(logK_b) + 0.09477(logK_c) - 0.06206(logK_b)^2 -$$
$$0.03641(logK_b)(logK_c) - 0.004514(logK_c)^2 + 0.004133(logK_b)^3 + 0.0044(logK_b)^2(logK_c)$$
$$+ 0.0005143(logK_b)(logK_c)^2 \qquad (8.4)$$

The coefficient of determination (R^2) was 0.99 for equations (8.3) and (8.4), indicating a high degree of accuracy of the regression models. Under the soil and straw conditions of the simulation model, the true values were calculated as $(A_{soil})_t = 0.056$ m^2 and $(A_{straw})_t = 0.072$ m^2 based on the analytical model of Liu et al. (2008), which had the same working speed as the simulation of 5 km h^{-1}. Substituting equations (8.3) and (8.4) into the objective function (eq. 8.2) and using the calculated true values, the K_b and K_c that yielded the minimal relative error were 8,730 and 332 N m^{-1}, respectively. This set of model micro-parameters was used throughout the following simulations.

8.4.2. Model performance

Using the calibrated micro-parameters, the straw-sweep-soil model was evaluated in terms of the straw forward displacement monitored using the straw tracers shown in Figure 8.3. The straw forward displacement was defined as the translational movement of the centre of gravity of a straw tracer in the direction along sweep travel speed. The soil particle density of 2081 kg m^{-3} was used in the model as calculated from the soil porosity and the bulk density in the experiment (Liu et al., 2007). A total of 310 clumps were randomly placed on top of the straw tracers to achieve a residue cover of 108 g m^{-2} as in

the experiment. After the sweep passage, the forward displacement curve of each of the four straw tracers is plotted against the time (Fig. 8.6). In the first 0.5 seconds, the sweep was travelling to establish a steady-state movement and the tracers were not disturbed. As the sweep came closer to the straw tracers, the tracer A was the first one to move followed by tracer B, C, and D in succession. The closer the straw to the bin centre, the earlier it would move. This reflected the triangular shape of the soil and straw moving areas, as the moving front was inclined toward the soil bin centre. The tracers rapidly moved forward a certain distance over a period of less than 0.5 s, then became relatively static until resting. The tracers reached their static status in the order from D to C to B to A. In summary, the earlier the tracer started to move, the longer the tracer would travel, and the later the tracer would land at rest. This explained the decreasing trend of straw forward displacement from tracer A to D. The tracer A, B, C, and D had a final forward displacement of 441, 167, 119, and 29 mm respectively. The average forward displacement was 189 mm. Comparing with the testing result of 173 mm by Liu et al. (2007), the model over-predicted the displacement by 9.2%. This concluded that the straw-sweep-soil model was reasonably accurate in simulating the straw movement.
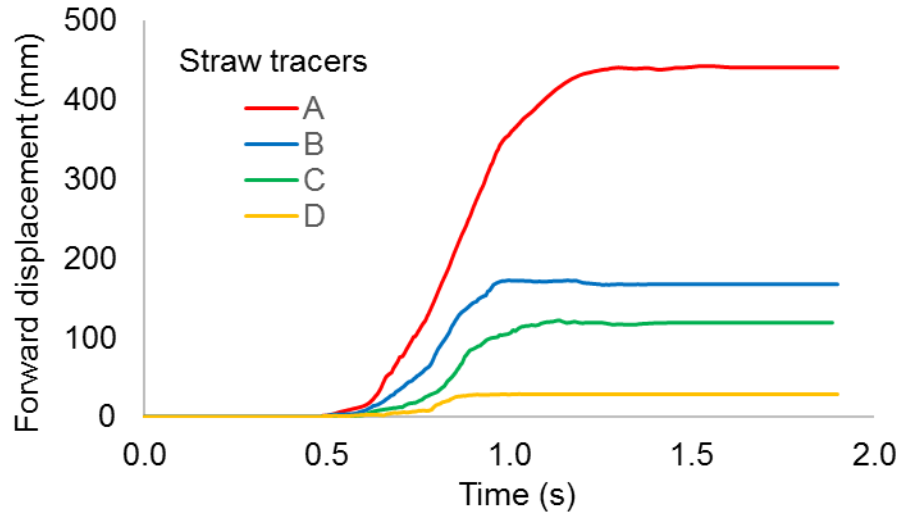
Figure 8.6. The forward displacement curve of four straw tracers.

8.4.3. Model prediction

8.4.3.1. Residue cover

The validated model was used to predict the residue cover and straw displacement as affected by sweep working speed under different initial residue amounts. A total of 230, 431, and 631 clumps were randomly spread on the soil surface to represent the initial residue amount of 80 (R_L), 150 (R_M), and 220 (R_H) g m^{-2}, which corresponded to an initial residue cover of 37.2%, 54.2%, and 67.5%, respectively, as measured through image processing in MATLAB. After the sweep passage, the residue cover remaining of R_M and R_H ranged from 30.9% to 51.1%, which met the minimum 30% requirement of conservation tillage systems; whereas, the residue cover remaining of R_L was less than 30% regardless of the working speed (Fig. 8.7). Increasing the working speed increased the residue cover reduction, and thus reduced the residue remained on the surface. The effect of working speed on surface residue reduction was more pronounced with heavier initial residue cover. For instance, increasing the speed from 8 (S_M) to 11 (S_H) km h^{-1}

resulted in a higher level of residue cover reduction of 8.3%, 5.1%, and 0.1% in R_H, R_M, and R_L, respectively. The average residue cover remaining (or reduction) was 45.3% (22.2%), 36.4% (17.8%), and 24.5% (12.7%) for R_H, R_M, and R_L, respectively. The sweep had a higher residue cover reduction at higher initial residue amount. Therefore, the sweep was effective in reducing residue cover and yet keeping residue cover maintained at a sustainable level when it was used at fields with high initial residue amount.
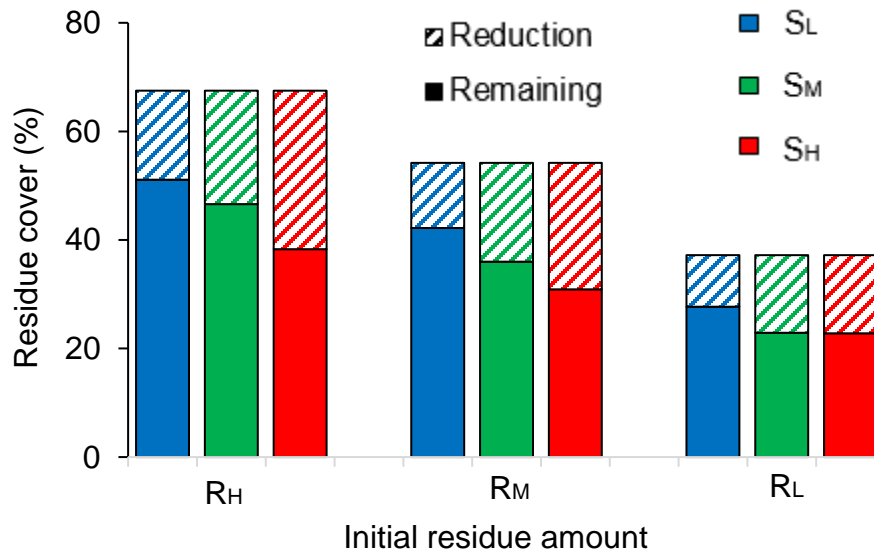
Figure 8.7. The effect of working speed (S_L: 5 km h^{-1}; S_M: 8 km h^{-1}; S_H: 11 km h^{-1}) on residue cover under different initial residue amounts (R_L: 80 g m^{-2}; R_M: 150 g m^{-2}; R_H: 220 g m^{-2}).

8.4.3.2. Straw displacement

The sweep moved the straw tracers farther away from their original positions in both forward and lateral direction as the working speed increased (Fig. 8.8). This agreed well with the experiment results of Liu et al. (2010), in which the sweep produced

significantly larger straw displacement at 10 km h^{-1} as compared with that at 5 km h^{-1}. The effect of speed on straw displacement was more noticeable in the forward direction than that in the lateral direction. For example, the straw tracers moved farther by 164 and 84 mm in forward and lateral directions as the speed increased from 8 (S_M) to 11 (S_H) km h^{-1} with the high residue amount (R_H). However, the effect of speed on the straw displacement did not show any specific trend as the initial residue amount varied. In general, the straw displacement decreased as the amount of initial residue increased, which was possible because the surface straws suppressed the movement of the tracers. The forward displacement was greater than the lateral displacement, except that at S_L-R_H, where the displacement was the smallest among all cases. Compared to the lateral displacement at S_H, the forward displacement increased by 41% at R_H, 35% at R_M, and 54% at R_L. The greater values of forward displacement were also found in the soil bin experiments of Liu et al. (2010) and Fang et al. (2016), where the forward displacement was greater than the lateral displacement with insignificant differences. The "straw dragging" phenomenon reported in Liu et al. (2010) was observed in some of the simulation runs, where straws were caught on the tool and dragged for a while before falling off. This was possible due to straw tangling since the dragging was more likely to occur as the initial residue amount increased. However, the rigid straws used in the model were not allowed to investigate straw tangling and dragging phenomena.
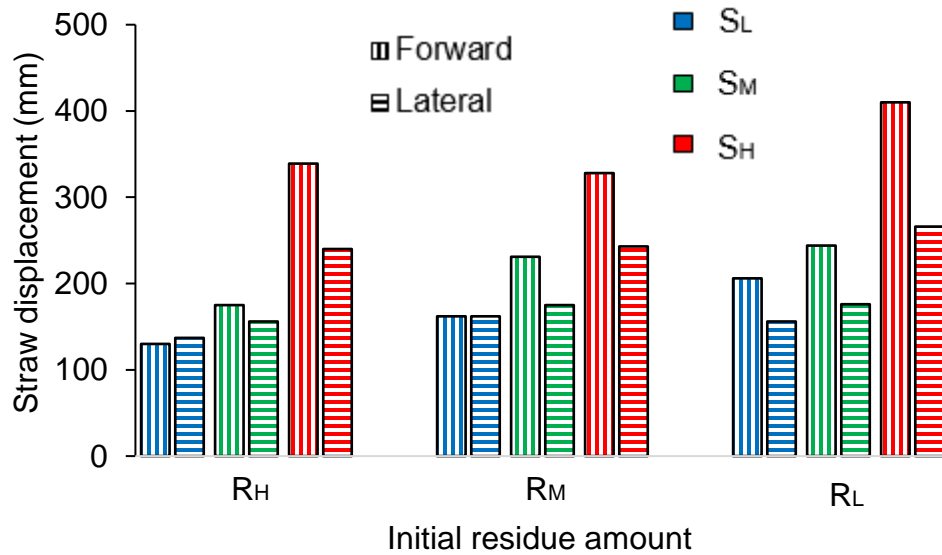
Figure 8.8. The effect of working speed (S_L: 5 km h^{-1}; S_M: 8 km h^{-1}; S_H: 11 km h^{-1}) on straw displacement under different initial residue amounts (R_L: 80 g m^{-2}; R_M: 150 g m^{-2}; R_H: 220 g m^{-2}).

8.4.3.3. Other straw dynamic attributes

Using the validated model as an example, several straw dynamic attributes were monitored. On the system level, the straw kinetic energy is plotted against the time (Fig. 8.9). Within the first 0.5 s of the tillage, the sweep did not disturb the surface straws, which resulted in a zero kinetic energy. Then, the kinetic energy started to accumulate and reached the peak value of 10 mJ at the time of 1.0 s. Subsequently, the kinetic energy gradually decreased as the sweep moved away from the straws. The surface straw regime came to the resting state at the time of 1.8 s, as indicated by the zero kinetic energy. The rate of kinetic energy accumulation was greater than the rate of dissipation. This was correlated to the damping coefficients used in the model. The straw kinetic energy was dissipated through local damping at each clump and through friction and viscous damping at the contacts. As a principal mechanism of energy dissipation, the local

damping applied a damping force with a magnitude proportional to the unbalanced force of each clump as dictated by the local damping coefficient. The relatively low value of the local damping coefficient (0.05) used in the simulation accounted for the low rate of kinetic energy dissipation. The kinetic energy of any particular straw could be tracked if desired.
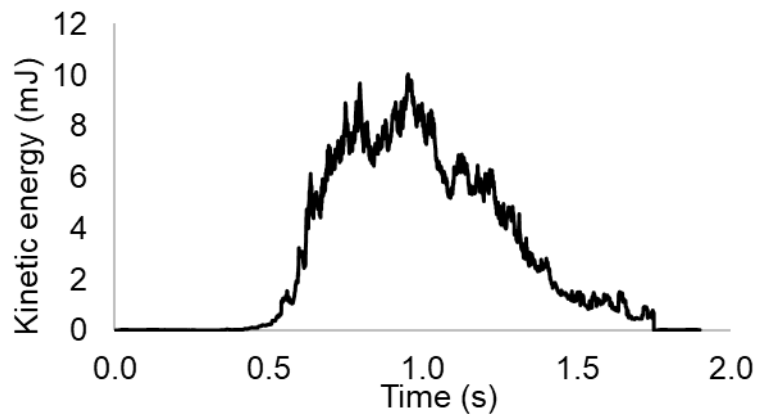

Figure 8.9. The total kinetic energy of all straws.

The moving trajectory of the straw tracers shown in velocity contour is plotted in isometric, front, side, and top views (Fig. 8.10). Comparing the velocity among tracers, one found that the closer the straw was to the soil bin centre, the higher the moving speed it experienced. This indicated that the centre tracers had more kinetic energy than the side tracers, which attributed to the greater moving displacement of the centre tracers. Straw movement during tillage was modelled as three phases, namely forced, projectile, and overturning displacement, by means of video recording, mathematical modelling, and experimental validation (Liu, 2005). The forced movement happened in the forepart of the straw displacement where the straws were forced to move along with the soil underneath by the sweep, as witnessed by the straw velocity equal or smaller than the

189

sweep travel speed (1.4 m s^{-1}) (Fig. 8.10a). A small straw velocity was attributed to the

resistance from the surface straws and the slippage between the tracers and soil. The

forced movement ended when a straw tracer was raised to the highest point (Fig. 8.10b).

After that, the straw tracers were projected away from the sweep and their velocities

increased to the peak value around 2 m s^{-1}. Meanwhile, the tracers fell down, which

completed the projectile movement (Fig. 8.10c). While bouncing on the ground, the straw

tracers were overturned by the rolling soil clods (Fig. 8.10d). Three tracers were turned

counter-clockwise and one was in the opposite direction. The tracer A had the maximum

turning angle while the tracer D was the least turned. The straw movement behaviours in

the proposed DEM-based numerical model agreed well with that in the physically based

mathematical model of Liu (2005).

(a)

Straw velocity (m s⁻¹)

(b)

(c)

(d)
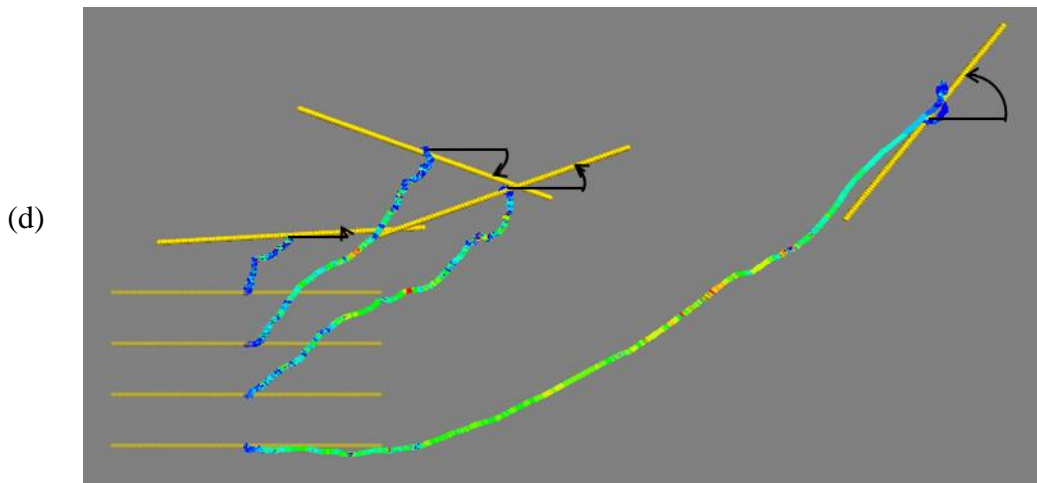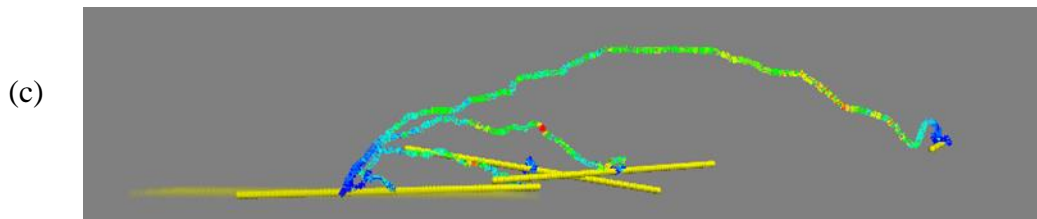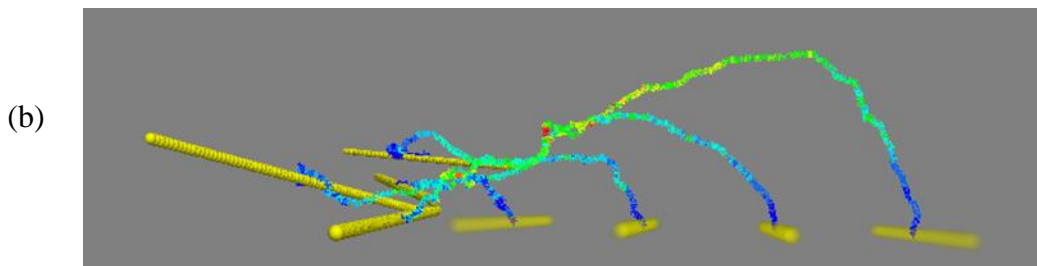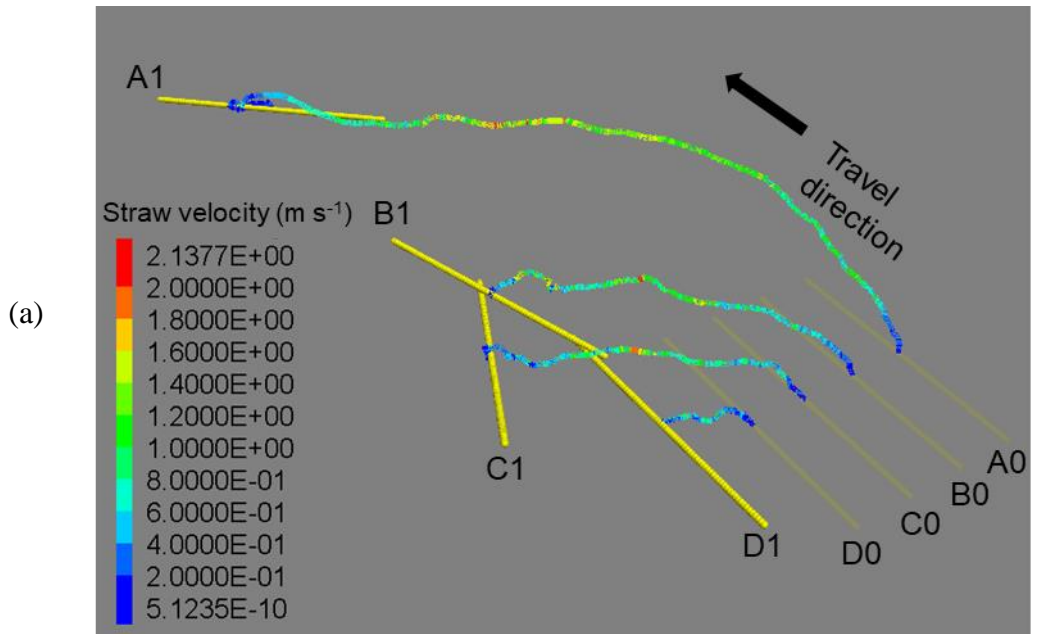
Figure 8.10. The moving trajectory and velocity of the straw tracers in isometric (a), top (b), side (c), and top (d) views (number 0 and 1 indicates the initial and ultimate position of the tracer respectively).

The model also allowed users to acquire kinematic information of any given straw. Taking straw tracer A as an example, its translational velocity, translational acceleration, angular velocity, and angular acceleration were tracked as the sweep travelled through the soil bin (Fig. 8.11). They had a similar single-peaked overall trend with different degrees of fluctuation. Generally speaking, the acceleration fluctuated more than its corresponding velocity. The translational velocity fluctuated the least among the four attributes (Fig. 8.11a). The maximum translational acceleration occurred at the time of 1.0 s, which corresponded to the projectile motion of the straw (Fig. 8.11b). The overturning movement of the straw was witnessed by the two jumps of angular velocity between 1.1 and 1.4 s (Fig 8.11c). All these kinematic attributes would be fundamentally critical in understanding straw dynamics in a straw-sweep-soil interaction system.
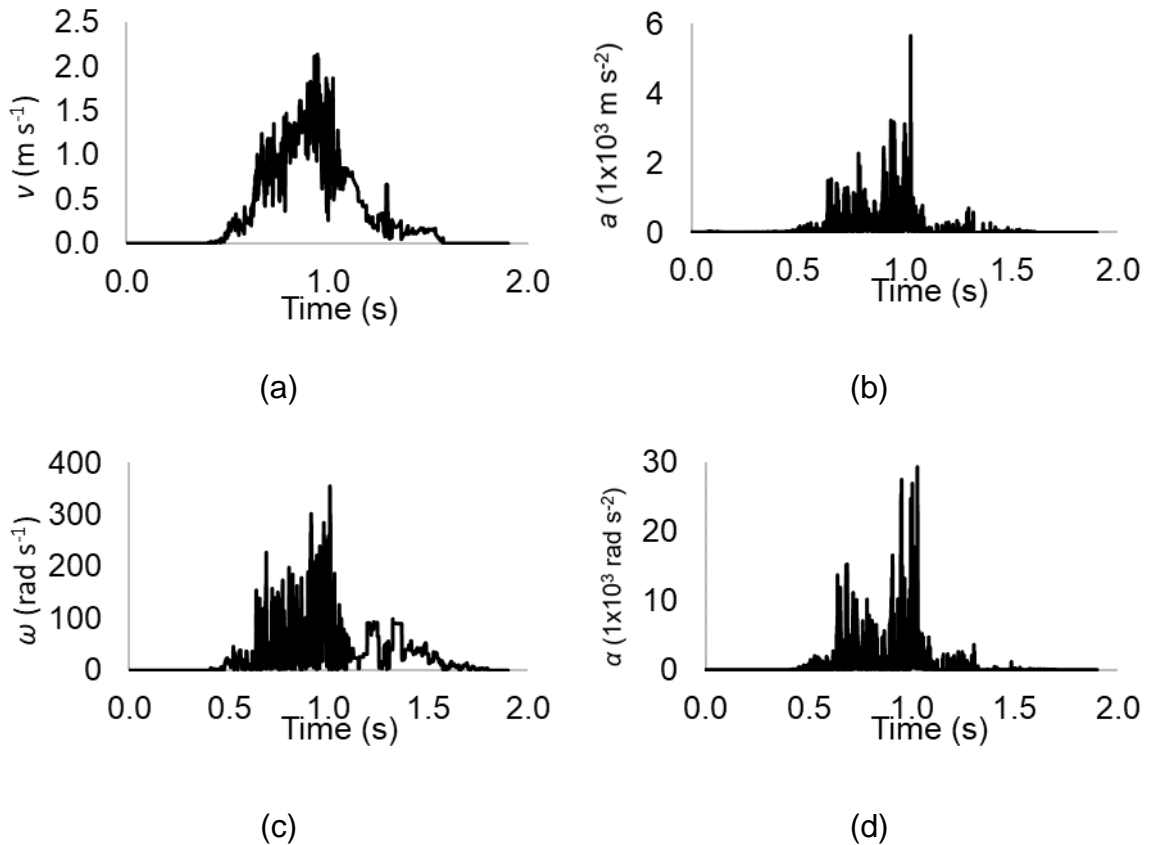
Figure 8.11. Several dynamic attributes of straw tracer A: (a) translational velocity (v);

(b) translational acceleration (a); (c) angular velocity (ω); (d) angular acceleration (α).

8.5. Conclusions

A straw-sweep-soil model was developed using the DEM. The model was able to

simulate dynamic attributes of bulk materials (such as soil and straw moving areas and

residue covers) and individual particles (such as straw displacements and trajectories).

Model parameters calibrated were 8730 N m^{-1} for ball stiffness and 332 N m^{-1} for clump

stiffness. The calibrated model produced a straw forward displacement of 189 mm, which

was 9.2% higher than the measurement data in the literature. The moving trajectories and

velocity contours of the straw tracers clearly demonstrated the three stages of the straw

movement, i.e., forced, projectile, and overturning movements. The closer the straw to

193

the sweep centre, the higher the speed, the longer the projectile period, and therefore the greater the straw displacement. Increasing the working speed of the sweep increased the residue cover reduction and the effect was more pronounced when the initial residue amount was high. The sweep showed a decreasing trend in reducing the residue cover as the initial residue amount decreased. Increasing the working speed from 5 to 11 km h^{-1} increased the straw forward displacement by 99% to 161%, depending on the initial residue amount. The increase in the straw lateral displacement was from 50% to 75% as the initial residue amount varied. The straw would travel farther if the amount of initial residue was low. The results provided critical information in designing tillage tools for straw management. Further research incorporating flexible straws as in practice is desired in modelling residue-soil-tool interaction.

8.6. Acknowledgement

8.7. References

Arvidsson, J., Hillerstrom, O., 2010. Specific draft force, soil fragmentation and straw incorporation for different tine and share types. Soil & Tillage Research 110, 154–160.

ASABE Standards. 2015. D497.7 Agricultural Machinery Management Data. St. Joseph, Mich.: ASABE.

Asaf, Z., Rubinstein, D., Shmulevich, I., 2007. Determination of discrete element model parameters required for soil tillage. Soil & Tillage Research 92, 227–242.

ASTM Standards. 2013. D6467 Standard Test Method for Torsional Ring Shear Test to Determine Drained Residual Shear Strength of Cohesive Soils. ASTM International, USA.

Barker, M.E., Plouffe, C., 2017. Simulation of planter row cleaner in corn residue using discrete element modelling. Paper No. 1700095. In: ASABE 2017 Annual Conference. Spokane, Washington, USA. July 16–19.

Chandio, F.A., 2013. Interaction of Straw-Soil-Disc Tool under Controlled Conditions. Ph.D. Thesis, Nanjing Agricultural University, Nanjing, China.

Eltom, A.E.F., Ding, W., Ding, Q., Tagar, A.A., Talha, Z., Gamareldawla, 2015. Field investigation of a trash-board, tillage depth and low speed effect on the displacement and burial of straw. Catena 133, 385–393.

Fang, H., Zhang, Q., Chandio, F.A., Guo, J., Sattar, A., Arslan, C., Ji, C., 2016. Effect of straw length and rotavator kinematic parameter on soil and straw movement by a rotary blade. Engineering in Agriculture, Environment and Food 9(3), 235–241.

Falagush, O., 2014. Discrete Element Modelling of Cone Penetration Testing in Granular Materials. Ph.D. Thesis, University of Nottingham, Nottingham, UK.

Itasca, 2018. Particle flow code in 3 dimensions (PFC^{3D}). Theory and Background. Itasca Consulting Group Inc., Minneapolis, Minnesota, USA.

Korn, C., Herlitzius, T., 2017. Coupled CFD-DEM simulation of separation process in combine harvester cleaning devices. Landtechnik 72(5), 247–261.

Leblicq, T., Smeets, B., Ramon, H., and Saeys, W., 2016a. A discrete element approach for modelling the compression of crop stems. Computers and Electronics in Agriculture 123, 80–88.

Leblicq, T., Smeets, B., Vanmaercke, S., Ramon, H., Saeys, W., 2016b. A discrete element approach for modelling bendable crop stems. Computers and Electronics in Agriculture 124, 141–149.

Lenaerts, B., Aertsen, T., Tijskens, E., Ketelaere, B.D., Ramon, H., Baerdemaeker, J.D., Saeys, W., 2014. Simulation of grain-straw separation by discrete element modelling with bendable straw particles. Computers and Electronics in Agriculture 101, 24–33.

Liu, J., 2005. Study of Tillage Tool-Soil-Crop Residue Interactions. Ph.D. Thesis, University of Manitoba, Winnipeg, Canada.

Liu, J., Chen, Y., Kushwaha, R.L., 2010. Effect of tillage speed and straw length on soil and straw movement by a sweep. Soil & Tillage Research 109, 9–17.

Liu, J., Chen, Y., Lobb, D.A., Kushwaha, R.L., 2007. Soil-straw-tillage tool interaction: field and soil bin study. Canadian Biosystems Engineering 49, 2.1–2.6.

Liu, J., Lobb, D.A., Chen, Y., Kushwaha, R.L., 2008. Steady-state models for the

    movement of soli and straw during tillage with a single sweep. Transactions of the

    ASABE 51(3), 781–789.

Ma, Z., Li, Y., Xu., L., 2015. Discrete-element method simulation of agricultural

    particles' motion on variable-amplitude screen box. Computers and Electronics in

    Agriculture 118, 92–99.

Mak, J., Chen, Y., 2014. Simulation of draft forces of a sweep in a loamy sand soil using

    the discrete element method. Canadian Biosystems Engineering 56, 2.1–2.7.

Mak, J., Chen, Y., Sadek, M.A., 2012. Determining parameters of a discrete element

    model for soil-tool interaction. Soil & Tillage Research 118, 117–122.

Mari, I.A., Chandio, F.A., Ji, C., Chaudhry, A., Asma, S., Tagar, A.A., Fang, H., 2014.

    Performance and evaluation of disc tillage tool forces acting on straw

    incorporation soil. Pakistan Journal of Agricultural Sciences 51, 1–6.

Sadek, M.A., Chen, Y., 2015. Feasibility of using PFC3D to simulate soil flow resulting

    from a simple soil engaging tool. Transactions of the ASABE 58(4), 987–996.

Zeng, Z., Chen, Y., 2018a. The performance of fluted coulters for vertical tillage as

    affected by working speed. Soil & Tillage Research 175, 112–118.

Zeng, Z., Chen, Y., 2018b. Performance evaluation of fluted coulters and rippled discs

    for vertical tillage. Soil & Tillage Research 183, 93–99.

Zeng, Z., Chen, Y., Zhang, X., 2017. Modelling the interaction of a deep tillage tool with

    heterogeneous soil. Computers and Electronics in Agriculture 143, 130–138.

Chapter 9: General Conclusions and recommendations

9.1. General conclusions

The experimental studies investigated the tillage performance of new soil-engaging tools of vertical tillage and compact disc harrow by measuring a variety of performance indicators. The numerical models of various tools and their interaction with soil and residue were successfully developed through calibration and validation for a micropenetrometer, a subsoiler, and a sweep. The results obtained in this thesis have advanced the science of soil dynamics by gaining insights into the dynamic systems of soil-tool-residue interactions. Furthermore, the results also provided engineering knowledge required to design a high-performance soil-engaging tool that creates the optimal field conditions for crop growth while consuming minimal tractor power. More importantly, the measurement methods and modelling approaches developed in this study could be used for other agricultural machines to achieve a comprehensive understanding of the soil-tool-residue interactions behaviours, which would be beneficial to the sustainable design and management of agricultural machinery. Specific conclusions toward each objective listed in Chapter 1 are as follows.

9.1.1. Vertical tillage

Field experimental studies showed that the fluted coulters resulted in less surface residue, incorporated more residue into the soil, created a wider furrow, and disturbed a larger area, as compared with the rippled discs. On the other hand, the coulters had a 73% higher draft force demand and a 729% higher possibility of soil sticking than the discs. The effect of working speed was more dominant than the coulter geometry on the tillage performance of the fluted coulters. Increasing the working speed (from 12 to 16 km h^{-1}

and from 12 to 20 km h^{-1}) increased the soil disturbance width by 7.0 and 13.1% and the soil throw width by 14.3 and 45.1% respectively, but decreased the soil sticking by 1.4 and 76.6% and the residue cover by 5.1 and 11.0% respectively.

9.1.2. Compact disc harrow

Soil bin experiments demonstrated that the disc spacing and offset had significant effects on the tillage performance, and the effects varied with the tillage depth. At the shallow tillage depth, larger disc spacing resulted in smaller cutting area ratios with negligible changes in the soil loosening efficiency. At the deep tillage depth, increasing in disc spacing resulted in increased cutting area ratios and increased soil loosening efficiencies. As for the effect of the disc offset, the centre offset position had the highest cutting area ratios, while the right offset position had the maximum efficiencies, regardless of the tillage depth.

9.1.3. Micropenetrometer

The soil-micropenetrometer model developed using PFC^{3D} produced comparable results as the laboratory measurements, in terms of the variation of cone index over penetration depth. The model was calibrated and validated using laboratory and field testing results respectively. The model was able to predict soil cone indices for different soil bulk densities and showed that the two variables had a linear proportional relationship.

9.1.4. Subsoiler

The subsoiler model was capable of predicting soil cutting resistance and soil disturbance characteristics with relative errors ranging from 2.63 to 10.2%. Simulation

results indicated that the shallow tillage, where the subsoiler-type tool worked at either 5 or 20 mm deeper than the hardpan layer, could achieve the best performance for breaking the hardpan.

9.1.5. Sweep

The straw-sweep-soil model was able to simulate dynamic attributes of bulk materials (such as soil and straw moving areas and residue covers) and individual particles (such as straw displacements and trajectories). Increasing the working speed of the sweep increased the residue cover reduction and the effect was more pronounced when the initial residue amount was high. The closer the straw to the sweep centre, the higher the speed, the longer the projectile period, and therefore the greater the straw displacement.

9.2. Recommendations

9.2.1. Experiments

Similar experiments of the new tillage tools need to be conducted in different crop production systems to investigate the suitability of the tools in varying conditions. A long-term field experiment embracing some agronomic factors related to the soil-tool-residue interactions would be helpful. The conclusions gained from the soil bin test would need to be verified in field tests since the tool tested was typically employed when field crop residue was presenting.

9.2.2. Simulations

The nature of the modelling studies in this thesis was the application of the simulation method of DEM in the area of soil-tool-residue interactions. No attempts were

made to modify the method itself. However, the exercises of DEM in this research topic suggested that some improvements to the method might be beneficial to the engineering application. For example, the constitutive law of soil could be integrated into a contact model specifically compiled for agricultural soil. The current approach of representing agricultural soil in DEM is adjusting model parameters of an adopted contact model until the model behaviours of interest are satisfactory, which sounds technically expedient. A contact model exclusively for the agricultural soil, and similarly another one for the crop residue, would significantly improve the model accuracy. Also, a new set of model parameters that have physical material meaning, rather than those of the microscopic constituents, would not only alleviate the difficulties of model calibration but also improve the accountability and universality of the model. Nevertheless, the feasibility of implementing these advancements in the DEM needs a long-term exploration. Finally, the capacity of DEM for modelling a complex system like residue-soil-tool interaction would highly depend on the advance of computational power.